VTT SCIENCE 46 Cantilever-enhanced photoacoustic spectroscopy in the analysis of volatile...

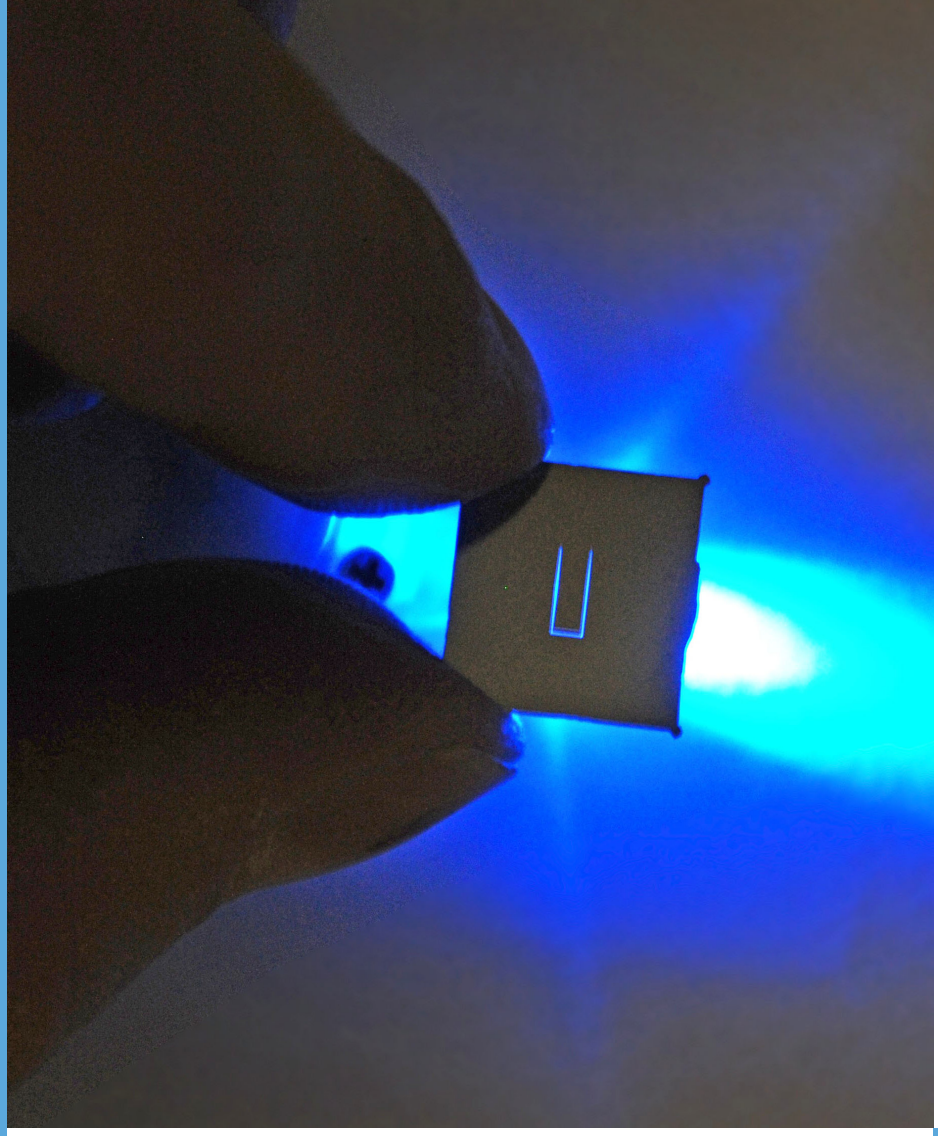

SCIENCE • TECHNOLOGY • RESEARCH HIGHLIGHTS • VISIONS •
Dissertation
46

Cantilever-enhanced photoacoustic spectroscopy in the analysis of volatile organic compounds

Christian Bernd Hirschmann

VTT

VTT SCIENCE 46

Cantilever-enhanced photoacoustic spectroscopy in the analysis of volatile organic compounds

Christian Bernd Hirschmann

University of Oulu Graduate School

Graduate School in Chemical Engineering

University of Oulu, Faculty of Technology,
Department of Process and Environmental Engineering

VTT Technical Research Centre of Finland

Academic dissertation to be presented with the assent of the Doctoral Training Committee of Technology and Natural Sciences of the University of Oulu for public defense in Kuusamonsali (Auditorium YB210), Linnanmaa, on 14 December 2013, at 12 noon.

ISBN 978-951-38-8105-4 (Soft back ed.)
ISBN 978-951-38-8106-1 (URL: http://www.vtt.fi/publications/index.jsp)

VTT Science 46

ISSN-L 2242-119X
ISSN 2242-119X (Print)
ISSN 2242-1203 (Online)

JULKAISIJA – UTGIVARE – PUBLISHER

VTT
PL 1000 (Tekniikantie 4 A, Espoo)
02044 VTT
Puh. 020 722 111, faksi 020 722 7001

VTT
PB 1000 (Teknikvägen 4 A, Esbo)
FI-02044 VTT
Tfn. +358 20 722 111, telefax +358 20 722 7001

VTT Technical Research Centre of Finland
P.O. Box 1000 (Tekniikantie 4 A, Espoo)
FI-02044 VTT, Finland
Tel. +358 20 722 111, fax +358 20 722 7001

Cover illustration: Cantilever photograph printed with the permission from Gasera Ltd.

Kopijyvä Oy, Kuopio 2013

Cantilever-enhanced photoacoustic spectroscopy in the analysis of volatile organic compounds

Christian Bernd Hirschmann. Espoo 2013. VTT Science 46. 109 p. + app. 49 p.

Abstract

Accurate and reliable measurement of volatile organic compounds (VOCs) is an important need in many application areas in industry, air pollution and atmosphere, health and well-being, defense and security as well as in many other fields. In this thesis, cantilever-enhanced photoacoustic spectroscopy (CEPAS) has been applied for the measurement of VOCs. A key feature in CEPAS is the non-resonant operational mode of the detector, which enables the broadly tunable wavelength ranges needed to resolve the spectral interferences that are typical in VOC measurement applications. Due to the large variation in VOC applications, the objective of this work was to build several, differently optimized CEPAS measurement systems and characterize their performance in certain applications.

The Fourier transform infrared (FT-IR) technique was applied for multi-compound VOC mixtures because of its capability to resolve spectral interference between the compounds. A compact, industry-ready FT-IR-CEPAS system was tested and reached multivariate detection limits (3σ, 25 s) at the single ppm level with the average sum of the cross-selectivity numbers in a four compound mixture being <0.01 ppm ppm^{-1}. To achieve better analytical sensitivity, the CEPAS detector was set up with a quantum cascade laser (QCL). The QCL-CEPAS system provides a univariate detection limit (3σ, 0.951 s) of 1.3 ppb for formaldehyde, which is ~1000 times better than the FT-IR-CEPAS system. However, in case of several compounds, spectral interferences are usually difficult to resolve because the mode hop-free tuning range of QCLs is limited to a few wavenumbers. For sensitive and selective trace gas detection, a compact optical parametric oscillator (OPO) was combined with CEPAS and applied to the multi-compound measurement of benzene, toluene, *p*-, *m*- and *o*-xylene (BTX). The achieved multivariate detection limits (3σ, 3237–3296 nm, 591 spectral points each 0.951 s) were around 10 ppb and the average sum of the cross-selectivity numbers <0.04 ppb ppb^{-1}.

Another achievement was the construction of a CEPAS measurement system capable of measuring at gas temperatures up to 180 °C. This enables applications where gases can only be measured in the hot state, e.g. the monitoring of many industrial emissions. Since the cantilever pressure transducer can withstand 180 °C, it was in direct contact with the hot sample gas and the need for cooling the gas or for using a signal tube was eliminated.

In summary, this thesis shows that modern CEPAS is a suitable technique for measuring VOCs. CEPAS is now robust and reliable enough for industrial and other applications outside the laboratory. Several measurement systems based on CEPAS and relevant for VOC applications have been demonstrated in this thesis.

Keywords Cantilever-enhanced photoacoustic spectroscopy, volatile organic compounds, FT-IR, quantum cascade laser, optical parametric oscillator, multi-compound analysis, science-based calibration

Preface

The research summarized in this thesis was carried out at the University of Oulu, Department of Process and Environmental Engineering and at VTT Technical Research Centre of Finland between 2009 and 2013. The financial support of the Graduate School in Chemical Engineering is greatly acknowledged.

First of all, I am deeply grateful to my principal supervisor Prof. Riitta Keiski for the possibility to conduct my thesis in her work group and the professional supervision of my thesis. Thank you for having a lot of confidence in me and my work. Special thanks go to my supervisor Doc. Satu Ojala, who always took time for my concerns. I enjoyed your support and advice. I owe a particular debt of gratitude to Dr. Ralf Marbach and M.Sc. Jussi Tenhunen, with whom I had uncountable and mind-opening technical discussions and professional guidance. Thanks to Lic.Sc.(Tech.) Jouko Malinen, Dr. Kimmo Solehmainen and Dr. Mikko Juuti for supporting my doctoral studies at VTT. Also, I would like to thank all my colleagues for their support and the cooperative atmosphere in both workgroups, at the university and at VTT.

Aside from University and VTT, I would like to extend my thanks to Gasera Ltd. and its employees, namely Dr. Ismo Kauppinen, Dr. Jussi Raittila, Dr. Juho Uotila, M.Sc. Sauli Sinisalo and M.Sc. Jaakko Lehtinen for providing equipment and excellent technical guidance. You always warmly welcomed me in your facilities. I am much obliged to Prof. Rudolf Kessler from Reutlingen University, who brought me to the interesting field of spectroscopy and process analysis and supported me with general advice over the years.

I am indebted to my parents Margit and Bernd Hirschmann and my brother Steffen Hirschmann who stood wholeheartedly by my side and helped me in every circumstance. Above all, the greatest thanks go to my wife Sarah Hirschmann for her wonderful love, enormous support, and generous practical help in everyday life during the research and dissertation. Finally, I also want to thank our children Vivien and Mathilda, who allowed me to refresh my mind after intensive working days.

Oulu, September 2013,

Christian Bernd Hirschmann

Academic dissertation

Principle Supervisor	Prof. Riitta L. Keiski Mass and Heat Transfer Process Laboratory Department of Process and Environmental Engineering University of Oulu, Finland
Supervisor	Doc. Satu Ojala Mass and Heat Transfer Process Laboratory Department of Process and Environmental Engineering University of Oulu, Finland
Reviewers	Prof. Markus Sigrist Laser Spectroscopy and Sensing Lab Institute for Quantum Electronics Swiss Federal Institute of Technology in Zurich, Switzerland
	Doc. Juha Toivonen Optics Laboratory Department of Physics Tampere University of Technology, Finland
Opponent	Dr. habil. Michael Maiwald Division Process Analytical Technology BAM Federal Institute of Materials Research and Testing Berlin, Germany

List of publications

This thesis is based on the following original articles which are referred to in the text as I–IV. The articles are reproduced with kind permission from the publishers.

I C. B. Hirschmann, J. Uotila, S. Ojala, J. Tenhunen, and R. L. Keiski, "Fourier transform infrared photoacoustic multicomponent gas spectroscopy with optical cantilever detection," Appl. Spectrosc. **64**, 293–297 (2010).

II C. B. Hirschmann, N. S. Koivikko, J. Raittila, J. Tenhunen, S. Ojala, K. Rahkamaa-Tolonen, R. Marbach, S. Hirschmann, and R. L. Keiski, "FT-IR-cPAS – New photoacoustic measurement technique for analysis of hot gases: A case study on VOCs," Sensors (Basel) **11**, 5270–5289 (2011).

III C. B. Hirschmann, J. Lehtinen, J. Uotila, S. Ojala, and R. L. Keiski, "Sub-ppb detection of formaldehyde with cantilever enhanced photoacoustic spectroscopy using quantum cascade laser source," Appl. Phys. B **111**, 603–610 (2013).

IV C. B. Hirschmann, S. Sinisalo, J. Uotila, S. Ojala, and R. L. Keiski, "Trace gas detection of benzene, toluene, *p*-, *m*- and *o*-xylene with a compact measurement system using cantilever enhanced photoacoustic spectroscopy and optical parametric oscillator," Vib. Spectrosc. **68**, 170–176 (2013).

C. B. Hirschmann was the main and corresponding author of all four articles.

Other related publications

- S. Ojala, S. Pitkäaho, T. Laitinen, N. Niskala Koivikko, R. Brahmi, J. Gaálová, L. Matejova, A. Kucherov, S. Päivärinta, C. Hirschmann, T. Nevanperä, M. Riihimäki, M. Pirilä, and R. L. Keiski, “Catalysis in VOC Abatement,” Top. Catal. **54**, 1224–1256 (2011).
- J. Lehtinen, C. B. Hirschmann, R. L. Keiski, and T. Kuusela, “Human Hair in the Identification of Cocaine Abuse with Cantilever-Enhanced Photoacoustic Spectroscopy and Principal Component Analysis,” Appl. Spectrosc. **67**, 846–850 (2013).

Contents

List of abbreviations

AD	Analog to digital
AM	Amplitude modulation
arb.	Arbitrary, the unit of the photoacoustic signal in CEPAS
BTX	Benzene, toluene, *p*-, *m*- and *o*-xylene
CEPAS	Cantilever-enhanced photoacoustic spectroscopy
CRDS	Cavity ring down spectroscopy
CS	Cross-selectivity
CW	Continuous wave
DFB	Distributed feedback
DL	Detection limit
DOAS	Differential optical absorption spectroscopy
DSP	Digital signal processing
EC	European Council
ECD	Electron capture detector
EMFi	Electromechanical film
EU	European Union
FFT	Fast Fourier transform
FID	Flame ionization detector
FT-IR	Fourier Transform Infrared
FWHM	Full width at half maximum
GC	Gas chromatography
HITRAN	High-resolution transmission molecular absorption database

InAs	Indium arsenide
InAsSb	Indium arsenide antimonide
IR	Infrared
LIDAR	Light detection and ranging
MS	Mass spectrometry
MSD	Mass selective detector
m-xylene	*meta*-xylene
NDIR	Non-dispersive infrared
NNEA	Normalized noise equivalent absorption coefficient
OPO	Optical parametric oscillator
o-xylene	*ortho*-xylene
PA	Photoacoustic
PAS	Photoacoustic spectroscopy
PID	Photoionization detector
PNNL	Pacific Northwest National Laboratory
ppb	Parts per billion (10^{-9}), refers to volume ratio if stated by the author
ppm	Parts per million (10^{-6}), refers to volume ratio if stated by the author
ppt	Parts per trillion (10^{-12}), refers to volume ratio if stated by the author
p-xylene	*para*-xylene
QCL	Quantum cascade laser
QEPAS	Quartz-enhanced photoacoustic spectroscopy
QTF	Quartz tuning fork
SBC	Science-based calibration
SNR	Signal-to-noise ratio
TDLAS	Tunable diode laser absorption spectroscopy
TLV	Threshold limit value
VOC	Volatile organic compound
WM	Wavelength modulation

1. Introduction

1.1 Background

The measurement of gases has become an important need in our modern life. Besides others, volatile organic compounds (VOCs) are a group of molecules that are of particular interest. The major issue with VOCs is their potential adverse effects on human health and nature [1–5]. They can deplete the stratospheric ozone layer [2,6–8], have acute and systematic toxic effects on human organs [1,3–5,9,10] and can even be carcinogenic [11], just to mention a few. Anthropogenic VOC emissions arise mainly from the usage and processing of organic material [2,12]. Therefore, many states have adopted legislation to limit VOC emissions from industry [3,13], their occurrence in the air and their presence in products, e.g., in fuel [14,15]. Still, VOCs are present in our everyday life. They outgas, for example, from commodities inside buildings or are emitted from industries and combustion processes into the atmosphere [2,4,12,16]. The motivation to measure VOCs is versatile and includes:

- process control in industry and other quality assessment applications such as ripening of fruits [17,18]
- industrial emissions and air pollution measurement, environmental and atmospheric monitoring and climate research [19–21]
- health and well-being related applications as workplace security and medical diagnostics, such as in breath gas analysis or cancer detection [22–26]
- detection of explosives and chemical warfare agents in defense and security applications [27,28], and
- many other applications [17,18,21,29,30].

The most commonly applied VOCs measurement techniques are chromatography, mass spectrometry, optical spectroscopy, electrochemical and other sensors [31–33]. Each technique has its own strengths, weaknesses and thus limited applicability as discussed later on in Chapter 2.5. To date, many unresolved VOC measurement problems and applications where the measurement performance can be improved still exist, such as in the monitoring of industrial emissions [3]. Photoa-

coustic spectroscopy (PAS) is a promising measurement technique in the analysis of VOCs, because it is sensitive and non-destructive, requires only small sample volume, offers linear response of the signal, a large dynamic range and can be combined with different light sources [19,30,34–36]. The sensitivity of PAS can be further improved by selecting the novel and recently developed cantilever microphone [37–40]. Since cantilever-enhanced photoacoustic spectroscopy (CEPAS) is an up-and-coming technology, many application fields are still undiscovered, including the measurement of VOCs. Therefore, the scope of this thesis is to develop CEPAS setups for the measurement of VOCs and apply them in different demanding VOC measurement applications, where other methods do not exist or have proven to be laborious.

1.2 Objectives and outline of the thesis

Analytical measurement instruments are typically application-specific, i.e., they are built according to the requirements of a specific measurement problem. It is also the case in VOC measurement, where possible applications are versatile as pointed out in Chapter 1.1 and one single instrument cannot satisfy all the potential measurement applications. Usually, the most important requirements are set by the need for single- or multi-compound analysis, the measurable analyte concentration range, which can vary for VOCs from percent in process industry to ppt in breath gas analysis, the measurement time, the tolerable cross-selectivity and the instrument properties of size, weight, supplies and resistance against possibly corrosive samples [19,31,41]. Therefore, the objective of this thesis is to develop CEPAS measurement systems for VOC measurement applications with different requirements. Figure 1 gives an overview of the content of this thesis: the used techniques, the measured analytes, and the objectives and novelty of each CEPAS measurement system. The built CEPAS measurement systems are tested in the laboratory by measuring the VOCs of the selected application and based on that, the performance of the systems is characterized. The performance is mainly characterized by the figures of merit selectivity, sensitivity and multi-compound ability.

Articles I and II describe Fourier transform infrared (FT-IR) CEPAS setups for the multi-compound measurement of various VOCs. The setup in Article I is robust and can be used for industrial measurements. Article II presents an FT-IR-CEPAS setup for the measurement of hot gases, for which the PA cell and the cantilever as the pressure transducer operate at 180 ºC. In Article III, CEPAS is combined with a quantum cascade laser (QCL) and is applied to the trace gas detection of formaldehyde. In Article IV, high sensitivity is achieved along multi-compound analysis in the measurement of benzene, toluene, *p*-, *m*- and *o*-xylene (BTX) by means of an optical parametric oscillator (OPO).

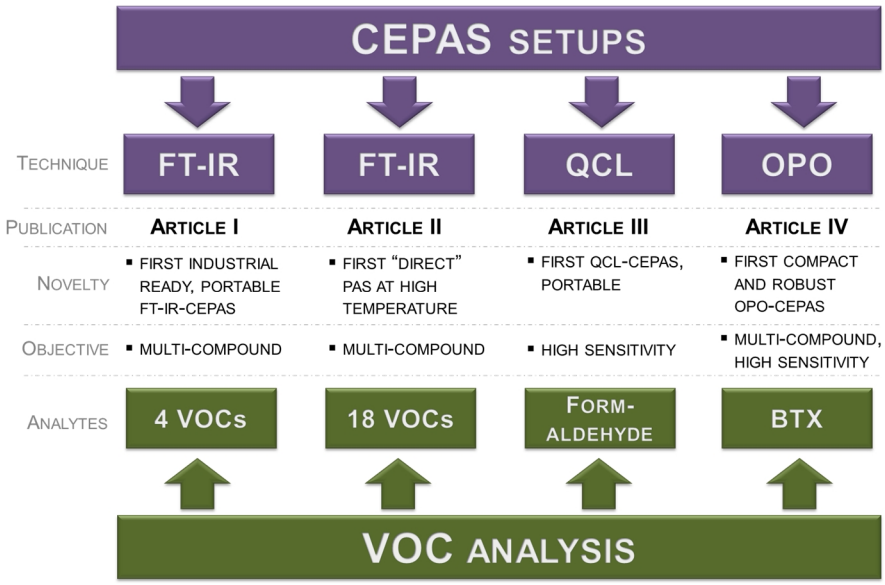

Figure 1. Overview of the thesis content.

2. Volatile organic compounds (VOCs)

2.1 Background and definitions

Organic molecules with a high vapor pressure at room temperature rapidly evaporate into the gas phase, for example, the ambient air, and are accordingly classified as volatile organic compounds (VOCs). No common conformance of the term VOC exists, as the definitions differ depending on the technical area and the country [3]. The United States Environmental Protection Agency defines VOC as “any compound of carbon, excluding carbon monoxide, carbon dioxide, carbonic acid, metallic carbides or carbonates, and ammonium carbonate, which participates in atmospheric photochemical reactions” [42]. In the European Council (EC) Directive 1999/13/EC (as known as the Solvent Emissions Directive), “VOC shall mean any organic compound having at 293.15 K a vapor pressure of 0.01 kPa or more…” [43]. The European Union (EU) Directive 2004/42/CE (as known as the Paint Directive) states “VOC means any organic compound having an initial boiling point less than or equal to 250 °C measured at a standard pressure of 101.3 kPa” [44]. Directive 2001/81/EC (also known as the National Emission Ceilings Directive) gives an even looser definition: “VOC mean all organic compounds arising from human activities, other than methane, which are capable of producing photochemical oxidants by reactions with nitrogen oxides in the presence of sunlight” [45].

From the chemical point of view, VOCs include a sheer limitless number of compounds from classes such as aliphatics, aromatics, alcohols, aldehydes, acids, amines, ketones, esters and ethers as well as halogenated and sulfurated hydrocarbons. Some commonly used VOCs are acetaldehyde, acetone, benzene, carbon tetrachloride, ethyl acetate, ethylene glycol, formaldehyde, heptane, hexane, isopropyl alcohol, methyl ethyl ketone, methyl chloride, monomethyl ether, naphthalene, styrene, toluene, and xylene [6,46].

2.2 Sources of VOC emissions

VOCs are emitted from natural as well as man-made, so-called anthropogenic sources. Vegetation, volcanoes, and natural forest fires produce most of the natural VOC emissions. Vegetation emissions come from plants, trees, wild animals,

and bacteria [2,9,47,48]. As an example, the Stone Pine (*Pinus pinea*) tree emits 0.1–0.9 µg g(LDW: leaf dry weight)$^{-1}$ h^{-1} of formaldehyde, 0.2–0.5 µg g(LDW)$^{-1}$ h^{-1} of formic acid and 0.1–0.3 µg g(LDW)$^{-1}$ h^{-1} of acetic acid [49].

Anthropogenic VOC emissions have numerous sources which primarily arise from the usage of organic material. Oil refining, storage and supply of fossil fuels, usage of organic solvents and solvent-containing products, combustion processes, industrial production processes and biological processes are the main anthropogenic sources of VOC emissions. The most important industrial production processes considered for VOC emissions include the production of food and beverages, wood processing as chipboard manufacturing, and the production of fine- and organic chemicals including solvent-containing and polymer products. Solvent-containing products include paints, printing inks, degreasers, cleaners, and lubricants. Examples of biological processes are the digestive processes of animals, agriculture, and disposal of organic wastes as landfills and manure. Combustion processes include power plants, vehicle engines, and home furnaces. [2,9,12,16,46,47]

This means that VOCs are not only emitted from industrial sites. VOC emissions also occur in urban areas and indoors. In urban areas the origin is mainly transportation; indoors the use of solvent-containing products including wood-based building materials, furnishings, personal care products, tobacco smoke, paints, and lacquers. In indoor air in particular, VOCs are the prevalent compounds causing air pollution. [1,3–5,50] Furthermore, the concentrations of many indoor pollutants are often higher than those typically encountered outside [4].

2.3 Effects of VOC emissions

VOC emissions can harm the atmosphere, nature, and human beings. Their individual effects are, however, diverse, because VOCs are a rather manifold group of molecules. The lifetime of VOCs in the troposphere ranges from minutes to months [6,8]. VOCs with a long tropospheric lifetime, for example, hydro- and chlorofluorocarbons, are able to pass through the troposphere and enter the stratosphere (the troposphere extends from the earth's surface to 9 km at the poles and 17 km at the equator; following the troposphere, the stratosphere extends to approx. 50 km from the earth's surface). After photodecomposition, chlorine and bromine can react with ozone as well as with ozone precursors, both leading to a depletion of the ozone layer [2,6–8]. The depletion of stratospheric ozone results in a higher UV radiation intensity in the troposphere, because ozone absorbs ultraviolet radiation below 290 nm. Higher UV light intensity has potential effects on humans, flora, and fauna. [8]

VOCs are mainly responsible for ground level ozone. In the troposphere, VOCs undergo photochemical reactions with nitrogen oxides forming ozone. Ozone near the ground harms human health, has effects on animals, crops, plants, and trees and is the primary compound of smog. [2,4,6,7,46,47,51] Further, tropospheric ozone is greenhouse active and moreover some VOCs can absorb solar or terres-

trial infrared (IR) radiation in the stratosphere, contributing to the enhanced greenhouse effect [2,6]. Some organic molecules with higher molecular masses are persistent to environmental oxidation and removal processes. Persistent compounds accumulate in nature and may possibly be brought to humans via the food chain [2].

The effects of VOCs on the human body are complex and range from odor sensation and irritation, over systematic toxicity to carcinogenicity [1,2]. The concentration and the VOC a person is exposed to as well as the temporal length of the exposure mostly influence the measure of the health effect [1,5,10]. Irritation of eyes, nose, throat and skin as well as secondary effects of irritation and odor sensation, such as headache, dizziness, and vomiting, have been reported. Systematic toxic effects damage the lungs, liver, kidneys, the mucous membrane and the central nervous system. [1,3–5,9,10] Carcinogenicity effects become visible a long time after exposure. For example, benzene, formaldehyde, trichloroethylene and vinyl chloride are classified by the International Agency for Research of Cancer as group 1, meaning they are carcinogenic to humans [11]. Many other VOCs, such as polycyclic aromatic hydrocarbons, polychlorinated biphenyls, dioxins, and furans are classified as group 2A “probably carcinogenic to humans” and group 2B “possibly carcinogenic to humans” [11].

Sick building syndrome is used to describe a sickness with non-specific symptoms that occurs after time spent in certain buildings, for example office buildings during work or the home. Reported symptoms include headache and vomiting, nasal and chest congestion, eye and throat problems, fatigue, muscle pain, neurological symptoms, dizziness, and dry skin. The real cause of sick building syndrome is not yet known, but indoor air pollution by VOCs is very likely to be an agent. [4]

2.4 Legislation

In the past, the EU released several directives regulating the use and emissions of VOCs for environmental and human health reasons. This chapter discusses only the current legislation in the EU. An overview of present and previous legislation in the EU as well as other countries worldwide is given in [3].

Directive 2010/75/EC (also known as the Industrial Emissions Directive) is the current applicable EU legislation for VOCs emissions. It directs users to replace VOCs classified as carcinogens, mutagens, or toxic to reproduction and assigned to carry the hazard statements H340, H350, H350i, H360D or H360F “as far as possible, by less harmful substances or mixtures within the shortest possible time” [13]. If not replaced, these compounds and halogenated VOCs assigned to carry the hazard statements H341 or H351 “shall be controlled under contained conditions, as far as technically and economically feasible, to safeguard public health and the environment and shall not exceed the relevant emission limit” [13]. For emissions of the VOCs assigned to carry the hazard statements H340, H350, H350i, H360D or H360F, where the mass flow of the sum of the compounds causing

the hazard statements is ≥10 g h^{-1}, "an emission limit value of 2 mg Nm^{-3} shall be complied with. The emission limit value refers to the mass sum of the individual compounds" [13]. For emissions of halogenated VOC assigned to carry the hazard statements H341 or H351, with a "mass flow of the sum of the compounds causing the hazard statements … is ≥100 g h^{-1}, an emission limit value of 20 mg Nm^{-3} shall be complied with" [13]. Nm^3 stands for norm cubic meter and refers to a temperature of 273.15 K and a pressure of 101.3 kPa. Formaldehyde, for example, carries the hazard statements H350 (may cause cancer) and thus its emission limit is 2 mg Nm^{-3}, i.e., ~1.5 ppm. Benzene also carries the hazard statements H350 in addition to H340 (may cause genetic defects) and its corresponding emission limit is ~0.6 ppm.

In addition to industrial emissions, the EU has also proposed limit values for the presence of VOC in urban areas. In the case of benzene, the annual average occurrence in urban areas should not exceed 5 µg m^{-3} i.e., ~1.5 ppb [52].

The threshold limit value (TLV) is the maximal concentration of a substance that workers can be exposed to without adverse health effects. For example, the TLV (8h exposure) for benzene is 0.5 ppm and for formaldehyde 0.2 ppm [53].

2.5 Measurement of VOCs

2.5.1 Requirements for the measurement system

The measurement of VOCs is required in many applications like industrial emission and process measurements, environmental monitoring and urban and indoor air analysis as pointed out in Chapters 1.1 and 2.4. According to Sigrist [19,31,41], the ideal measurement system for trace gas monitoring possesses all the important technical performance features, such as:

1. multi-compound ability, i.e., it measures several analytes with a single instrument;
2. high sensitivity, i.e., it detects the analytes in trace concentrations of ppb (10^{-9}) and even ppt (10^{-12});
3. high selectivity, i.e., it discriminates the analytes at no or sufficiently low cross-selectivity;
4. large dynamic range, i.e., it is able to detect ppt level concentrations in environmental monitoring, for example, and percent level concentrations in process measurement, for example;
5. reasonable temporal resolution, i.e., it enables online measurement;
6. reasonable portability, i.e., to shift the measurement system to another location, and
7. automatic operation, i.e., it conducts all necessary actions autonomously, for example, sampling or data handling.

In practice, the requirements of the performance features are set by the measurement application. In other words, the application directs the required performance features and the measurement system will be designed according to these. Depending on the particular application, the emphasis on the individual performance features varies. In some applications it is sufficient to measure the total VOC content and therefore the selectivity is less important [19]. Another example is in the industrial process measurement that requires detection at ppm level and thus, high sensitivity is not a major concern. One final example is the monitoring of environmental pollutants, where the temporal resolution is of low importance.

Suitable techniques for the analysis of VOCs are wide-ranging and can be divided into spectroscopic and non-spectroscopic analytical techniques [41]. Due to the numerous measurement techniques and the wide field of possible applications, the objective here is not to give a comprehensive in-depth literature survey of all possible techniques, but rather to point out the techniques most frequently applied in the analysis of VOCs.

2.5.2 Non-spectroscopic techniques

Gas chromatography (GC) is the measurement technique most widely applied in the analysis of VOCs in air due to its capability to separate individual VOCs [32,33]. Different detectors can be attached to the GC, and the most frequently used ones are the flame ionization detector (FID), the electron capture detector (ECD), and the mass selective detector (MSD) [32,33,54]. Usually, GC measurement systems reach very good selectivity and sensitivity [33]. The common disadvantages of GC systems are the expensive supply materials, i.e., gases, the complex sampling and sample preparation and the analysis time [32] as well as the need for a highly qualified operator [33]. Miniaturized GCs, known as micro GC or µGC, offer shorter measurement time than traditional GCs and consume less supply materials [33,55].

Mass spectrometry (MS), flame ionization (FID) and photoionization detectors (PID) have also been used in a self-contained manner in the analysis of VOCs [19]. FID and PID are non-selective detectors used to measure the sum of the compounds that respond to the detector [48,56]. They are usually robust and used for monitoring the total organic carbon in industry, for example [57]. Direct-injection mass spectroscopic techniques offer good time and mass resolution, are sensitive and have been applied to rapid monitoring and quantification of VOCs. The main techniques are MS-e-noses, atmospheric-pressure chemical ionization, proton-transfer reaction mass spectrometry and selected ion-flow-tube mass spectrometry. [58] However, these systems are usually labor-intensive and expensive [32].

Metal oxide semiconductor sensors, quartz microbalances, surface acoustic wave and other sensors, relying on electrochemistry, calorimetry, conductivity and other phenomena, may be made in silicone and are usually inexpensive and small in size [32]. However, they mainly respond to a certain compound or to a class of

compounds. Most of these sensors can be considered non-selective, some tend to drift and some have limited lifetimes [35]. To offer better selectivity, multiple sensors can be arranged in a so-called sensor array. [32] In addition, combinations of electrochemical sensors with PID and ion mobility spectrometry have been demonstrated [59].

2.5.3 Spectroscopic techniques

In general, spectroscopic measurement techniques offer fast response times, minimal drift and a high selectivity, if configured correctly [35]. The measurement is non-destructive, and can be carried out in real time as well as in-situ, which is important for process measurements [35]. Certain spectroscopic techniques can be used for remote sensing of VOCs in the atmosphere because they do not require a sample cell and the measurement can be carried out from the open path [32,60]. General disadvantages of spectroscopic techniques are their costs. Compared to silicone sensors, spectroscopic measurement systems are considerably more expensive. [35] To show significant absorption in the mid-infrared, the dipole moment of the molecule needs to change during the vibration [61]. VOCs typically have dipole moments, since they consist of carbon atoms combined with other atoms such as hydrogen, oxygen, chlorine, etc. However, the change in dipole may be small for some compounds and thus their absorption coefficients are small, which makes their detection challenging. VOC samples typically contain several compounds that may also absorb infrared radiation. In that case, their spectra can overlap, i.e., interfere with the spectrum of the compound of interest. Resolving interferences is usually challenging and increases the complexity of the measurement system. [17,35,41] By increasing the size of the molecules, the absorption bands become broader as shown in Chapter 7. As a consequence, achieving selectivity is more challenging and results as well in more complex measurement systems that offer, for instance, a wider spectral coverage. [35]

The most frequently used spectroscopic technologies in the analysis of VOCs are: Differential optical absorption spectroscopy (DOAS), non-dispersive infrared (NDIR) sensors, tunable diode laser absorption spectroscopy (TDLAS), Fourier transform infrared (FT-IR) spectroscopy, light detection and ranging (LIDAR), cavity-enhanced techniques such as cavity ring down spectroscopy (CRDS) and photoacoustic spectroscopy [19,35,60].

DOAS is mainly used to monitor VOCs in the atmosphere and the optical path length can range from meters to 1000 km. In DOAS, the light intensity emitted by the source (I_0) is not measured, but is instead estimated from the measured spectrum, which involves very complex data analysis. [60,62]

NDIRs are used for VOC measurement applications in the environment and industry, mainly to measure the total organic carbon [35]. Broadband, non-dispersive gas measurement systems consist of only a few parts and can be built cheaply and in a compact way. An NDIR sensor for carbon dioxide detection is of great commercial interest and a mass market application because chemical car-

bon dioxide sensors tend to drift and have a rather short lifetime. [35] Different setups of NDIR sensors exist, but the main principle of these sensors is to measure the absorption of the analyte via optical filters. Depending on the sample mixture and the selected filters, other compounds may interfere and affect the analyte reading. [35]

TDLAS became field-usable during the last two to three decades [60], and since then it was applied for industrial and environmental VOC measurement. In TDLAS a laser with a narrow bandwidth is tuned over the absorption band of the analyte and the transmitted light is recorded. The sensitivity of the measurement can be enhanced by using multi-reflection gas cells, such as the White or Herriott cell or wavelength modulating the laser, for example [21]. TDLAS can be highly selective if a spectral band without interference can be found. [35]

FT-IRs have been applied in environmental and industrial measurements of VOCs [32,35]. In FT-IR spectroscopy, an interferometer modulates mid-IR light emitted by a broadband light source. After passing the sample, the detector records the transmitted light as an interferogram. Fourier transformation of the interferogram gives the spectrum of the sample. [61] As in TDLAS, different multi-reflection gas cells with varying path lengths can be applied, and open path FT-IRs are also used [63]. FT-IRs offer high selectivity, because they record the whole mid-IR spectrum. Hence, they are used in multi-compound analysis, i.e., when the spectra of the individual compounds interfere [35]. Data analysis and chemometric means help to resolve the interference.

LIDAR can be used for remote sensing of VOCs in the atmosphere from distances of up to several kilometers [32]. LIDAR is a technique related to RADAR (radio detection and ranging), but instead of radio waves, laser light is used. The laser light pulses are sent into the atmosphere and the temporal evolution and the intensity of the backscattered light is measured. By applying different lasers or laser tuning, analyte specific information is received. Lasers ranging from 250 nm to 11 µm have been used in LIDARs. [64]

Cavity-enhanced techniques such as CRDS are nowadays mature technologies and have been used in process and environmental measurement applications, for example [65]. Cavity-enhanced techniques measure the decay time of a light pulse in a stable resonator. The decay time is dependent on mirror losses, scattering and the absorption of the gas. If the decay time of the cavity is determined with a non-absorbing gas beforehand, the difference in decay time is proportional to the concentration of the analyte [35,60,65,66]. Typical optical path lengths in CRDS are 1 to 10 km [21].

PAS will be described later in more detail. It has been used in VOC analysis [32,34,67,68] and trace gas analysis [17], particularly with laser sources [41,69] and also in mobile setups as in [70]. Schmid [18] gives examples of photoacoustic VOC measurement in process analytical chemistry.

2.5.4 Sampling

Depending on the application and the applied measurement technique, different sampling techniques are available. In process analytics, Kessler classified the sampling into off-, at-, on- and inline, according to the distance from the analyzer to the process [71]. In offline sampling, the drawn sample is transported to the analyzer, i.e., to the next laboratory. In atline, the sampling is manual or semi-automated and the analyzer is close to where the sample was taken. Online sampling usually involves a bypass, from where the measurement is carried out. The bypass feed is then returned to the reactor. Inline, or in other words *in-situ*, sampling means the measurement is carried out directly in the process and is usually done via a probe. [71] On- and inline are often used as synonyms in the literature, particularly in application fields such as environmental air sampling.

Off- and atline gas sampling techniques used in the VOC analysis include canister and bag sampling, cryogenic, passive and diffusive sampling as well as sampling on sorbents [32,33,54]. In on-/inline sampling, the sample gas is usually inserted directly into the measurement system. Filtering, extraction or preconcentration are commonly used steps in the preparation of the sample [32,33].

Although the sampling chapter is kept rather short here, correct sampling is a key factor in the analysis procedure. Without correct sampling, the analysis carried out will give incorrect readings. According to Kessler, more than 80% of the malfunctions in process analysis is due to wrong sampling [71].

3. Photoacoustic spectroscopy (PAS)

3.1 Background and principle

Molecules can absorb radiation in the mid-infrared if the energy of the radiation matches the energy required for a transition between two quantized vibrational or rotational energy states. If so, the radiation, i.e., the photon becomes absorbed and the molecule is promoted to the higher vibrational or rotational energy state. In the commonly used transmission spectroscopy, the part of the light transmitted through the sample $I(v)$ is measured by the detector. Still, the amount of photons reaching the detector without the sample $I_0(v)$ is required in order to calculate the absorbance $A(v)$ [-] of the sample, according to

$$A(v) = -\ln\left(\frac{I(v)}{I_0(v)}\right) = -\ln(T(v)) = r(v)dl \qquad (1)$$

where T is transmission through the sample [-], $r(v)$ is the absorption cross section of the molecule [cm^2 molecule^{-1}], d the density of the absorber [molecules cm^{-3}], l the absorption path length [cm], v the wavenumber of the radiation [cm^{-1}] and $\lambda = v^{-1}$ the wavelength [cm]. For gases $r(v)\ d = \alpha(v)\ p$ is true, where $\alpha(v)$ is the absorption coefficient [atm^{-1} cm^{-1}] and p the partial pressure of the gas [atm].

This means that in transmission spectroscopy, two measurements are needed to determine the absorption spectrum of the sample: the sample spectrum $I(v)$ and the $I_0(v)$, which is usually known as the background spectrum. Transmission spectrometers, such as FT-IRs, are mostly built as single beam devices, and thus the measurement of $I(v)$ and $I_0(v)$ are carried out at different times. This gives rise to baseline errors, occurring from a change in the temperature of the light source or in the optical alignment due to temperature instabilities, for example [72]. Another drawback of transmission spectroscopy is the fact that in the case of small absorption, as is typical in trace gas detection, the small absorption signal is superimposed on a huge background signal [34] as illustrated in Figure 2. As a result, even a small change in the huge background signal can shroud the small absorption signal of the sample. To minimize this problem and to increase the absorption, long optical path lengths have been realized in so-called multi-pass cells. Howev-

er, multi-pass cells have two major drawbacks. Firstly, the cell volume, physical sizes, complexity and price increase [73] and secondly, the measured signal becomes non-linear. Because the signal of matrix gases such as water is also non-linear and in addition dependent on the temperature and pressure, the calibration becomes complicated and expensive. [73,74] The photoacoustic technique measures the absorption directly, without the huge background signal and can thus overcome the drawbacks of the transmission method explained above.

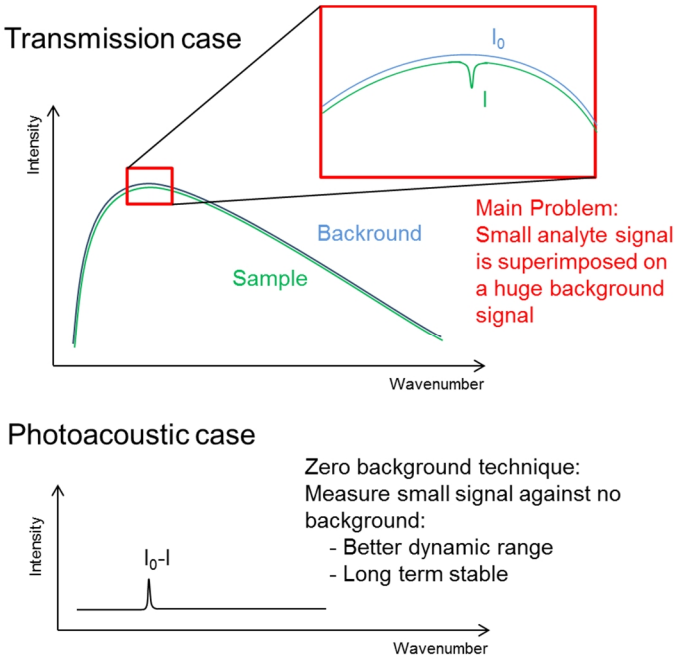

Figure 2. Graphical illustration of the indirect transmission and direct photoacoustic measurement.

A schematic of the photoacoustic effect is shown in Figure 3. If a molecule absorbs infrared radiation it is excited from the ground state to an energetically higher, vibrational or rotational quantum state. However, the molecule is not stable in the excited state and wants to dissipate the energy. The molecule can, in principle, decay through two different pathways: either through radiative or non-radiative energy transfer. In the radiative pathway, a photon is emitted with a longer wavelength than the excitation photon. The non-radiative decay will happen, if the relaxation can compete with the radiative lifetime of the excited energy levels. The lifetime of the radiative decay varies from 10^{-7} s at visible wavelengths to 10^{-2} s at 10 µm. The non-radiative decay time varies from 10^{-3} to 10^{-8} s, depending on the pressure, since the decay time is inversely proportional to the pressure. [17] In the non-radiative decay, the energy is converted to translational energy. This increas-

es the temperature and that in turn increases the pressure of the gas, located in a closed cell. If the irradiated light is periodically modulated, the pressure variation also occurs periodically and thus forms an acoustic wave with the same frequency at which the irradiated light was modulated. The acoustic wave can be detected by a microphone. [17,34,56,75–77]

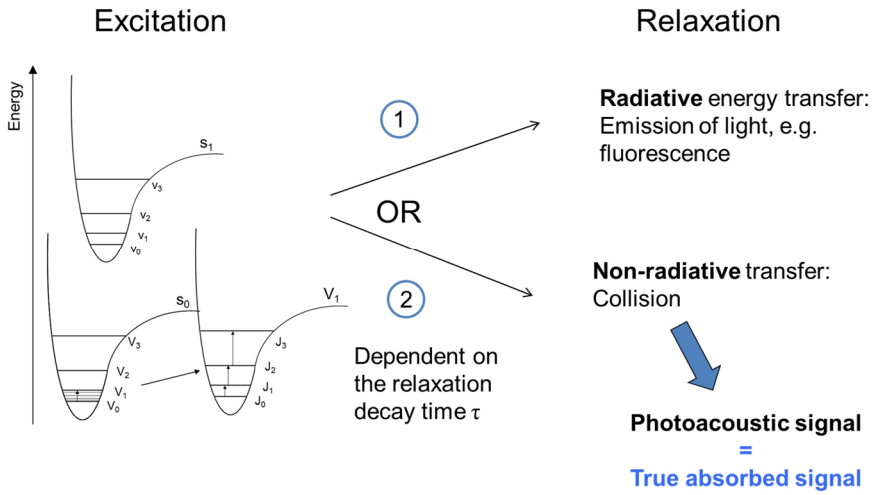

Figure 3. Decay pathways of an exited molecule. *V* are the vibrational, *s* the electronical, and *J* the rotational energy states.

As a result, photoacoustic spectroscopy directly measures the absorbed intensity $I_0(v)$-$I(v)$ as illustrated in Figure 2. The absorbed intensity is proportional to the amplitude of the acoustic wave and the amount of the light absorbing molecules. [34,37,72] The PA signal is formed according to

$$S(v) = P(v)\, M\, (K\, \eta\, r(v)\, d + B) \qquad (2)$$

where $S(v)$ is the generated photoacoustic signal, $P(v)$ the exciting light power, M the sensitivity of the microphone, K the cell constant, η the efficiency of the conversion of absorbed light energy into heat and B is the background signal generation efficiency. Equation (2) is only true for small absorptions, in the absence of absorption saturation and when the relaxation times are shorter than the modulation times.

In addition, PAS is background free, which means that if no light is absorbed, no signal is produced [17,21,34]. And so, Bozóki et al. [34] concluded that photoacoustics have the potential to be more accurate and sensitive than traditional spectroscopic techniques as the transmission spectroscopy.

3.2 History of PAS

The photoacoustic effect was reported for the first time by Bell in 1880 [78], after he found disks emitting sound under exposure of modulated sunlight. In a later experiment [79], he replaced the eye piece of a commercial spectroscope with a hearing tube and observed audible sounds of the sample. Bell's initial works arose interest in the scientific community and researchers such as Röntgen [80], Tyndall [81], and Preece [82] contributed to the early research in photoacoustic spectroscopy. However, interest soon faded due to the lack of a quantitative description of the photoacoustic effect, sensitive microphones and intense light sources [17,67]. The second milestone in the evolution of PAS was a groundbreaking article published in 1968 by Kerr and Atwood on the photoacoustic detection of infrared absorption in gases [67]. Kerr and Atwood [83] used a CO_2 laser in a set up they called the "absorptivity spectrophone" and achieved high sensitivity in the detection of CO_2. The last milestone, indicating the start of modern photoacoustics, was in 1981, according to Michaelian [67]. At that time the photoacoustic technique reached maturity and acceptance among the vibrational spectroscopic community.

Since then, numerous pieces of research on PAS were carried out. It has been applied in many fields of analysis, on solids, liquids, and gaseous samples [67]. Different instrumental techniques and setups have been developed [67] and PAS has been applied in a wide wavelength range, reaching from UV to IR [84]. Nowadays, PAS is a routine technique in many measurement applications [34].

3.3 Sensitivity enhancement techniques

In the past, great efforts were made to enhance the inverse analytical sensitivity of the photoacoustic technique. Advances have been made, particularly in optimizing the light source and increasing its power, optimizing the photoacoustic gas cell and operating the cell in resonance as well as introducing improved detectors such as quartz- or cantilever-enhanced detectors. Resonance operation of the cell and novel microphones will be discussed hereafter, because these are relevant for the present work.

Photoacoustic sample cells can be operated in resonant and non-resonant mode. In the non-resonant mode, the modulation frequency of the irradiated light is clearly lower than the lowest acoustical resonance frequency of the cell. The wavelength of the created sound wave is larger than the cell dimensions, so the sound cannot propagate and no standing waves can be formed. In the non-resonant operation, the average pressure in the cavity oscillates with the modulation frequency [34,73]. For the resonant operation, the irradiated light is modulated at a resonance frequency of the photoacoustic cell. This leads to an amplification of the photoacoustic signal by the quality factor (Q-factor) of the cell [17,34,73,77]. Depending on the photoacoustic cell geometry, Q-factors from <10 to several hundreds can be achieved [34]. In quartz-enhanced PAS, Q-factors of $>10^4$ are

typical [30,85,86]. Resonance enhancement in PAS has been extensively used in the past [17,35]. However, commitment to the resonance has considerable disadvantages. First, the background noise is usually amplified by an equally large amount as the photoacoustic signal is amplified [35]. Second, the system design is more complex, because the resonance frequency needs to be exactly adjusted and maintained. If the modulation frequency drifts marginally apart from the resonance frequency, a loss in amplification results in a strongly reduced PA signal [30]. For example, cells with a high Q-factor of >500 require active temperature stabilization to maintain the resonance. Without that, temperature induced variation of the sound velocity cause drifts in the resonance frequency [35]. Miklos et al. [77] reported that the product Q ΔT needs to be kept at ≤56 for a PA signal stability of ±1%. And third, the usage of broadly tunable light sources is difficult to realize with photoacoustic setups working in resonance mode due to the wide frequency response required for tuning.

The most frequently used conventional detectors applied in PAS are the condenser and electret microphones. The condenser, also known as the capacitor microphone, measures the change in capacity that is generated when one side of the capacitor, i.e., the sensitive membrane, stretches. The electret microphone is similar to the condenser, but without the need for a polarizing power supply, because the electret is a permanently charged material. [30,68,73,87] However, capacitive microphones have a fundamental performance limitation, which will be discussed in the next chapter. To overcome these limitations, novel detectors for gas phase PAS have been developed [35,37–39,88,89].

In 2002, Kosterev and Tittel [90] introduced quartz-enhanced photoacoustic spectroscopy (QEPAS). The key element of QEPAS is the quartz tuning fork (QTF). QTFs are mass-produced and used in watches and clocks as the timing element with the resonance frequency of ~32 kHz. The idea of QEPAS is not to accumulate the absorbed energy in the gas but in the sensor element, the QTF [86,90,91]. For photoacoustic operation, the excitation light beam is guided through the gap between the QTF prongs, filled with sample gas. The generated acoustic wave lets two prongs bend in opposite direction. This bend is piezoelectrically active, resulting in an electric signal. The read-out electrical signal is proportional to the concentration of the excited gas molecules. Piezoelectric crystal quartz is well suited as detector material due to its high Q-factor and Q-factors of $>10^4$ are typical in QEPAS. Even though QEPAS has optical path lengths of only a few millimeters, it has shown to be very sensitive. [86,90,91] Reported normalized noise equivalent absorption coefficients (NNEA, 1σ) for QEPAS are (all in W $(cm)^{-1}$ $(Hz)^{-1/2}$) 1.0 x 10^{-8} for CO_2, 5.3 x 10^{-7} for CO, 2.2 x 10^{-8} for formaldehyde [91], 2.7 x 10^{-10} for SF_6 [92] and 4.1 x 10^{-9} for acetylene [93]. The main advantage of QEPAS is its immunity to acoustic noise. Sound waves originating from acoustical noise are generated outside and not in between the prongs. An outside generated sound wave let the prongs move in the same direction and does not generate a signal. Due to its immunity to acoustical noise, it is a suitable technology for portable gas sensors for field and industrial applications. [94] The signal generation model of QEPAS is reported in [95] and its optimization in [93].

Until now, QEPAS has been applied in many trace gas measurement applications with various laser light sources as near-IR distributed feedback (DFB) diode lasers, QCLs and OPOs [35,67,92,96–99]. Even an optical read-out of the prong's bending has been realized [100]. The drawbacks of QEPAS are the restriction in light sources due to the high resonance frequency of the QTF and the very accurate control of the modulation frequency. A minor drift in the modulation frequency leads to an enormous loss in the photoacoustic signal because of the very narrow resonance peak and the high Q-factor [73]. Although QEPAS is a promising technology, it has not yet achieved its commercial breakthrough and only a few field and industrial measurement applications have been reported.

Recently, an electromechanical film (EMFi) has been used as a pressure transducer in PAS. The EMFi is a cellular polypropylene film with an internal charge and a thickness of approx. 70 µm. Metal electrodes are attached on each side of the film. A sound wave striking the film leads to opposite charges on the two electrodes, which can be read-out as an electric signal. The EMFi is easily formable, inexpensive and several layers of the film can be stacked together, increasing the sensitivity. [101,102] Saarela et al. [102] achieved a detection limit of 22 ppb and a NNEA (1σ) of 3.2 x 10^{-9} W $(cm)^{-1}$ $(Hz)^{-1/2}$ for NO_2 with a five-layer EMFi in a multipass PA cell. Apart from these good results, EMFi has not yet reached wider application in PAS.

Another novel detection technique in PAS is cantilever-enhanced photoacoustic spectroscopy. Cantilever-enhanced photoacoustic spectroscopy will be discussed in the next chapter.

3.4 Cantilever-enhanced photoacoustic spectroscopy (CEPAS)

In 2003, the group of J. Kauppinen initially reported a novel microphone for PAS based on a silicon cantilever [38]. Earlier, FT-IR-PAS was known to be less sensitive than the FT-IR transmission technique. This is because in FT-IR instruments, the spectral elements are modulated at a wide range of audio frequencies and thus the PA cell needs to be operated in non-resonant mode to enable a wide frequency response of the detector [38]. To improve the sensitivity of the FT-IR-PAS gas measurement, Kauppinen identified the microphone as the performance limiting part and therefore, their investigations was focused on developing a new pressure sensor that overcomes the limitations of the traditional capacitive microphones. The capacity C of a condenser microphone is given as

$$C = \frac{\varepsilon E}{h} \tag{3}$$

where E is the area of the electrodes, ε the dielectric constant of the gas between the electrodes, and h the distance between the electrodes. A pressure difference Δp is proportional to a difference in capacity ΔC via Δh according to

$$\Delta p \propto \Delta C = \frac{-\varepsilon E}{3h^2} \Delta h \, (\Delta h \ll h). \quad (4)$$

By increasing the electrode area *E* while decreasing the distance *h*, Kauppinen et al. [37] achieved a sensitivity typical for the best commercial capacitive microphones. However, a further increase in *E* and a decrease in *h* did not improve the sensitivity anymore, i.e., they reached the physical limitation of the capacitive microphones. In an experiment described in [37], they were able to show that the so-called “damping effect” is the limiting factor of capacitive microphones. The air flow between the rigid electrode and the flexible membrane being deformed requires energy and therefore induces damping of the membrane. More flexible membrane material increases the amplitude but also the damping effect and offers only a very limited dynamic range. [37,73]

The “damping effect” can be resolved if the rigid electrode is left out and the sensitivity is improved by using optical methods for the read-out of the membrane stretch. Appropriate optical read-out methods are optical beam deflection or interferometry. Still, the membrane has its own mechanical limitations, such as the non-linear pressure response due to the radial stretch and the temperature dependent response. To resolve the membrane related issues, Kauppinen et al. replaced the membrane with a cantilever. The cantilever was made out of silicone and was 5 µm thick, 4 mm long and 2 mm wide. The fabrication of the cantilever is described in [103,104]. Under pressure, the cantilever bends and does not stretch as the membrane does. Thus, the movement of the free end of the cantilever can be about two orders of magnitude greater than the movement of the membrane center under the same pressure variation. Furthermore, the dynamic range of the cantilever is larger than the one of the membrane. The movement of the cantilever can be read-out by optical beam deflection or interferometry. Kauppinen and his group selected the interferometric read-out because it offers a larger dynamic range. [37,73]

In practice, the cantilever frame is mounted in the PA cell and the read-out light beam is guided through an additional window in the cell wall. The read-out interferometer consists of a small He-Ne laser, a Michelson type interferometer, the cantilever and a detector. In the beginning photodiodes were used, but nowadays a linear sensor array reads the interference fringes. When the cantilever bends, the interference fringes move spatially on the detector. The signal is read-out and processed with analog preamplifiers and a digital signal processor. [37,72,105]

Although the original idea was to improve FT-IR-PAS, the novel cantilever microphone was quickly applied in many other setups. Setups with FT-IRs have been demonstrated in [40,72–74,106], with a broadband IR light source in [40,107,108], with light emitting diodes in [109], with diode lasers in [89,105,110–113], and very recently with an OPO in [114]. The interesting combination of the cantilever photoacoustic technique and long path absorption is realized in the so-called “selective differential method”. This technique has been extensively studied in [40,115–118].

CEPAS has been applied in the detection of several gases. The detection of carbon dioxide was initialized by Laurila et al. [105,119] and they achieved an NNEA (1572 nm, DFB laser, 1σ) of 4.6 x 10^{-9} W $(cm)^{-1}$ $(Hz)^{-1/2}$. In an improved experimental set up [112,120], they advanced the NNEA (1572 nm, DFB laser, 1σ) to 2.2 x 10^{-9} W $(cm)^{-1}$ $(Hz)^{-1/2}$. Koskinen et al. [111] reached an NNEA (1572 nm, DFB laser, 1σ) of 1.7 x 10^{-10} W $(cm)^{-1}$ $(Hz)^{-1/2}$ after optimizing the setup and reducing the cell diameter from 10 to 3 mm. Cattaneo et al. [113] measured oxygen and found an NNEA (760 nm, DFB laser, 1σ) of 4.8 x 10^{-9} W $(cm)^{-1}$ $(Hz)^{-1/2}$. Acetylene was measured by Lindley et al. [39] and an NNEA (6518.486 cm^{-1}, DFB laser, 2σ) of 2.2 x 10^{-9} W $(cm)^{-1}$ $(Hz)^{-1/2}$ was reported. Kuusela et al. [109] measured propane and methane with an Indium arsenide (InAs) LED emitting in the range of 3.1–3.5 µm and CO_2 with an Indium arsenide antimonide (InAsSb) LED emitting 4.2–4.4 µm and reached detection limits (1σ, 1 s) of 6, 26 and 11 ppm, respectively. The detection of methane was also studied in several works. Kauppinen et al. [37] reported a detection limit (broadband IR source, bandpass filter 2600–3400 cm^{-1}, 1σ, 100 s) of 0.8 ppb. Fonsen et al. [108] used an electrically modulated broadband IR source with an optical filter at 2950 cm^{-1} and achieved a detection limit (2σ, 5 s) of 0.5 ppm. Very recently Peltola et al. [114] detected methane with an NNEA (~3057 cm^{-1}, mid-IR continuous wave OPO, 1σ) of 1.8 x 10^{-9} W $(cm)^{-1}$ $(Hz)^{-1/2}$ and a detection limit (1σ, 30 s) of 65 ppt. For a better overview, Table 1 briefly sums up the measured analytes, the techniques used and the achieved figures of merit.

Lindley et al. [39] compared the performance of the cantilever to a single electret capacitive and a differential dual microphone and came to the conclusion that the cantilever microphone obtained a ~100x better normalized sensitivity. However, this result should be viewed critically, because the systems did not reach state of the art due to residual ambient noise in their laboratory.

Apart from the high sensitivity, further advantages of CEPAS are its wide dynamic range and linear response of the signal [37]. Koskinen et al. [40] reported a linear response in the cantilever movement from pico- to several micrometers. For methane they found a linear response of the photoacoustic signal from sub-ppb levels up to thousands of ppm. In CEPAS, the photoacoustic cell is operated in non-resonant mode, because the electronic noise is well below the Brownian noise level [74]. Even without the resonance enhancement, CEPAS is very sensitive and achieved the best ever reported NNEA in TDL-PAS, for example [111]. The non-resonant operation of the photoacoustic cell makes the measurement system design simpler and easier to apply in field and industrial applications. Another advantage is the ability of the cantilever to be heated. This enables the photoacoustic measurement to be carried out directly in the hot gas as reported in Chapter 5.2 of this work. The drawbacks of CEPAS are its complex construction and the higher price compared to traditional microphones. Over the years, CEPAS became a mature technology and is nowadays commercially available from Gasera Ltd., Finland [121].

Table 1. Brief overview of CEPAS-based setups used for gas measurement applications and their figures of merit. Details are provided in the text.

Analyte	Technique	Detection limit or NNEA (both 1σ)	Reference
Carbon dioxide	DFB laser, 1572 nm	4.6×10^{-9} W $(cm)^{-1}$ $(Hz)^{-1/2}$	Laurila et al. [105,119]
Carbon dioxide	DFB laser, 1572 nm	2.2×10^{-9} W $(cm)^{-1}$ $(Hz)^{-1/2}$	Laurila et al. [112,120]
Carbon dioxide	DFB laser, 1572 nm	1.7×10^{-10} W $(cm)^{-1}$ $(Hz)^{-1/2}$	Koskinen et al. [111]
Oxygen	DFB laser, 760 nm	4.8×10^{-9} W $(cm)^{-1}$ $(Hz)^{-1/2}$	Cattaneo et al. [113]
Acetylene	DFB laser, 1534 nm	1.1×10^{-9} W $(cm)^{-1}$ $(Hz)^{-1/2}$	Lindley et al. [39]
Propane, Methane	InAs LED 3.1–3.5 µm	6 ppm (1 s) 26 ppm (1 s)	Kuusela et al. [109]
Carbon dioxide	InAsSb LED 4.2–4.4 µm	11 ppm (1 s)	Kuusela et al. [109]
Methane	Broadband IR source, 2600–3400 cm^{-1}	0.8 ppb (100 s)	Kauppinen et al. [37]
Methane	Electrically modulated broadband IR source, 2950 cm^{-1}	0.25 ppm (5 s)	Fonsen et al. [108]
Methane	OPO, ~3057 cm^{-1}	1.8×10^{-9} W $(cm)^{-1}$ $(Hz)^{-1/2}$, 65 ppt, (30 s)	Peltola et al. [114]

4. Science-based calibration (SBC)

Another novel aspect of this work is the use of the science-based calibration (SBC) method for data analysis and calibration in the cases of multivariate photoacoustic measurement. Since the SBC is not yet very widespread, the calibration method will hereafter be briefly introduced.

4.1 Background and advantages

In contrast to univariate measurements, a multivariate measurement instrument measures more than one quantity at the same time, for example the absorbance values at different wavelengths. Multivariate, sometimes in literature also found as multichannel measurement [61], is standard nowadays for various spectroscopic techniques such as VIS, near-IR or Raman spectroscopy. Array detectors and suitable optics allow the measurement at a number of wavelengths simultaneously. In PAS, the measurement is usually carried out univariate, i.e., one wavelength at a time, except FT-IR-PAS which is considered as a multivariate measurement instrument. Nevertheless, also univariate PAS can record multivariate data by tuning the laser, for example. However, this increases the measurement time [34]. The common reason to record multivariate data in PAS is spectral interference of compounds present in the sample. By measuring the sample at multiple wavelengths, the interference, i.e. the cross-selectivities may be reduced to an acceptable level [17,34,36].

Multivariate data analysis requires advanced chemometric methods compared to univariate analysis. In the past, two different approaches to multivariate calibration existed side by side: statistical calibration methods, for example, PLS or PCR; and physical calibration methods, i.e., spectral fitting methods. It can be shown, however, that all calibration methods, regardless of approach, are based on the same principle and share a common notation. The solutions of all multivariate calibration methods can be written in the form of Equation (6) [122,123] and depend on only two parameters, namely, the estimate of the spectral signal, g, used by the method, and the estimate of the spectral noise, Σ, used by the method. The true values of these two fundamental parameters describe the measurement situation completely (as long as the measurement situation is linear and time-

stationary, as is usually assumed). It can be shown that the different calibration methods merely differ in their way of estimating the two parameters. Statistical calibration methods estimate both the spectral signal and the noise implicitly, i.e., both are computed by the algorithm and are not controllable by the user. For physical calibration methods the signal estimate is explicit, i.e., controlled by the user, but the noise estimate is again implicit. Looking at the algorithmic details involved in making the various implicit estimates, one can say, in summary, that physical calibration methods usually make a good estimate of the signal but a bad one of the noise, whereas statistical calibration methods usually make a bad estimate of the signal and a good, but expensive, estimate of the noise. [123] In the case of the SBC method, both estimates are explicit, i.e., under direct user control. In this sense, the method is not so much an algorithm but a science-based procedure. The analyst can use whatever experimental data and a-priori knowledge about the application and spectroscopy are available to him to estimate the two parameters, and then insert the two estimates into Equation (6). If both estimates are close to describing the actual measurement situation, the solution is close to the globally optimal solution alias “matched filter”. In practice, the SBC method combines the best properties of the two earlier approaches, i.e., the prediction accuracy of statistical calibration and the simplicity and reliability of classical calibration [122,123]. Originally named “matched filter” or “Wiener filter” by its inventor R. Marbach [124], it was renamed to its current name by the pharmaceutical industry [122] in the course of the PAT initiative [125]. The advantages of SBC over other calibration methods are described in detail in [122,123,126] and only the key advantages are listed hereafter:

- The need for lab-reference values is substantially reduced, because the SBC does not need to “learn” the shape of the analyte’s spectral response. This significantly reduces calibration cost compared to statistical calibrations, often by 80%.
- The generation of calibration standards with artificially increased variation in analyte concentration is no longer needed. This advantage is particular appreciated for smoothly running industrial processes.
- Selectivity of response can be proven based on causality and “first principles”.
- Best possible sensitivity in the sense of minimal mean square error is achieved.
- New possibilities become available to master calibration transfer from instrument to instrument.
- By defining the signal and the noise estimate directly, the calibration becomes transparent to the user and is science-based. The user can include a-priori knowledge about spectroscopy and the application.

To be able to utilize the SBC method, the spectral response of the analyte needs to be identified and justified based on causality and “first principles”. This is feasi-

ble for most applications and typically rather simple. [122] In some truly statistical applications, however, this is not possible, for example, calibration of near-IR spectra to predict the "taste" determined by a test panel [127]. In these cases, the SBC method cannot be applied and the method of choice is statistical calibration, for example, PLS. In the SBC method the noise is explicit, meaning the user is required to make an accurate noise estimate of the measurement situation, which can in some cases be quite tricky. As in other calibration methods, a design of experiments might be useful to verify the calibration afterwards.

Since the SBC has not yet been widely used, only a few applications are published. In a demanding chromatographic application with diode array detection, it could improve the selectivity and sensitivity [128]. The use of SBC in some industrial near-IR spectroscopic applications is reported in [123].

4.2 Implementation

The theory behind SBC and the mathematical derivation are well described and discussed in the literature [126,129]. Therefore, this section will briefly explain the practical implementation of the SBC method. For explanatory reasons, a gas measurement application is assumed where the analyte concentration is given in [ppm] and the photoacoustic signal in arbitrary units [arb.]. A SBC is implemented according the following steps:

Step 1: The spectrum of the pure analyte needs to be found and scaled to the concentration, which forms the response spectrum g [arb. ppm^{-1}]. From a mathematical point of view, g is also called response vector, whereby g is written as a column vector while g^T denotes a row vector. In PAS, the spectrum of the pure analyte can usually be measured, but literature data, such as from a spectral library, can also be used. As always, the analyte response should be linear over the calibration range, i.e., the shape of the response spectrum should not vary with analyte concentration.

Step 2: The noise matrix Σ [arb.^{2}] is the multivariate form of the (standard deviation)^2. This parameter describes the sum of all spectral variations that still occur in the measured spectra when the analyte concentration is assumed to be held constant. Σ can be estimated in two ways: experimentally and theoretically and also by a combination of both. In the experimental method, a representative population (no reference values needed) of "noise" spectra is measured containing no or only minor variation in analyte concentration and Σ computed as

$$\Sigma \cong \frac{\tilde{X}^T \tilde{X}}{n-1} \tag{5}$$

where n is the number of spectra measured, X [arb.] the matrix containing the measured spectra and "~" over the matrix means that the matrix is mean-centered. If measured noise spectra are not at hand, Σ can be estimated theoretically. In the theoretical method, the user estimates the noise variance Σ by identi-

fying and adding up individual variance components, e.g., the hardware noise floor of a typical diode array spectrometer contributes a variance matrix with non-zero numbers only on the matrix diagonal and the amplitude of these numbers can easily be determined by measuring repeat spectra of a typical sample. Comparing the two methods, the experimental method is easier to conduct and safer in the sense that no components are "forgotten." However, measurement of a fairly high number of typically several ten noise spectra is required in order to achieve a reliable statistical estimate of the true noise matrix. Also, since the experimental approach does not force the user to also estimate the spectra of the interfering compounds, it may not be possible to prove selectivity from "first principles". Using the theoretical method, the user's noise estimate is usually not perfect, but is often close enough to the desired matched filter. And since the theoretical method requires the user to estimate the spectra of the (most important) interfering compounds, a main benefit of this method is the ability to calculate the cross-selectivities. [122]

The matrix inversion Σ^- [arb.$^{-2}$] usually works with the "normal", i.e., full-rank inverse. In the case of FT-IR instruments, however, a rank-reduced pseudo inverse has to be computed because the usual practice of zero-filling the interferogram before FT computation lets the matrix Σ become singular. For large matrixes, such as high resolution FT-IR spectra, so-called Krylov subspace methods like the preconditioned conjugate gradient can be used to solve the system of linear equations without actually computing the inverse matrix, which saves memory and increases computation speed.

Step 3: After g and Σ^- have been defined, the regression vector b [ppm arb.$^{-1}$] of the analyte is

$$b = \frac{\Sigma^- g}{g^T \Sigma^- g} \tag{6}$$

Step 4: The analyte concentration of a new measured spectrum is calculated by

$$c_{\mathrm{calc}} = c_{\mathrm{OP}} + b^T \left(\mathrm{W}_{\mathrm{meas}} - W_{\mathrm{OP}}\right) \tag{7}$$

where c_{calc} is the calculated concentration of the analyte [ppm] of the measured spectrum W_{meas} [arb.], and W_{OP} [arb.] the spectrum and c_{OP} the concentration [ppm] at the chosen operation point. The user can define the operation point of the calibration freely as is reasonable for the application at hand; typically the mean analyte concentration and the mean spectrum are chosen.

Step 5: Calculation of the calibration's figures of merit: sensitivity and selectivity. The term sensitivity is used throughout this work as meaning the inverse analytical sensitivity. The detection limit is the smallest amount of analyte that can be measured with a certainty of three standard deviations (3σ) [130,131]. Assuming the realized calibration is close to the desired matched-filter case, the multivariate detection limit DL [ppm] of the SBC method can be computed as

$$\mathrm{DL} = 3\sqrt{\frac{1}{g^T \Sigma^{-} g}} \tag{8}$$

Note that the detection limit in Equation (8) can be computed from the same two fundamental parameters that also create the calibration, so that the expected performance of measuring "that g against that Σ" can be assessed even before the calibration is deployed.

The cross-selectivity (CS) number states how much the presence of a certain interferent affects the analyte reading and is given by

$$\mathrm{CS}_{\mathrm{Analyte/Interferent}} = b^T_{\mathrm{Analyte}}\, g_{\mathrm{Interferent}} \tag{9}$$

where $CS_{Analyte/Interferent}$ is the cross-selectivity with which the interferent affects the reading of the analyte. The cross-selectivity numbers are usually given in [ppm ppm^{-1}] or [ppb ppb^{-1}], sometimes also in % values.

5. Multi-compound VOC measurement using the Fourier transform infrared (FT-IR) technique

This chapter presents the work published in Articles I and II. Chapter 5.1 continues the earlier work on FT-IR-CEPAS and presents a rugged measurement system for industrial use. In Chapter 5.2 the focus is on the industrial emission measurement application, and for that an FT-IR-CEPAS measurement system capable of operating at 180 ºC is developed and its performance tested.

5.1 Measurement system for industrial use

5.1.1 Background

Spectrometers based on the Fourier transform infrared (FT-IR) technique for the mid-IR spectroscopic measurement of solids and liquids have been employed for around three decades in laboratory and more recently also in industrial applications [61]. In FT-IR gas phase spectroscopy, the transmission technique has played a major role, because the FT-IR-PAS instruments were clearly less sensitive [37]. Over the years, the transmission FT-IR gas analyzers have been developed and their performance is now close to the theoretical limits. The light source is difficult to improve further and the optical semiconductor IR detectors work close to the mentioned theoretical performance limit. Therefore, the sensitivity of these instruments cannot be significantly improved any more. [37,73] The main option to further increase the sensitivity of the FT-IR transmission technique is by enlarging the optical absorption path length, which is done in practice and absorption paths from a few up to several tens of meters are used in modern multi-pass cells. This, however, leads to bulky cell designs with a bigger gas volume and expensive mirrors [73]. Also, the signal response becomes non-linear, which makes quantitative calibration more demanding, particular if wet gases are measured due to the non-linear response of the analyte and water as already mentioned in Chapter 3. [73,74] PAS is a zero background technique, offers small optical path lengths and thus has the potential to overcome the mentioned challenges [37,38,73]. However, as

already mentioned above, gas phase FT-IR-PAS has not been widely applied and only a few publications are known to exist [67]. This is mainly because of the low spectral radiance available from the broadband IR source with interferometer compared to e.g., laser sources, the non-resonant operation enabling a wide frequency response and the low sensitivity of the earlier microphones [38,73]. To overcome the limitations, Kauppinen invented the cantilever microphone [38]. Based on the cantilever microphone, a novel technique known as CEPAS evolved, as explained in Chapter 3.4. FT-IR-CEPAS setups were reported in previous works by Wilcken and Kauppinen in [38] and Kuusela and Kauppinen in [73]. Uotila and Kauppinen [106] built an FT-IR-CEPAS setup able to measure solids, liquids and gases in a single PA cell and found a detection limit (2σ, 168 s) for methane of 3 ppm by using a Mattson Galaxy 6020 series FT-IR interferometer, with 1.6 kHz mirror velocity, a resolution of 8 cm^{-1}, 100 scans and univariate data analysis at 3012 cm^{-1}. All these setups were for measurement purposes in the laboratory with rather bulky FT-IRs that are not easy to transport and capable of operating in rough environments. Therefore, a complete analyzer for industrial application was built that is rugged, easy to transport and capable of operating outside of the laboratory. The objective of this work is to describe the first industry-ready FT-IR-CEPAS measurement system and characterize its performance in the measurement of some selected VOCs.

5.1.2 Experimental

5.1.2.1 Measurement system

Bruker's IRcube is a modular FT-IR OEM spectrometer with permanent aligned optics. It is insensitive to vibrations and temperature changes. For these reasons, it was selected as the FT-IR for the analyzer that should be capable for operating in rough environments. The collimated output beam of the FT-IR had a diameter of 25 mm and the cylindrical shaped PA cell (Gasera PA101) an inner diameter of 4.5 mm. A focusing mirror with a focal length of 76.2 mm was used to achieve a focal spot size of 4.4 mm. The beam splitter of the FT-IR was made of KBr-Germanium and the FT-IR window material was KBr. The PA cell was made out of aluminum, had a length of 100 mm and a volume of <8 mL. A BaF_2 window was used to pass the beam into the cell. On the other side of the cell a gold coated window reflected the light beam back, resulting in 200 mm optical path length. The dimensions of the silicone cantilever were 6 x 1.5 x 0.01 mm (LxWxH). Both, the cantilever and the PA cell were coated with gold. The resonance frequency of the cantilever was above 480 Hz at 500 mbar pressure and the cell was operated in non-resonant mode. The digital cantilever readout signal was converted to analog, fed to the FT-IR and the measurement signal was read from the IRcube via the LabVIEW™ program "FTIR analysis software". The software Fourier transformed the measured interferogram to the final spectrum.

The function of the gas exchange system was to purge the PA cell, draw a sample and condition it inside the PA cell to the correct pressure and temperature. For that, a membrane pump, several solenoid vales and a pressure sensor were used. The total volume of the sampling system was ~13 mL. An illustration of the whole system including the gas exchange module is given in Figure 4.

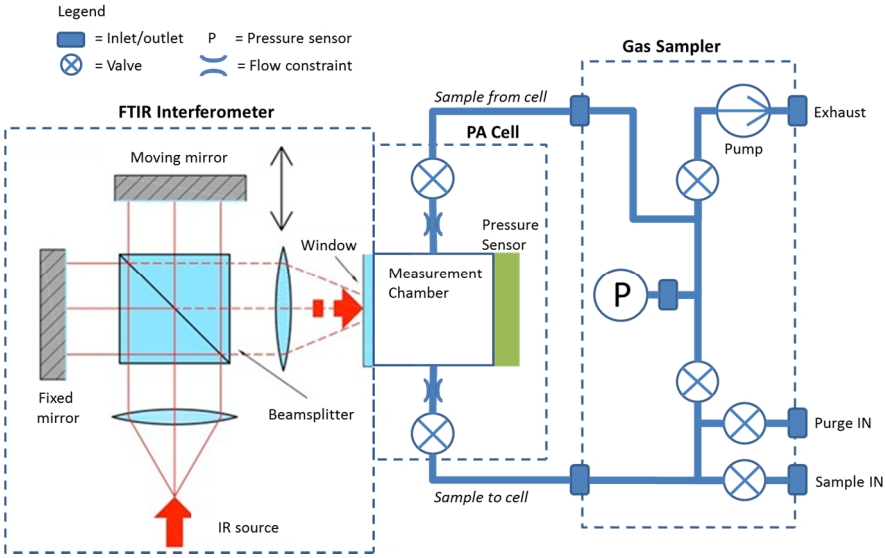

Figure 4. Illustration of the whole measurement system including FT-IR, PA cell and sampling module (printed with the permission from Gasera Ltd.).

The casing in which the whole measurement system was arranged had the dimensions of 475 x 482 x 266 mm (LxWxH) and a weight of 25 kg. A notebook was needed in addition to communicate with the instrument, set the operation parameters, read the signal with the "FTIR analysis software" and for further data processing and analysis. Figure 5 shows a photograph of the whole measurement system without the notebook. The FT-IR-CEPAS system was manufactured by Gasera Ltd., Finland.

5.1.2.2 Measurement parameters

The sample gas pressure was adjusted to 470 mbar and the temperature of the cell and the sample gas to 50 °C. The full spectral range was recorded from 200 to 6000 cm^{-1} and the aperture was selected to be 4 mm. The mirror velocity of the FT-IR was set to 1.6 kHz and the resolution to 4 cm^{-1}. With these parameters, one scan took 5 s. For methane and carbon dioxide, 5 spectra were averaged and the AD converter gain was 5. For methanethiol and propene, 10 spectra were averaged and the AD converter gain was 10.

High resolution FT-IR reference spectra from the Pacific Northwest National Laboratory (PNNL) [132] are used for modeling purposes in this work. The PNNL spectra measured at 50 °C and 1013 mbar were selected.

Figure 5. Photograph of the FT-IR-CEPAS measurement system.

5.1.2.3 Gas supply

The gases were not selected according to a particular application as was done in the following chapters. The objective of the work described in this chapter was to test the FT-IR-CPEAS system and therefore some typical VOCs were selected, as described below. Methane (CH_4) was chosen because it is a commonly used analyte to compare the performance of measurement systems. Propene (C_3H_6) has a slightly longer aliphatic chain than methane without functional groups. Methanethiol (CH_3SH) has the same molecular structure as methane but one hydrogen atom is replaced with a thiol (SH) group. Carbon dioxide (CO_2) is sometimes interesting to quantify as well and it might even be useful to be able to subtract it from the measured spectra in some cases. The subtraction of water is studied in Chapter 5.2 and will therefore be omitted here.

The analyte gases were supplied in gas cylinders as custom blends from AGA, Finland. Methane and carbon dioxide came as a blend in nitrogen in the same cylinder; methane as 10 000 ppm in nitrogen and carbon dioxide as 50 000 ppm. Propene and methanethiol were procured in individual cylinders as 5000 and 2000 ppm, respectively. Nitrogen (AGA, 5.0) was used for dilution. All ratios (ppm, ppb and ppt) stated in this work by the author refer to the volume ratio, which is the same as the mole ratio for an ideal gas.

Dilution of the gas blends was done with a self-built gas mixing setup. The gas mixing setup included the gas cylinders with each having a pressure reducer, two mass flow controllers (Brooks Instrument model 5878-2 for analyte gas and AALBORG mass flow meter GFM17 for nitrogen), a pressure control unit (Tekmar-Dohrmann 14-3938-000) with an over pressure valve and a sample reservoir made out of steel. From the reservoir, which acted as a buffer, the gas exchange system of the FT-IR-CEPAS measurement system drew the sample. To keep a continuous flow through the gas mixing setup, the excess gas was passed from the reservoir to the fume hood. An illustration of the gas mixing setup is shown in Figure 6.

Several different concentrations of each analyte were prepared and measured. The spectra used for calibration were measured at a concentration of 1000, 5000, 2000 and 1000 ppm for methane, carbon dioxide, methanethiol, and propene, respectively. The spectra for the calculation of the cross-selectivities were measured at the same concentration as the calibration spectra.

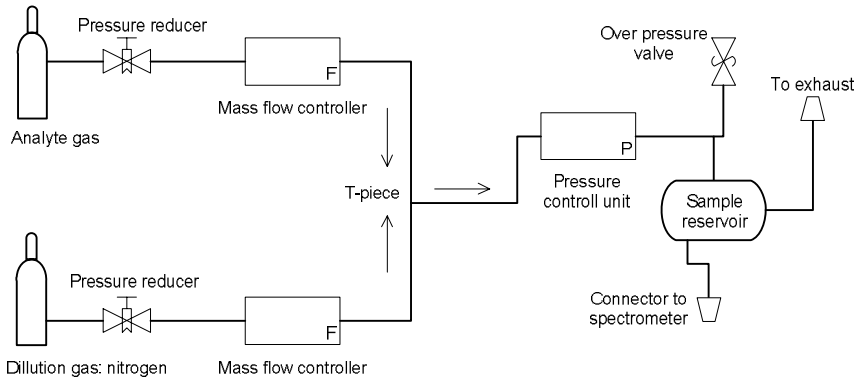

Figure 6. Illustration of the gas mixing setup.

5.1.3 Results and discussion

5.1.3.1 Data processing

The background and water features were subtracted from the measured spectra with previously determined spectra of the pure cell response and water. Methane and carbon dioxide came in the same cylinder and thus the spectrum contains bands of both analytes. For both methane and carbon dioxide, the band of the other analyte were filled with baseline pieces taken from 1800 to 2200 cm^{-1}. Finally all spectra were divided by their concentration to become the response spectra *g* that are plotted in Figure 7.

The measured spectra were compared to PNNL reference spectra presented in Figure 8. The position of the bands in the measured and reference spectra match.

The band shape and intensities look somewhat different, which comes from the instrument response function, different resolution and sample gas pressure. PNNL spectra are recorded at 0.112 cm^{-1} and 1013 mbar and in the present work at 4 cm^{-1} and 470 mbar. The only exception makes CO_2 with an absorption band intensity of a factor of ~10 times lower than expected. The reason for that is unknown, but might be related to the gas cylinder or the sampling system. With a different gas cylinder and without a sampling system, the carbon dioxide concentration was later evaluated to be ~10 times higher than in this work. Nevertheless, the carbon dioxide spectra were not adjusted or further manipulated. Therefore, the evaluated detection limit of carbon dioxide in this work is rather pessimistic and can be up to ~10 times better.

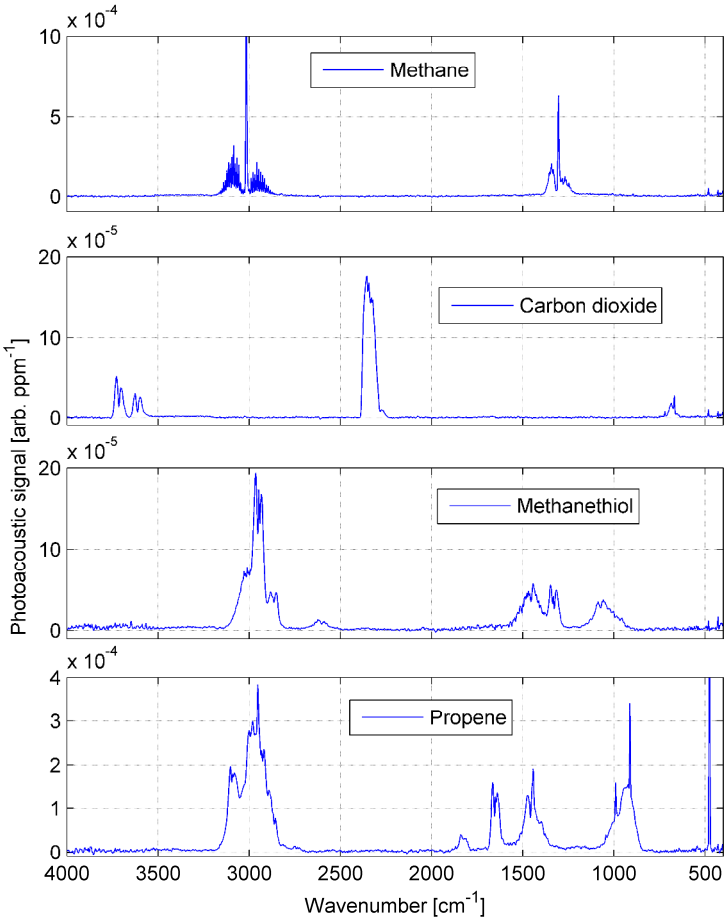

Figure 7. The measured response spectra *g* of the analytes. The photoacoustic signal in CEPAS is in arbitrary units [arb.]. The spectra were background and water corrected and divided by the concentration.

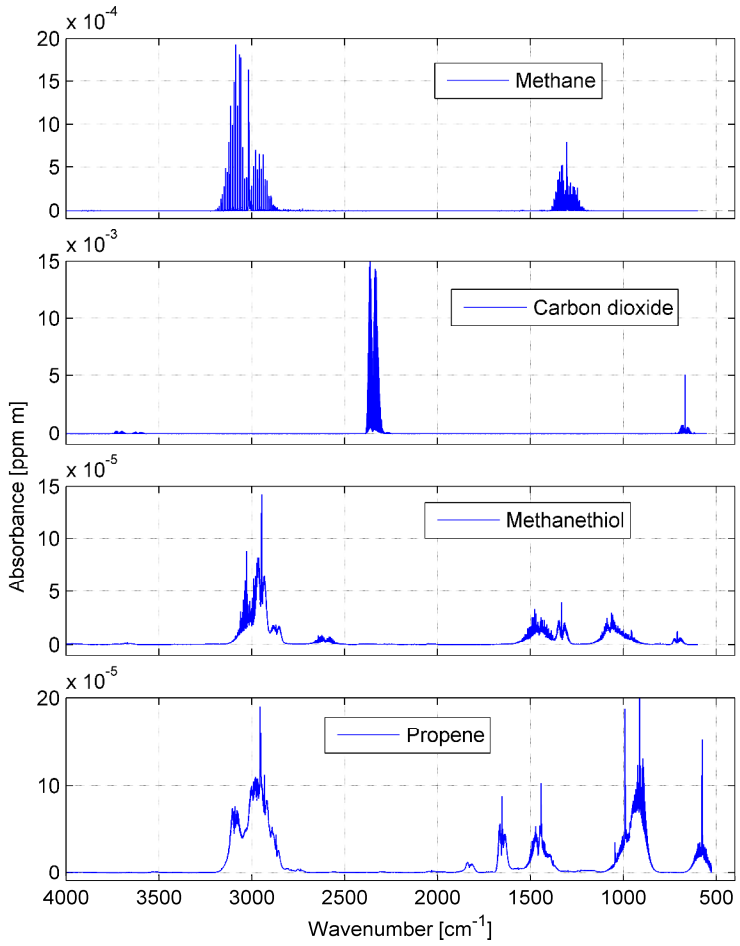

Figure 8. PNNL reference spectra of the analytes. The ordinate scale is in absorbance and in addition referred to an analyte concentration of one ppm and a path length of one meter.

5.1.3.2 Univariate data analysis

For the univariate detection limit, the maximum band intensity of each analyte response spectrum is divided by the instrument noise. The instrument noise is the standard deviation of the baseline variation in the range of 3200 to 3500 cm^{-1}. The standard deviation was calculated from the raw spectra that were not yet divided by their concentration and averaged over all analytes. The calculated noise was 2.10×10^{-3} (photoacoustic signal is in arbitrary units). The signal intensity and the univariate detection limits are shown in Table 2 in the column titled “Univariate data analysis”.

Table 2. The detection limits for uni- and multivariate data analysis.

	Univariate data analysis			Multivariate data analysis	
	Wavenumber of signal [cm^{-1}]	Signal intensity [arb. ppm^{-1}]	Detection limit (3σ, 25 s) [ppm]	Detection limit (3σ, 25 s) [ppm]	
				Single-compound	Multi-compound
Methane	3016.6	1.32×10^{-3}	4.8	2.2	2.5
Carbon dioxide	2355.1	1.76×10^{-4}	35.7	6.7	6.7
Methanethiol	2964.6	1.94×10^{-4}	32.6	5.6	9.8
Propene	2953.0	3.83×10^{-4}	16.5	2.2	3.9

The univariate detection limits (3σ, 25 s) range from best 4.8 ppm for methane to 35.7 ppm for carbon dioxide, whereas the carbon dioxide signal was a factor of ~10 lower than expected, meaning that the detection limit could be better by up to a factor of ~10. The achieved detection limit of methane is better than what Uotila and Kauppinen [106] reported: 3 ppm (2σ, 168 s, 1.6 kHz, 8 cm^{-1}). The detection limit of 4.8 ppm achieved here can be converted as follows: The 4.8 ppm are multiplied by 2 / 3 to become 2σ and divided by √(168 / 25) to take the shorter measurement time into account. The converted detection limit is 1.2 ppm and still measured at a better resolution of 4 cm^{-1}. The reason for the lower performance of their system is the compromise to measure solid, liquid and gaseous samples in the same cell.

The detection limits stated in Article I differ from the numbers given here for the following reasons: First, the noise is taken here as 3σ and in Article I as 1σ. Second, measurement time for the noise in Article I was 100 s and here only 25 s. And finally, the noise was calculated differently. The noise in Article I was calculated more optimistically by fitting a line through the baseline variation between 3200 and 3250 cm^{-1}. Then, the standard deviation was calculated from the fitted line to the measured points. In this work, the standard deviation was calculated directly from the baseline variation and is more realistic. The detection limits can be compared as done here for methane: The detection limit of 4.8 ppm is divided by 3 to become 1σ and divided by √(100 / 25) to take the shorter measurement time into account, resulting in 0.8 ppm, which is close to the 0.5 ppm stated in Article I.

Univariate data analysis may even be selective, if for each analyte a spectral region can be found, where only the analyte is absorbing and no interference occurs. In the presented case, methane could be determined without interference at 1270 cm^{-1}, carbon dioxide at 2355 cm^{-1}, propene at 1665 or 910 cm^{-1} and methanethiol at 1090 cm^{-1}. However, lower absorption coefficients and the risk of still run into interferences with increasing concentration of the other analytes speak

against univariate analysis here. Multivariate data analysis can incorporate the whole spectral range and resolve the interference, as shown in the next chapter.

5.1.3.3 Multivariate data analysis

Multivariate data analysis and calibration were performed with the SBC method. As the analyte signal, the response spectra *g* were taken in the range of 500–4000 cm^{-1}. The instrument noise was assumed to be 2.10 x 10^{-3} for the whole wavelength range, which might not be perfectly true, but is a good estimate for this calibration. Two regression vectors *b* were calculated for each analyte representing the single- and multi-compound case. The $\Sigma_{\text{multi-compound}}$ included the instrument noise and the interference noise of the other analytes. This will become the calibration where the spectral interference of the analytes will be resolved and each analyte can selectively be measured. However, resolving the interference costs signal and depending on the extent of the interferences the detection limit will be worse. To evaluate by how much the sensitivity worsens, the single-compound calibration is calculated assuming only the analyte to be present in the sample. Accordingly, the noise matrix $\Sigma_{\text{single-compound}}$ contained only the instrument noise. In real-world applications, water vapor is commonly present in samples and interferes as well with the analyte spectra. To make a water insensitive calibration, water was added as another interferent to $\Sigma_{\text{multi-compound}}$. Finally, the multi-compound calibrations were optimized for selectivity. The calculated detection limits are shown in Table 2 in the column titled “Multivariate data analysis”, the cross-selectivities in Table 3 and the regression vectors in Figure 9.

Table 3. Cross-selectivities (500–4000 cm^{-1}, 25 s) in [ppm ppm^{-1}] of the individual analytes, water and in sum. For instance, if methane’s concentration increases by 100 ppm, then it affects the methanethiol reading by -0.233 ppm.

	Interferent →					
Analyte ↓	Methane	Carbon dioxide	Methanethiol	Propene	Water	Sum
Methane	1.00	4.98 x 10^{-5}	2.44 x 10^{-3}	4.59 x 10^{-4}	-4.07 x 10^{-4}	3.35 x 10^{-3}
Carbon dioxide	-7.74 x 10^{-4}	1.02	1.61 x 10^{-3}	6.92 x 10^{-4}	-2.46 x 10^{-3}	5.53 x 10^{-3}
Methane-thiol	-2.33 x 10^{-3}	-4.41 x 10^{-6}	0.95	4.11 x 10^{-3}	-3.85 x 10^{-3}	1.03 x 10^{-2}
Propene	5.44 x 10^{-3}	9.78 x 10^{-5}	8.30 x 10^{-3}	0.99	-1.16 x 10^{-3}	1.50 x 10^{-2}

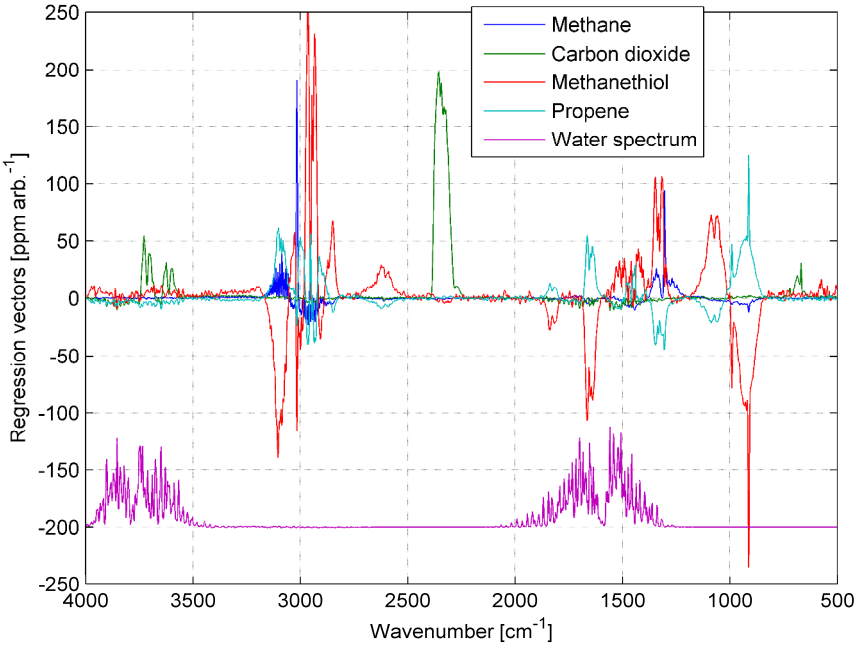

Figure 9. Regression vectors *b* of methane, carbon dioxide, methanethiol and propene. For comparison reasons the water response spectrum is also shown.

FT-IRs are multivariate measurement instruments, what means that the measurement time does not depend on the measured spectral range, i.e., the amount of spectral elements. In other words, FT-IRs measure the spectral elements parallel in time, since the spectral elements are modulated at different frequencies with the interferometer and resolved by the fast Fourier transform (FFT). The measurement time of FT-IRs is determined by the amount of scans, the optical resolution and the mirror velocity. Therefore the measurement time for multivariate data analysis does not increase as compared to laser-based systems, for example, where the laser is tuned once at a time through the spectrum. With the same measurement time as for univariate data analysis, the multivariate single-compound detection limits are better by a factor of 2.2 for methane and 7.5 for propene. Propene gains most when using multivariate data analysis, because it is the analyte with the most and broadest absorption bands. The multivariate multi-compound detection limits worsen compared to multivariate single-compound detection limits by up to a factor of 1.77 for propene due to the interference with the other analytes and water. Methane's detection limit worsens only slightly, because the methane spectrum shows rotational bands which let the spectra look different from the others and that makes it easier to discriminate. The detection limit of carbon dioxide does not worsen because it can be measured free of interferences. The cross-selectivity number of carbon dioxide as an interferent is on average only 5.07 x 10^{-5} ppm ppm^{-1}

and the carbon dioxide detection is interfered by the other analytes by only 5.52 x 10^{-3} ppm ppm^{-1}. The average of the sum of the cross-selectivity numbers per analyte was 9.55 x 10^{-3} ppm ppm^{-1}. This means that if all other analytes rise by 100 ppm, then the reading of the analyte of interest will be biased by +0.955 ppm.

The interference of water could be kept on a low level of 1.81 x 10^{-3} ppm ppm^{-1} on average. Water shows the smallest cross-selectivity number against methane, because the water and methane bands overlap only in a short region between 1300–1500 cm^{-1} as shown in Figure 9. Carbon dioxide has a higher cross-selectivity number against water than methane, which looks strange on first view. The reason for that is the combination band occurring between 3550 and 3750 cm^{-1} that interferes with the asymmetric OH stretch vibration band of water.

As already suspected before, the sensitivity of the FT-IR-CEPAS system cannot reach those of laser or broadband IR sources with filter CEPAS systems due to the limited spectral radiance of the broadband IR source with interferometer. Fonsen et al. [108] reached a detection limit for methane of 0.5 ppm within 5 s of measurement time with CEPAS and an electrically modulated broadband IR source combined with a filter. Kauppinen et al. [37] reported a detection limit of 0.8 ppb of methane within 100 s of measurement time with CEPAS and broadband IR source with optical filter. Uotila et al. [117] achieved 13 ppb as the detection limit for methane within a measurement time of 0.37 s using the selective differential CEPAS method. But the FT-IR still has the advantage of being a multivariate measurement instrument and therefore, multivariate data analysis is always recommended in the case of FT-IRs. Further, FT-IRs are able to measure several analytes in parallel. Therefore, the figure of merit comparison based on the measurement time is just half the truth and the amount of determined analytes should also be taken into account when comparing FT-IRs to laser and broadband light sources with filter systems, for example. As here, where four analytes were selectively detected, and the interference of water was removed within 25 s of measurement time.

5.1.3.4 Future system improvements

The optimization of the main important measurement parameters resolution and measurement time depends on the particular application. However, a general guide is given as follows. According to Ahro and Kauppinen [133], the optimal resolution is to have vibrational information included, but to avoid the rotational information, because the full rotational structure can usually not be resolved. In practice this means a resolution of ~4 to 8 cm^{-1}. In case the resulting cross-selectivities are better than needed, the resolution can be reduced, which will result in better detection limits because the power output of the interferometer is proportional to the aperture. Finally, the measurement time will be adjusted according to the required detection limit.

This work describes the very first FT-IR-CEPAS measurement system that was assembled, and in the future, the system performance can still be improved. The

main point of improvement is the aperture of the FT-IR. The biggest possible aperture in the IRcube is 4 mm and gives a best resolution of 1 cm^{-1}. However, the resolution used here was 4 cm^{-1} and in commercial FT-IR transmission gas analyzers even 8 cm^{-1} are commonly used [134]. Therefore, the sensitivity can be enhanced by using a larger source and aperture without the need for very tight focusing.

This work was done in 2009 and until now, some progress on the CEPA detector has been made. The read-out interferometer has been enhanced and the photodiodes were replaced by a line detector. The PA cell has also been improved and the diameter increased to 8 mm. The vibration isolation has been revised and the cantilever dimensions changed from 6 x 1.5 x 0.01 mm to 5 x 1.2 x 0.01 mm (LxWxH) leading to a better sensitivity. The overall performance increase compared to the CEPA detector used here is difficult to estimate, but is probably around a factor of 2.

5.2 Photoacoustic spectroscopy at elevated temperatures

5.2.1 Background

As stated in the previous chapter, FT-IR-CEPAS performs best in applications that require multi-compound detection down to ppm level. Many such applications can be found in industry. The one selected here is the measurement of industrial VOC emissions.

Many industrial products and processes require organic solvents and in some cases they are crucial. A wide variety of industrial sectors utilize organic solvents such as painting, chemicals, coating, pharmaceuticals, printing, paper, textiles and resins enterprises [9]. The exhaust emissions of VOC vary greatly in composition and concentration depending on the industrial sector and the particular process [3,58]. VOC emission abatement technologies exist and are applied in more than ~40% of the cases in Europe in 1999 [135]. However, a major problem is the accurate and reliable VOC measurement [57]. Such a analyzer would help to optimize the existing and develop new manufacturing processes with lower VOC emissions. Further, it would facilitate the development of abatement systems and it could be used as a process analyzer while operation, to drive the abatement systems in an optimal way. Finally, it allows the verifications of the emissions, which is a statutory obligation. [57]

The measurement of industrial VOC emissions is not trivial. Depending on the application, the concentration of the compounds varies from ppm to percent, the emission stream is usually a mixture of many different organic compounds and moisture and the measurement system should be corrosion resistant [33,57,58]. FT-IR systems match the measurement system requirements that are ppm level sensitivity, selectivity and multi-compound ability. However, the transmission FT-IR analyzers suffer from the non-linear response, the high calibration effort and the poor stability in rough and corrosive industrial environments. CEPAS offers a

linear signal response of several orders of magnitude [37,40], and thus can be calibrated with low cost and PA cells can be built corrosion resistant [136,137]. Therefore, FT-IR-CEPAS was selected for this application.

Quite often in industry and in industrial emission measurement, the gas to be measured has a higher temperature than ambient. In a measurement system operating at ambient temperature, condensation of the sample in the analyzer may happen, which leads to wrong readings and trouble in the operation of the analyzer. To avoid these problems, all parts of the analyzer that are in contact with the measurement gas need to be heated, including the PA cell. Since almost all microphones are limited in the operational temperature, the microphone is usually placed outside the PA cell at lower temperature and often at ambient conditions [138]. Advanced cell designs and coupling techniques were invented to operate a heated PA cell with an externally connected microphone. Possibly the first technique was the heat-pipe cell reported in [139–141]. Later investigations used signal tubes to connect the microphone to the heated PA cell. Various setups for different temperature ranges and applications have been built and reported in [138,142–144]. The problem of applying the signal tubes are the lower signal intensity at the microphone, the more complex setup and calibration. Therefore, the approach of this work is to have the pressure transducer inside the heated PA cell. The novel cantilever microphone can be heated up to 180 °C, and therefore enables the pressure sensing at elevated temperatures inside the PA cell eliminating the need of a signal tube. The objective of this work is to develop and build a novel FT-IR-CEPAS measurement system where all parts that are in contact with the sample to be measured, including the PA cell and the cantilever, are operating at 180 °C. The performance of the system will be tested by the measurement of VOCs typical for industrial emissions.

5.2.2 Experimental

5.2.2.1 Heatable photoacoustic detector

As already explained earlier in this work in Chapter 3.4, the cantilever is the pressure transducer of the optical cantilever microphone. The cantilever is made out of silicone and can withstand temperatures of at least 180 ºC. In the heatable PA cell, the cantilever was mounted and the cell including cantilever heated up to 180 ºC, as will be explained in the next sub-chapter. The movement of the cantilever is read-out via an interferometer. This read-out interferometer needs to be at ambient temperature due to the electronics and the laser. The red laser beam with a wavelength of 650 nm is guided from outside through a quartz glass window into the cell and focused on the moving end of the cantilever. The distance between the read-out interferometer and the outer cell wall was 17.5 mm and filled with thermal insulation material (Aerogel). Figure 10 shows an illustration of the heatable cantilever microphone. Although the heatable detector was set up here with an

FT-IR, it can be used with any other light source suitable for PAS, such as those reported later on in this work.

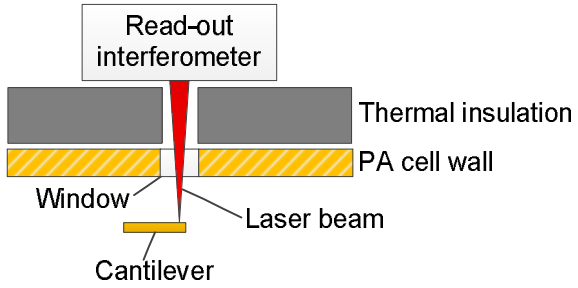

Figure 10. Illustration of the heatable cantilever microphone and its read-out at ambient temperature.

5.2.2.2 Measurement setup

Bio-Rad's FTS 6000 laboratory FT-IR forms the basis of the built measurement system. A custom-made oven was installed in the sample compartment of the FTS 6000. The oven contained the photoacoustic detector and the sampling system and was heated to 180 ºC.

The PA cell (Gasera PA101h) had a cylindrical shape with an inner length of 100 mm and diameter of 4 mm. The focal spot size of the IR beam leaving the FTS 6000 was 11.94 mm. To irradiate all optical power into the PA cell, the focal spot size was reduced by an ellipsoidal mirror with a ratio of 3:1 to 3.98 mm. The IR light beam was guided into the cell through a BaF_2 window. The window at the other end of the cell was gold coated, resulting in 200 mm optical path length. The cell was made out of stainless steel and was operated in non-resonant mode. The cantilever made from silicone had the dimensions of 5 x 1.2 x 0.01 mm (LxWxH). Both cantilever and the PA cell were coated with gold. The PA cell had an internal volume of ~8 mL, can be used at temperatures from 15 to 180 ºC and sample gas pressures from 0 to 2 bar.

The role of the gas exchange system was to purge and clean the PA cell with fresh sample and adjust the pressure of the sample inside the cell. Figure 11 shows an illustration of the gas exchange system. The following components were used: a 0.5 µm particle filter at the inlet (F1, Swagelok, SS-2TF-05-12457), a membrane pump (P1, Air Dimensions, B161-GP-HJ0-L) to circulate the gas, valves (V1–3, Swagelok, 6LVV-ALD3TFR4-P-C) to seal the sample gas in the PA cell, a pressure sensor (PS1, Wika, 35064269) to read the actual pressure in the cell and a taper (T1, Swagelok, SS-SS2-D). The sample gas pressure in the PA cell was precisely adjusted by the taper and valve V3. Efforts were made to select parts that withstand temperatures of at least 180 °C and are corrosion resistant. The material choice for the parts in contact with the gas was PTFE or stainless steel grade SS316, if available, coated with a Silcosteel.

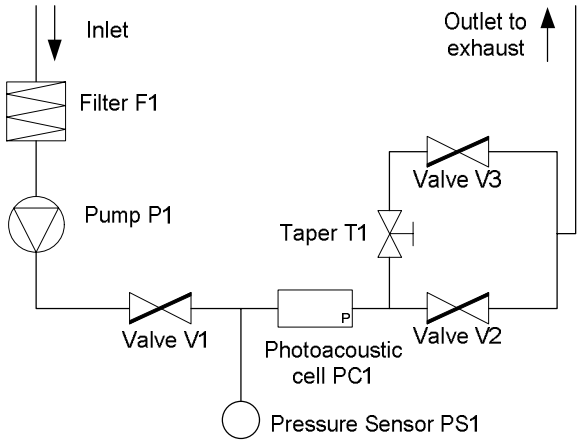

Figure 11. Illustration of the gas exchange system.

The self-built oven was made from aluminum and isolated with Aerogel and heated with 10 direct current resistors (Tyco THS50) placed on the inside of the oven and the PA cell. The shape of the oven extends in height, because the width was fixed by the sample compartment of the FTS 6000. Figure 12 shows a photograph of the oven with an open side cover.

The electronics controlling the whole oven including temperature and gas exchange system was placed in a separate box and attached to the back of the oven. The control was realized with a National Instrument board (USB 6501) and LabVIEW™ software. The digital signal of the microphone displacement was converted to analog and fed to the FT-IR. The Bio-Rad software (Digilab Win-IR Pro 3.4) collected the interferograms from the FTS 6000 and Fourier transformed them to the final spectrum.

5.2.2.3 Measurement parameters

The PA cell was heated to 180 °C and the sample gas pressure inside the cell was set to 1300 mbar. The aperture of the FT-IR was 11.94 mm and the resolution 8 cm^{-1}. The spectral range from 400 to 8000 cm^{-1} was recorded at a mirror velocity of 2.5 kHz. One measurement is the average of 300 individual scans. With these parameters the measurement time for one measurement was 8.5 min.

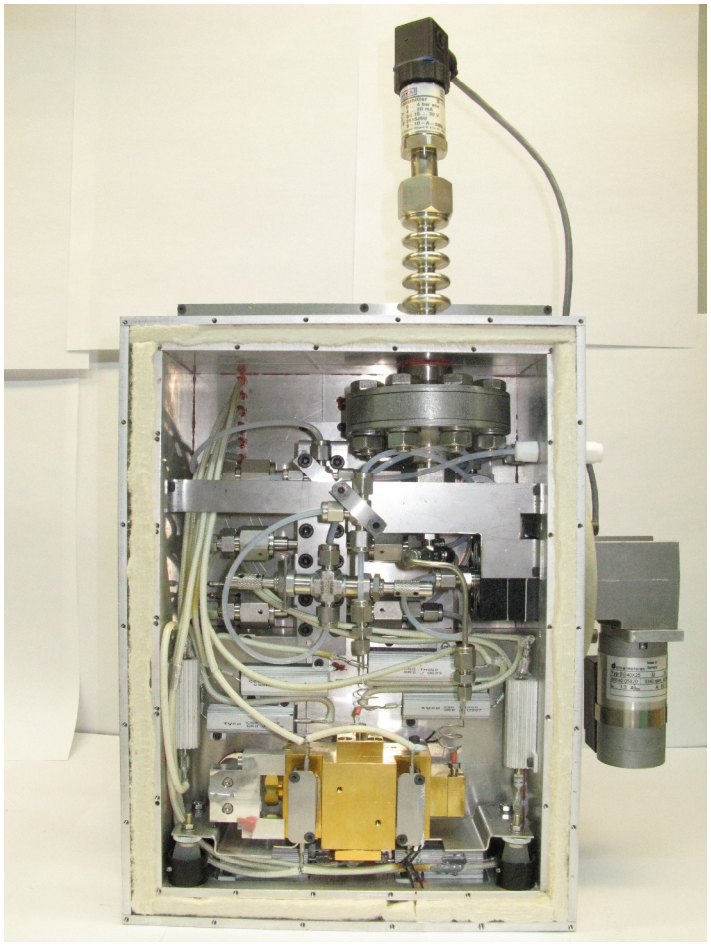

Figure 12. Picture of the self-built oven. The metal side cover was removed for the picture. The gold-colored PA cell sits on the bottom of the oven. The other parts belong to the gas exchange and heating system.

5.2.2.4 Gas supply

For characterizing of the heated FT-IR-CEPAS measurement system, VOC were selected that typically occur in industrial emissions. Table 4 lists the measured VOCs. Each VOC was measured in a concentration of 100 and 200 ppm, diluted in nitrogen (AGA, 5.0).

Table 4. Liquids from which the VOC vapors were generated.

Name	Boiling point [ºC]	Supplier, Purity
Acetone	56	Alfa Aesar, 99.5+%,
Ethanol	78	Altia Oy, 99.5%
Isobutanol	108	Alfa Aesar, 99.0+%
Isopropanol	83	Sigma-Aldrich, 99.9+%
Methanol	65	Merck, 99.80%
n-Butanol	117	Alfa Aesar, 99.0+%
Tetrachloroethylene	121	Sigma-Aldrich, 99.9+%
Methoxypropanol acetate	146	Sigma-Aldrich, 99.5+%
Methyl acetate	60	Alfa Aesar, 99.00%
Methyl ethyl ketone	80	Sigma-Aldrich, 99.7+%
Methyl isobutyl ketone	118	Alfa Aesar, 99.00%
o-Xylene	144	Alfa Aesar, 99.00%
m-Xylene	139	Alfa Aesar, 99.00%
p-Xylene	138	Alfa Aesar, 99.00%
Dimethylformamide	153	Alfa Aesar, 99.7+%
Dichloromethane	40	Sigma-Aldrich, 99.9+%
Butyl acetate	126	Fluka, 99.0+%
Toluene	111	J.T. Baker, 99.70%

The analyte gas mixtures were prepared with the Gasmet™ calibrator [145]. The calibrator contains a syringe pump that feeds the VOC analyte liquid from a syringe into an evaporation chamber. The chamber is flushed by an exact flow of nitrogen, controlled by a built-in mass flow controller. The temperature of the evaporator was set 5 °C higher than the boiling point of the organic liquid. To prevent condensation of the gases, all the tubing was heated up to 180 °C. Figure 13 shows an illustration of the VOC analyte vapor generator. For the water subtraction experiment in Chapter 5.2.3.4, an additional syringe pump (Scientific Lab Instruments, KDS-100-CE) was installed between the Gasmet™ calibrator and the heated line.

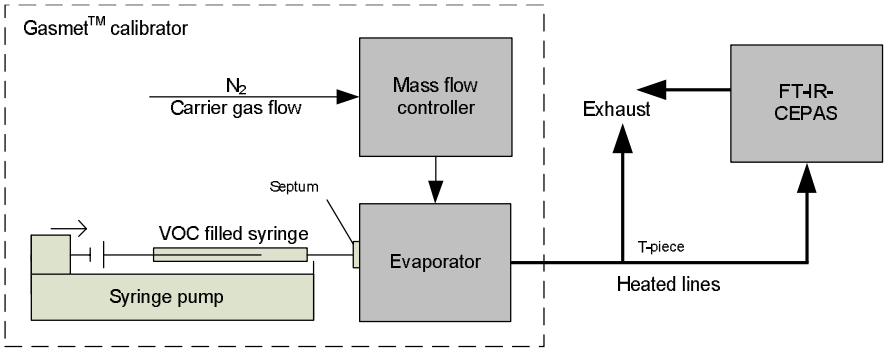

Figure 13. Illustration of the VOC analyte vapor generator.

5.2.3 Results and discussion

5.2.3.1 Data processing and selection

In this work, the background subtraction was refined and the background was subtracted in the complex plane, between the FFT and the power spectrum calculation. The reason for performing the background subtraction in the complex plane is that the cell background and the gas sample signal have different phases. Further details of the complex background subtraction, formulas and an example are given in Article II. The complex background spectrum used for the subtraction was determined earlier by measuring pure nitrogen and saving the spectra in complex numbers. After the power spectrum calculation, the spectra are finally divided by the concentration to become the response spectra *g* [arb. ppm^{-1}].

The univariate and multivariate single-compound detection limit was calculated for all analytes. The multivariate multi-compound detection limits and cross-selectivities were assessed for a case study. The spectra measured at 100 ppm are used for the uni- and multivariate single-compound detection limit calculation. The multivariate multi-compound calibration was done based on the 200 ppm and the cross-selectivities were calculated from the 100 ppm spectra.

5.2.3.2 Univariate data analysis

The univariate detection limit is found by dividing the maximum band intensity of each analyte response spectrum in the range between 500 and 4000 cm^{-1} by the instrument noise. The instrument noise is the standard deviation of the baseline variation in the range of 3200 to 3500 cm^{-1}, and was averaged over all 100 ppm analyte spectra. The standard deviation was calculated from the raw spectra before they were divided by the concentration. Since all 100 ppm spectra are an average of three measurements, i.e., 3 x 300 scans, the measurement time was 25.5 min. To be able to directly compare the results with multivariate data analy-

sis, where the measurement time was 8.5 min, the detection limits were multiplied by √(25.5 / 8.5). The instrument noise was 3.00 x 10^{-3}. The signal intensity and the univariate detection limits are shown in Table 5 in the column titled “Univariate data analysis”.

The univariate detection limits (3σ, 8.5 min) vary from the best 1.3 ppm for butyl acetate to the worst 23.1 ppm for *m*- and *o*-xylene. As in Chapter 5.1, also here, the detection limits differ from the values stated in Article II. The spectral range used for the calculation of the noise was here 3200 to 3500 cm^{-1} and in Article II 2400 to 2800 cm^{-1} and the analyte signal was not taken until 4500, but only until 4000 cm^{-1}. Both modifications were made to be in compliance with Chapter 5.1. However, these modifications let the numbers be only of a minimal difference. Further, the measurement time of the univariate data analysis was referred to 8.5 min as explained above.

The direct comparison of the noise and signal numbers with those of the IR-cube system described in Chapter 5.1 is not possible, because the FT-IRs rely on different output numbering systems. Therefore, the signal-to-noise ratio (SNR) is used to compare the sensitivity of the Bio-Rad system operated once at 180 ºC and another time at 50 ºC and the IRcube at 50 ºC. Methane was the test gas and in the case of the Bio-Rad, a custom blend of 100 ppm form AGA was used. In the case of the IRcube, the methane measurement at 1000 ppm was used. The Bio-Rad system reached an SNR of 139 at 50 ºC, 30 at 180 ºC and the IRcube 95 at 50 ºC. Whereby, the amount of averaged scans was equal for all measurements, but the mirror velocity and resolution were different. The Bio-Rad ran at 2.5 kHz and 8 cm^{-1} and the IRcube at 1.6 kHz and 4 cm^{-1}. The comparison of both the systems at 50 ºC is therefore not straightforward. The main reason why the IR-cube system has a lower SNR is that in addition to the overworked PA detector, the aperture of the IRcube was for a best resolution of 1 cm^{-1} and for the Bio-Rad 4 cm^{-1}, i.e., the Bio-Rad probably had a higher light throughput. Comparing the Bio-Rad system at 50 and 180 °C, it turns out that the 180 °C system was 4.6 times less sensitive. The performance can also roughly be compared by the measurement time, since the IRcube and the Bio-Rad systems are approximated to reach ppm detection limits. The ratio of the measurement time is √(60 x 8.5 / 30) = 4.1, which is not too far from 4.6. The reasons for the lower SNR at 180 °C are mainly the higher noise level besides the lower signal due to fewer analyte molecules in the cell. The higher noise came mainly from the vibration isolation, which did not work anymore optimally at 180 °C. The vibration isolation was realized with gel dampers, where the cell was placed onto. The gel dampers were capable of operating at >180 °C, but their damping capability decreased with the temperature in combination with the weight of the PA cell. Because the mass of the cell was not equally distributed on the dampers, the PA cell also got a little tilt, which could have further reduced the performance.

Table 5. The detection limits of all 18 VOCs for uni- and multivariate data analysis.

	Univariate data analysis			**Multivariate data analysis**
	Wavenumber of signal [cm^{-1}]	Signal intensity [arb. ppm^{-1}]	Detection limit (3σ, 8.5 min) [ppm]	Detection limit (3σ, 8.5 min, single-compound) [ppm]
Acetone	1744	4.02×10^{-1}	3.8	0.56
Ethanol	1053	1.08×10^{-1}	14.3	1.7
Isobutanol	1042	2.21×10^{-1}	7.0	0.84
Isopropanol	2978	1.73×10^{-1}	9.0	1.00
Methanol	1057	1.59×10^{-1}	9.7	1.5
n-Butanol	2943	2.07×10^{-1}	7.5	0.82
Tetrachloroethylene	910	5.61×10^{-1}	2.8	0.84
Methoxypropanol acetate	1242	1.12	1.4	0.33
Methyl acetate	1246	8.18×10^{-1}	1.9	0.37
Methyl ethyl ketone	1744	2.16×10^{-1}	7.2	1.2
Methyl isobutyl ketone	1724	2.68×10^{-1}	5.8	0.84
o-Xylene	2940	6.71×10^{-2}	23.1	1.7
m-Xylene	2940	6.71×10^{-2}	23.1	1.9
p-Xylene	1508	7.33×10^{-2}	21.1	1.9
Dimethylformamide	1724	7.27×10^{-1}	2.1	0.51
Dichloromethane	1277	1.21×10^{-1}	12.7	2.6
Butyl acetate	1234	1.16	1.3	0.31
Toluene	3040	1.00×10^{-1}	15.5	1.8

5.2.3.3 Multivariate data analysis

The 18 VOCs measured in this work were selected because they typically occur in industrial emissions. However, not all the selected VOCs occur together. Depending on the industrial sector and process, some of them can be found in the emission stream. Therefore the multi-compound detection limit and the cross-selectivities were not assessed for all VOCs than rather for a case study.

Multivariate data analysis and calibration were carried out by an SBC and as analyte signal, the response spectra *g* were used in the range of 500–4000 cm^{-1}.

For the single-compound analysis that was performed first, the noise matrix $\Sigma_{\text{single-compound}}$ contained only the multivariate instrument noise and no interference noise. The multivariate instrument noise is the standard deviation of each spectral point of three nitrogen spectra calculated over the whole spectral range. The noise spectrum was rather peaky, because only three spectra were used. Therefore, the noise spectrum was smoothed with the "rloess" filter in Matlab™ and a span of 1000. The single-compound multivariate detection limits are shown in Table 5 in the column titled "Multivariate data analysis". The improvement in the detection limit varied from the worst factor of 3.3 for tetrachloroethylene to the best of 13.2 for o-xylene when compared to univariate data analysis. The spectrum of tetrachloroethylene shows only one fine absorption band, which is the reason for the small improvement in the detection limit, as shown graphically in Article II.

For the multi-compound case study, the noise matrix $\Sigma_{\text{multi-compound}}$ included the instrument noise and the interference noise of the other analytes. In addition, an offset noise of 2×10^{-3} was added to correct the slight difference in the baseline. The multi-compound calibrations were optimized for selectivity and water was added as another interferent to $\Sigma_{\text{multi-compound}}$, to minimize the interference of water vapor.

The gases for the multi-compound case study were acetone, tetrachloroethylene, methyl isobutyl ketone, dimethylformamide and methanol. The selection of the VOCs was done based on an industrial example and because of their spectra overlap particularly as shown in the response spectra plot in Figure 14. For this reason, not very good cross-selectivity numbers were expected. However, only methyl isobutyl ketone and methanol had an unpromising sum of the cross-selectivity numbers of ~0.1 ppm ppm^{-1} as shown in Table 6. The other analytes tetrachloroethylene, acetone and dimethylformamide had an acceptable average sum of the cross-selectivity numbers of 3.10×10^{-2} ppm ppm^{-1}. The average of the individual cross-selectivity pairs is 1.47×10^{-2} ppm ppm^{-1}. The cross-selectivity of water is on an intermediate level with an average number of 1.03×10^{-3} ppm ppm^{-1}. The multivariate multi-compound detection limits worsen on average by a factor of 1.5 compared to single-compound as shown in Table 7.

The achieved figures of merit are adequate for some applications, although the two high cross-selectivity numbers of ~0.1 ppm ppm^{-1} for methyl isobutyl ketone and methanol need to be decreased to the level of the other ones. Before optimizing any other parameter, the high noise in the spectra should be removed, because it prevents better cross-selectivities. In other words, the calibration "interprets" the noise as many small analyte bands. These "noise bands" in turn affect the calibration and the calculation of the cross-selectivities. The methanol and methyl isobutyl ketone regression vectors are noisy, as can be seen in Figure 15. Therefore, reduction of the spectral noise of the heated setup will not only improve the sensitivity, but also the cross-selectivity.

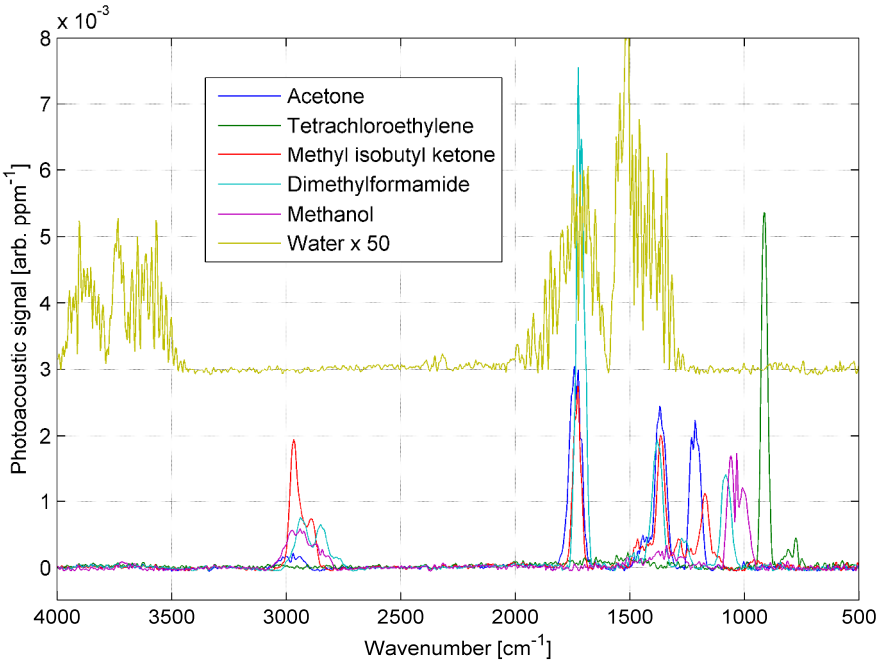

Figure 14. Response spectra *g* of the analytes and water. The water response spectrum is magnified 50 times and plotted with an offset of 3 x 10^{-3} arb. ppm^{-1}.

Table 6. Cross-selectivities (500–4000 cm^{-1}, 8.5 min) in [ppm ppm^{-1}] of the individual analytes, water and in sum. For instance, if acetone's concentration increases by 100 ppm, then it affects the tetrachloroethylene reading by -1.14 ppm.

	Interferent →						
Analyte ↓	Acetone	Tetrachloroethylene	Methyl isobutyl ketone	Dimethylformamide	Methanol	Water	Sum
Acetone	0.99	-1.11×10^{-2}	7.35×10^{-3}	4.32×10^{-4}	1.69×10^{-2}	-5.78×10^{-5}	3.58×10^{-2}
Tetrachloroethylene	-1.14×10^{-2}	1.00	-6.59×10^{-3}	-3.10×10^{-5}	9.38×10^{-3}	5.02×10^{-4}	2.79×10^{-2}
Methyl isobutyl ketone	2.83×10^{-3}	-1.62×10^{-2}	0.99	-7.14×10^{-2}	-4.65×10^{-3}	3.11×10^{-3}	9.81×10^{-2}
Dimethylformamide	4.78×10^{-3}	9.58×10^{-5}	-2.07×10^{-3}	1.01	-2.00×10^{-2}	-2.32×10^{-3}	2.93×10^{-2}
Methanol	-6.91×10^{-3}	1.01×10^{-2}	-1.51×10^{-2}	-6.64×10^{-2}	1.01	3.90×10^{-3}	1.02×10^{-1}

Table 7. Comparison of the multivariate detection limits of the analytes. Single-compound denotes the situation when only the analyte of interest is present in the sample and multi-compound when all other analytes and water interfere.

	Detection limit (3σ, 8.5 min) [ppm]	
	Multivariate, single-compound	Multivariate, multi-compound
Acetone	0.56	1.2
Tetrachloroethylene	0.84	0.96
Methyl isobutyl ketone	0.84	1.5
Dimethylformamide	0.51	0.71
Methanol	1.5	1.9

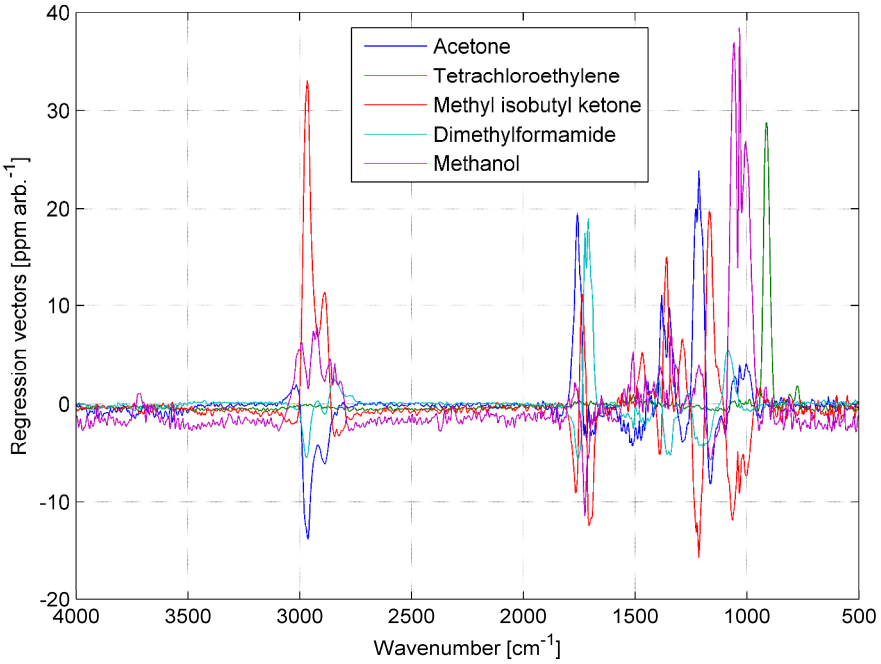

Figure 15. Regression vectors *b* of the analytes for the multi-compound calibration.

5.2.3.4 Water subtraction

Water is a major challenge in mid-IR spectroscopy, because of its broad and intense absorption bands that interfere with analyte bands. For that reason, the water features need to be removed from the measured spectrum before quantitative analysis, for example, can be carried out. The objective of this study is to prepare analyte water mixtures, set up a calibration that subtracts the water features and calculates the analyte concentration correctly. Methyl ethyl ketone (MEK) was chosen as the analyte, because it has four absorption bands, two overlapping and two non-overlapping with water bands as shown in Figure 16. MEK's concentration was kept constant at 200 ppm during the whole experiment, while the water concentration was successively increased to 1400, 4200, 12 000, 35 000 and 100 000 ppm. An SBC was set up, with MEK as the analyte and water as the interferent. For calibration, the response spectrum of MEK calculated from the 100 ppm spectrum was taken and the noise matrix Σ contained the instrument noise and the interference noise of water. The response spectrum of water used as interferent was measured at 10 000 ppm. For comparison purposes, a calibration without the interferent water was calculated. The measured spectra were multiplied with the regression vectors of both calibrations and the results are shown in Table 8.

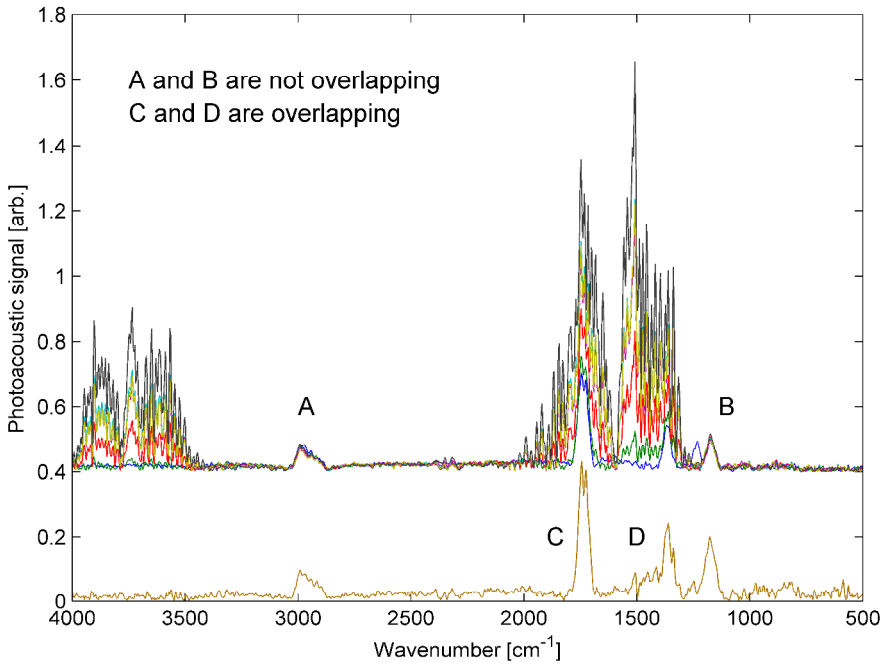

Figure 16. *Bottom:* Pure methyl ethyl ketone (MEK) spectrum at 200 ppm. *Above:* Spectra of MEK at 200 ppm mixed with different amounts of water varying from 1400 to 100 000 ppm.

Table 8. Calculated MEK concentrations with and without water subtraction.

MEK concentration [ppm]	Water concentration [ppm]	Calculated MEK concentration [ppm]	
		Without subtraction	With subtraction
200	1400	242	203
200	4200	339	198
200	12 000	482	199
200	35 000	455	188
200	100 000	648	198

Clearly, if the water features are not subtracted, the calculated MEK concentration increases with an increasing water concentration. However, with the subtraction the calculated concentrations scatter at around 200 ppm. The accuracy of the calculated values is good, which confirms the function of the subtraction method. However, the precision is rather poor with a coefficient of variation of 3%. The variation of the calculated MEK concentration does not come from the subtraction. The origin is the time-wise instable MEK feed of the experimental setup. This can be proven by calculating the coefficient of variation of the non-overlapping band A between 2900 and 2950 cm^{-1}, which is 3.7%.

5.2.3.5 Future system improvements

The performance of the built FT-IR-CEPAS measurement system operating at 180 ºC did not reach the state of the art. The main cause for that was the non-optimal vibration damping of the cell at 180 ºC, that resulted in a high noise level, a tilt of the cell and thus non-optimally aligned optics. Consequently, the most crucial point is to improve the vibration damping at 180 ºC. By that, the noise level can be reduced and the optical alignment assured. With correct damping, it should be possible to reduce the noise to the noise level of the IRcube system. If so, the performance of the system will improve by a factor of ~4, i.e., it reduces the measurement time by a factor of ~16 to a reasonable measurement time. Finally, a reduction in noise will also facilitate the improvement of the cross-selectivities.

After that, improvements of a lower priority can be considered. The resolution of the FT-IR was 8 cm^{-1}, but the maximal aperture was for a best resolution of 4 cm^{-1}. Thus, by selecting a low-resolution FT-IR, the performance may be further increased, as already discussed for the IRcube in Chapter 5.1.3.4. The oven was already built in a compact manner (approx. 200 x 300 x 400 mm LxWxH), which enables a portable measurement system if a smaller FT-IR, for example the IRcube is chosen. Finally, the heated CEPAS system built here can also be combined with other types of light sources.

From the mechanical point of view, a progress in the oven can be made by further miniaturization. In general, smaller components and a smaller system require less space and material, which speeds up heating and reduces the necessary heating power. The whole sampling system might be built from one metal block, which would improve the heating performance. The corrosion resistance can also be advanced, because not all parts were available in SS316 or with Silcosteel coating.

5.3 Summary and outlook

Two novel FT-IR-CEPAS measurement systems are reported. One was compact and robust for industrial measurements by using Bruker's IRcube FT-IR. This system reached multivariate single-compound detection limits (3σ, 25 s) of best 2.2 ppm for methane and propene and worst 6.7 ppm for carbon dioxide. In a multi-compound calibration, the detection limits became worse by only a factor of 1.4 on average. The average of the cross-selectivity numbers was found to be 9.55×10^{-3} ppm ppm^{-1} and the interference of water could be kept at around 1.81×10^{-3} ppm ppm^{-1}.

The other FT-IR-CEPAS was a laboratory system, where all parts in contact with the sample gas including the PA cell and the cantilever were heated to 180 ºC. The direct measurement of the sample at higher temperatures is novel and was enabled by the cantilever microphone. Although the optical read-out of the cantilever is at ambient temperature, the pressure transducer, the cantilever, sits inside the heated PA cell, which makes previously used signal tubes and cooling of the gas redundant. This system reached multivariate single-compound detection limits (3σ, 8.5 min) of best 0.3 ppm for butyl acetate and worst 2.6 ppm for dichloromethane. In a multi-compound calibration of five heavily overlapping VOCs, tetrachloroethylene, acetone and dimethylformamide had an acceptable sum of the cross-selectivity numbers of 3.10×10^{-2} ppm ppm^{-1} and methyl isobutyl ketone and methanol had an unpromising sum of the cross-selectivity numbers of ~0.1 ppm ppm^{-1}. The cross-selectivity of water was at an intermediate level with an average number of 1.03×10^{-3} ppm ppm^{-1}. The multivariate multi-compound detection limits worsens on average by only a factor of 1.4 compared to multivariate single-compound. The subtraction of water features from spectra of a mixture of methyl ethyl ketone and water was successfully demonstrated. The water concentration ranged from 1400 to 100 000 ppm and the subtraction was carried out with an SBC, resulting in accurate analyte readings.

Still, the built system did not reach the state of the art, mainly because of the non-optimal vibration damping of the PA cell at 180 ºC resulting in a high noise level. A univariate comparison of the Bio-Rad system operating at 50 and 180 ºC resulted in a factor of 4.6 better SNR at 50 ºC, which can be explained by the vibration damping. Further, the SNR of the Bio-Rad system at 50 ºC was better by a factor of 1.5 than the IRcube system, which is mainly due to the lower resolution of 8 cm^{-1} compared to the 4 cm^{-1} of the IRcube and the overworked PA detector.

In both cases, the improvement of the FT-IR will increase the system performance.

FT-IR-CEPAS is a valuable tool for gas measurements down to the ppm level. With further improvements in the PA detector and the FT-IR, possibly sub-ppm levels might be reached within reasonable measurement times, but much better detection limits are not possible. For better sensitivity, more powerful light sources need to be selected, as done in the next two chapters. Still, the FT-IR-CEPAS is a valuable tool for multi-compound gas measurement above and down to the ppm level. Many industrial applications of this kind exist, where multi-compound gas analysis is required. The heated setup needs to be made more stable and further engineered from the laboratory to an industrial setup. Then, the heated measurement system can also become a valuable tool for high temperature industrial gas analysis.

6. Sub-ppb detection of formaldehyde using quantum cascade laser (QCL)

This chapter presents the work published in Article III.

6.1 Background

One conclusion drawn in the previous chapter is that FT-IR-CEPAS cannot reach significantly better detection limits as sub-ppm within a reasonable measurement time. However, many VOC measurement applications require better detection limits, at ppb and even at ppt levels. The optical cantilever detector is quite well optimized and in an ideal case only limited by the Brownian noise and background signal instability [72–74]. Therefore, mainly a more powerful light source can improve the sensitivity of the measurement system. Diode lasers emitting in the near-IR have shown to be powerful light sources for spectroscopy [31,35,60], PAS [17,30,34,41,99,146,147] and CEPAS [89,105,110–113]. They are commercially available, of compact size and inexpensive [114]. The absorption coefficients, however, are typically two magnitudes higher in the mid-IR compared to near-IR [31]. Therefore, the idea of this work was to improve the sensitivity by using a mid-IR QCL as the light source. QCLs have been reported to be suitable light sources for trace gas analysis used in other fields of spectroscopy and PAS [21,23,29,35]. A combination of CEPAS and QCL has never been set up before, although a QCL was once proposed as a light source for the differential method by Uotila in [115]. Following, the first QCL-CEPAS measurement system is introduced and its performance tested by the trace gas measurement of formaldehyde.

Formaldehyde was chosen for this measurement application, because its detection at ppb and even ppt level is required in many measurement applications. Formaldehyde has, as already discussed in Chapter 2.3 for VOCs in general, adverse effects on environment and nature, but the main concern is the effect of formaldehyde on human health. Exposure to formaldehyde causes discomfort, irritation of eyes, nose, and throat, sneezing, coughing, and at high concentrations formaldehyde is lethal [148–151]. Further, formaldehyde is a mutagen, possibly carcinogen and accounts for the ‘‘sick building syndrome’’ [151]. The most prevalent form of exposure is via inhalation, but also via the oral or dermal route [152].

Despite these known adverse health effects, formaldehyde is still utilized in industry and also a number of products used in everyday life contain formaldehyde [151]. In industry, formaldehyde is a commonly used chemical and even necessary in the manufacturing of some products, such as plastic and resins. Formaldehyde measurement applications in industry contain process and emission measurements and range from ppb to percent. Household furniture, detergents, textile materials, paints and many other products have been in contact with formaldehyde during their production and thus still contain some formaldehyde [151]. Over time, these commodities release formaldehyde to the indoor and urban air. Typically, urban air contains 3–25 ppb of formaldehyde, normal indoor air 10–80 ppb and polluted indoor air 80–300 ppb [151]. The occupational health limit for 8 h exposure in Finland is 0.37 mg m^{-3} (~300 ppb) [153] and 200 ppb according to the International Labour Organization. No general replacement for formaldehyde has been found so far and its usage will continue for now.

In addition to the applications listed above, formaldehyde measurement is also required in diagnostics, for example breath gas analysis. Breast and lung cancer, for example, may be detected by elevated formaldehyde levels in the breath. [22,23,154] The required sensitivity in diagnostics ranges between ppt and ppb.

As a result, reliable and accurate formaldehyde measurement technology is needed and potential applications are found in industrial emission and process gas measurement, environmental monitoring, indoor and urban air quality monitoring as well as in diagnostics.

6.2 Experimental

6.2.1 Measurement setup

The measurement system was arranged on a Breadboard, although the components used were already assembled as modules. The cantilever-enhanced detector (Gasera PA201) module contained the photoacoustic cell including the cantilever, the readout optics and the digital signal processing (DSP) as well as the gas exchange system. The gas exchange system drew the sample gas into the PA cell and conditioned the sample to the desired temperature and pressure. The photoacoustic cell was operated in non-resonant mode had a cylindrical shape with a length of 95 mm and a diameter of 4 mm and was made from aluminum. The dimensions of the cantilever were 5 x 1.2 x 0.01 mm (LxWxH). The cell window material was BaF_2 and both the cell and the cantilever were coated with gold.

The light source module was based on the QCL mounting fixture (ILX Lightwave LDM 4872) and was equipped with a continuous wave (CW), DFB QCL. The QCL was acquired from III-V lab and is tunable over 1772–1777 cm^{-1} at 18 °C, to which the temperature of the chip was set with the thermoelectric temperature controller (Newport Model 350) and water cooling. The current for the laser was supplied by the laser current driver (ILX Lightwave LDX-3232). The laser beam was collimated by an aspheric lens sitting in the QCL mounting and conducted

through the photoacoustic cell. An aperture, placed in front of the PA cell, limited the laser beam to 4 mm, i.e. to the same diameter as the PA cell. In amplitude modulation (AM) operation, a tuning fork chopper was placed in between the aperture and the PA cell. After passing the PA cell, the transmitted power was registered by a laser power meter (Thorlabs S302C).

The third and final module was the data management and acquisition system. It set the parameter for the laser tuning to the laser current driver and red the microphone signal from the DSP unit. The time domain signal from the microphone, which is proportional to the cantilever movement, was transformed to frequency domain via FFT (power spectrum). The amplitude of the photoacoustic signal was recorded at the modulation frequency simultaneously with the laser current. Since the laser drive current is proportional to the wavelength of the laser, the photoacoustic spectrum could be formed. An illustration of the measurement setup is shown in Figure 17.

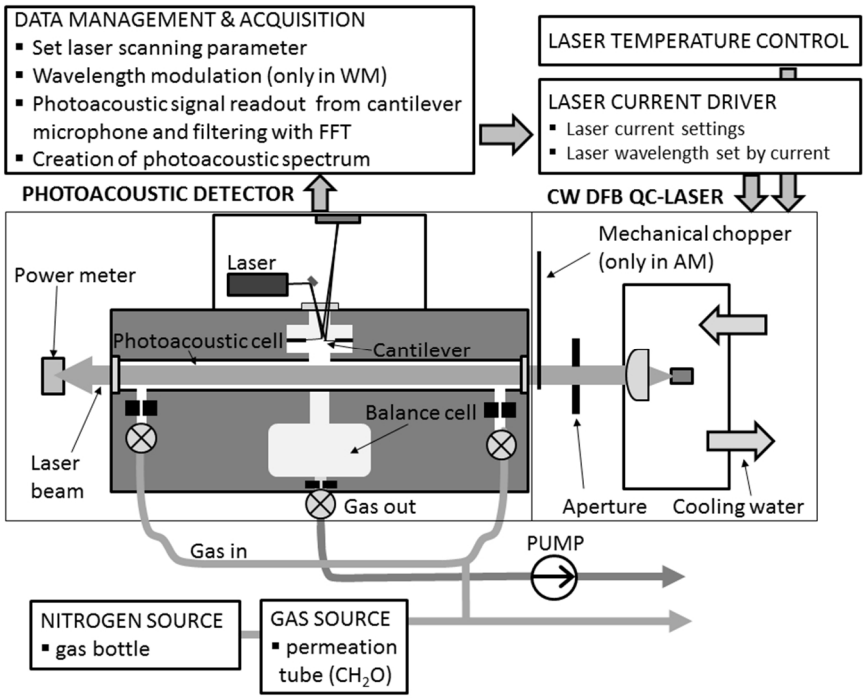

Figure 17. Illustration of the QCL-CEPAS measurement setup (reprint from Article III, with the permission from Springer).

6.2.2 Measurement parameters

To compare the performance of the system in amplitude and wavelength modulation (WM), the measurements were carried out with both modulation techniques.

In AM, the tuning fork chopper was operated at 135 Hz. The modulation frequency in WM was 70 Hz, with a triangular waveform and the signal was recorded at the second harmonic ($2f_{mod}$) at 140 Hz. The measurement time of a single measurement was 0.951 s. The temperature of the PA cell and of the sample was set to 50 °C and the sample gas pressure inside the PA cell to 350 mbar.

6.2.3 Gas supply

The formaldehyde (CH_2O) gas feed was prepared by a permeation tube system (Kin-Tek FlexStream™ Gas Standards Generator). The concentration of formaldehyde was adjusted to 2 ppm and as dilution gas, pure nitrogen (AGA, 5.0) was used. Special attention was paid to the sampling and the sampling system, because formaldehyde quickly adsorbs on surfaces. For this reason, the PA cell was heated to 50 °C, all tubing was designed as short as possible and when filling the PA cell with analyte gas, long purge times of approx. 10 min were observed.

6.3 Results and discussion

6.3.1 Noise characterization of the measurement system

The noise characterization of the system was done in AM, to include also the background signal instability. The PA cell was filled with nitrogen up to 350 mbar. The signal was recorded over about 2 mins with a single measurement time of 0.951 s. Seven of these records were performed, each with a different laser power, i.e. laser current, varying from 1.6 to 43.3 mW. The record measured at 450 mA laser current and 2.8 mW laser power is shown in Figure 18. As can be seen from Figure 18, the signal increases over the course of the record. The signal increase can be explained by water molecules desorbing from the cell interior into the gas phase and thus creating a photoacoustic signal. Although none of the noise measurements was carried out at the center of a water absorption band, the absorption coefficients on the tails are still sufficient to generate a photoacoustic signal. The signal increase caused by water is not noise. Therefore, to characterize the noise of the measurement system only, the water caused signal was subtracted. The true variation in the nitrogen signal is the residual of the record after the subtraction of its 4^{th} order polynomial fit. The 4^{th} order polynomial fit as well as the residual is shown in Figure 18. For each residual record, the standard deviation was calculated in blocks of 10 successive record values, giving 12 standard deviation values per record. This was done to avoid water subtraction residuals influencing the standard deviation value. The final noise value is the average of the 12 standard deviation values of each record. Figure 19 shows the calculated noise and the background signal over the laser power. The first value measured of each record was selected as the background signal.

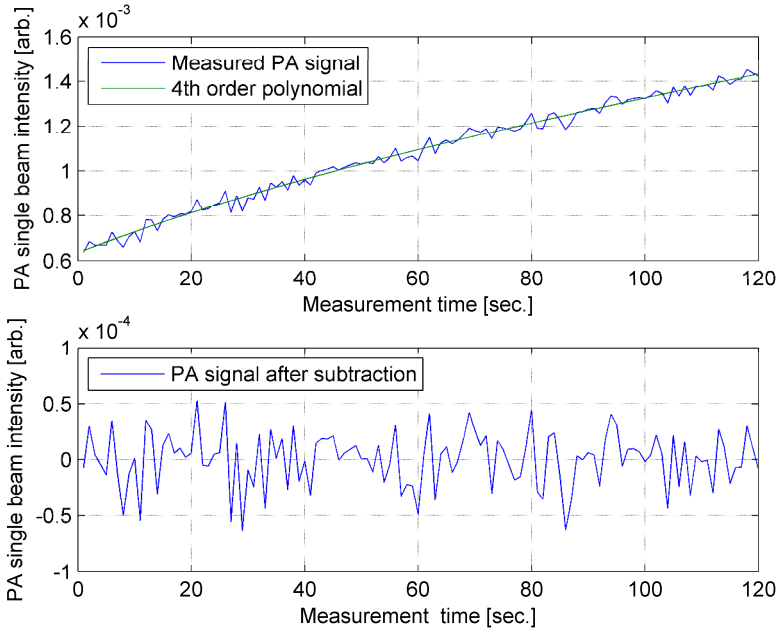

Figure 18. *Upper graph:* Record of the photoacoustic signal at 450 mA laser current and 2.8 mW laser power with the PA cell filled with nitrogen and its 4th order polynomial fit. Water molecules desorbing from the cell interior increasing the PA signal over time. *Lower graph:* Residual signal after subtraction of the 4th order polynomial fit (reprint from Article III, with the permission from Springer).

The noise sources in CEPAS are: acceleration noise, acoustical noise, electrical noise, background signal instability and the ultimate limiting Brownian noise [72–74]. As already stated in the introduction of this chapter, the primary noise sources are the Brownian noise and the background signal instability, because the electrical noise is below the level of all other noise sources [73] and acceleration and acoustical disturbances from the surroundings can usually be eliminated [73,74]. Acceleration noise is eliminated by a proper vibration damping of the PA cell, selecting a modulation frequency higher than the resonance frequency of the vibration dampers and the use of the balance cell geometry as described in [72–74]. Acoustical noise is eliminated by an appropriate system design with thick PA cell walls and by preventing the sound transmission from the rest of the instrument to the PA cell. In practice, these methods work well, because no acceleration and acoustical noise was observed during the measurements. Figure 20 shows the frequency spectrum of two measurements, one with the laser in operation and the other with the laser switched off. No peaks other than the signal and the cantilever resonance occurring at ~715 Hz, are present.

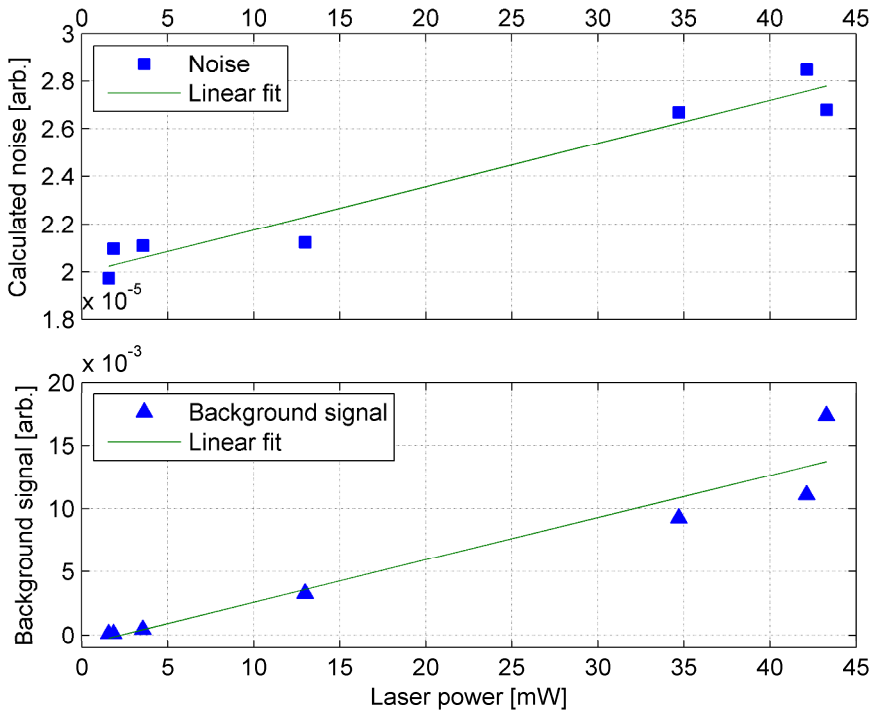

Figure 19. The calculated noise and the measured background signal as function of the laser power (reprint from Article III, with the permission from Springer).

The walls and windows of the photoacoustic cell as well as dust particles inside the cell can absorb light and cause an unwanted photoacoustic signal, the so-called background signal. The variation of the background signal over time is called the background signal instability and sometimes the term background noise is used in the literature instead [34]. The sources of the background signal instability are variations in the light source intensity and the precision of the cantilever read-out. For laser light sources, the variation in intensity is described by the relative intensity noise of the laser, which is a sum parameter of different individual noise sources [155,156]. As shown in Figure 19 the noise in this work shows a general offset (regression line ordinate intercept), the so-called noise floor, with a value of 1.99 x 10^{-5}. The noise floor is due to the Brownian noise, which was verified by measurements with the QCL turned off. The noise above the floor is background signal instability, which increases with the power.

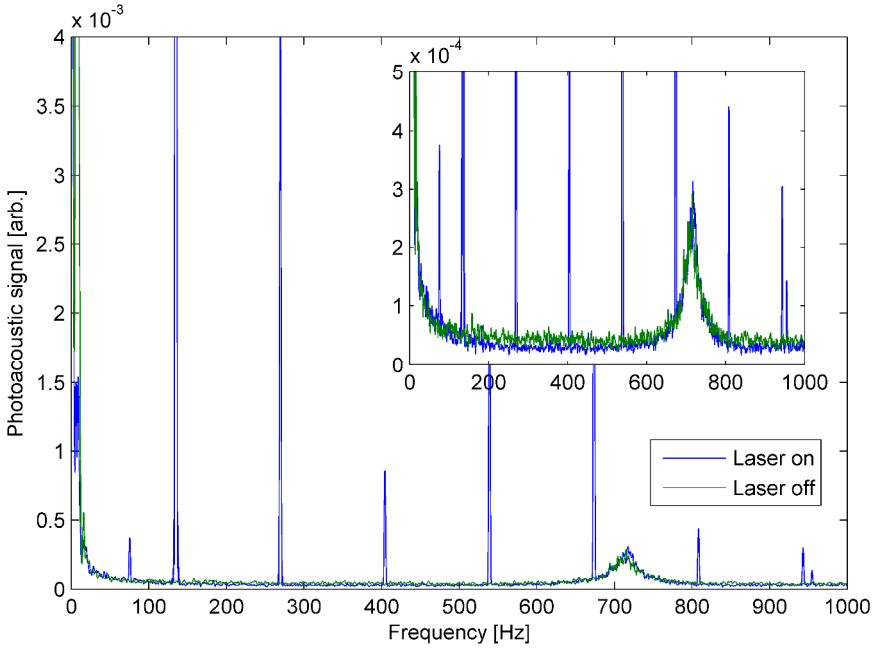

Figure 20. Frequency spectrum of the measured PA signal [arb.] with the laser in operation and when switched off.

6.3.2 Univariate data analysis

6.3.2.1 Amplitude modulation

The photoacoustic spectrum of formaldehyde was measured from 1772 to 1777 cm^{-1} by tuning the laser in steps of 0.018 cm^{-1}. For verification, the measured formaldehyde spectrum is compared to the formaldehyde spectrum modeled with HITRAN [157] at 350 mbar and 323.15 K. Both spectra, the measured and the modeled one, are shown in Figure 21. The absorption band shape and the band intensities of the two spectra match if the instrument response curve of the QCL-CEPAS system is taken into account. The response in mainly influenced by the emitted laser power, which increases with decreasing wavenumber as shown in Figure 21. The band positions match for most of the bands, but some show slight deviations due to the partially non-linear wavelength tuning of the laser. In the measured spectral region, two water absorption bands occur at approx. 1772.71 and 1775.63 cm^{-1} as also shown in Figure 21. The water bands occurring in the measured formaldehyde spectrum were subtracted by means of a measured water spectrum.

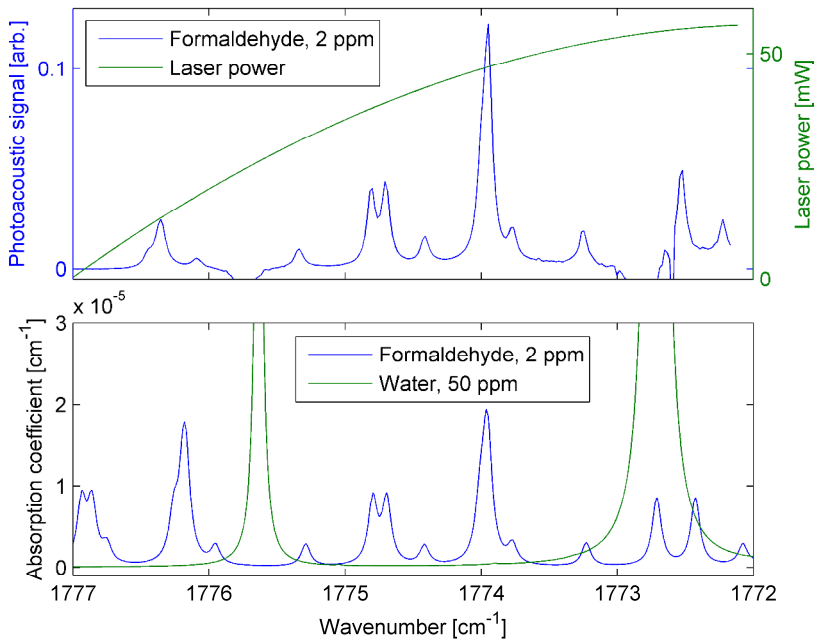

Figure 21. *Upper graph:* Measured formaldehyde spectrum with the subtracted water bands and the laser power emission curve. *Lower graph:* Modeled absorption coefficient spectrum of 2 ppm formaldehyde and 50 ppm water at 350 mbar and 323.15 K (reprint from Article III, with the permission from Springer).

The background corrected formaldehyde band at 1773.959 cm^{-1} was selected for the univariate calculation of the figures of merit. In the case of AM, the noise *N* was calculated from the noise regression line in Figure 19 at a laser power of 47 mW, which corresponds to the wavelength of 1773.959 cm^{-1} at which the analyte band sits. The signal-to-noise ratio SNR [-], the detection limit DL [ppb], the minimum detectable absorption coefficient α_{min} [cm^{-1}] and the NNEA [W cm^{-1} $(Hz)^{-1/2}$] (all 3σ) are calculated with the following equations:

$$\mathrm{SNR} = \frac{S}{3\,N} \tag{10}$$

$$\mathrm{DL} = \frac{c}{\mathrm{SNR}} \tag{11}$$

$$\alpha_{min} = \frac{\alpha}{\mathrm{SNR}} \tag{12}$$

$$\text{NNEA} = \alpha_{min} P \sqrt{t} \quad (13)$$

where *S* is the measured photoacoustic signal [arb.], *N* the calculated noise [arb.], *c* the formaldehyde concentration [ppb], *P* the power emitted by the laser [W] and *t* the measurement time [s].

The parameters used for the calculation, the resulting detection limit and the NNEA are shown in Table 9 in the column titled "AM". The achieved detection limit (3σ, 0.951 s) is 1.6 ppb and the NNEA (3σ) reached is 7.32 x 10^{-10} W cm^{-1} $(Hz)^{-1/2}$.

Table 9. Parameters, detection limit and NNEA for the formaldehyde measurement in amplitude modulation (AM) and wavelength modulation (WM) (reprint from Article III, with the permission from Springer).

	AM	**WM**
Laser power, *P* [mW]	47.0	47.0
Formaldehyde concentration, *c* [ppm]	2.00	2.00
Wavenumber, *v* [cm^{-1}]	1773.959	1773.959
Signal, *S* [arb.]	0.105	0.089
Noise (1σ), *N* [arb.]	2.85 x 10^{-5}	1.99 x 10^{-5}
Measurement time, *t* [s]	0.951	0.951
Signal-to-noise ratio (3σ), SNR [-]	1225	1486
Detection limit (3σ), DL [ppb]	1.6	1.3
Absorption path length, *l* [cm]	9.50	9.50
Absorption coefficient (2 ppm, 350 mbar, 323.15 K), *α* [cm^{-1}]	1.96 x 10^{-5}	1.96 x 10^{-5}
Minimum detectable absorption coefficient (3σ), α_{min} [cm^{-1}]	1.60 x 10^{-8}	1.32 x 10^{-8}
Minimum detectable optical density (3σ), $\alpha_{min} l$ [-]	1.52 x 10^{-7}	1.25 x 10^{-7}
NNEA (3σ) [W cm^{-1} $(Hz)^{-1/2}$]	7.32 x 10^{-10}	6.04 x 10^{-10}

6.3.2.2 Wavelength modulation

In WM, the spectrum of formaldehyde was also measured from 1772 to 1777 cm^{-1} in steps of 0.018 cm^{-1}, with a modulation amplitude of 0.15 cm^{-1}, i.e., a modulation index of 1.5 for the 1773.959 cm^{-1} band. Figure 22 shows the formaldehyde spectrum measured in WM.

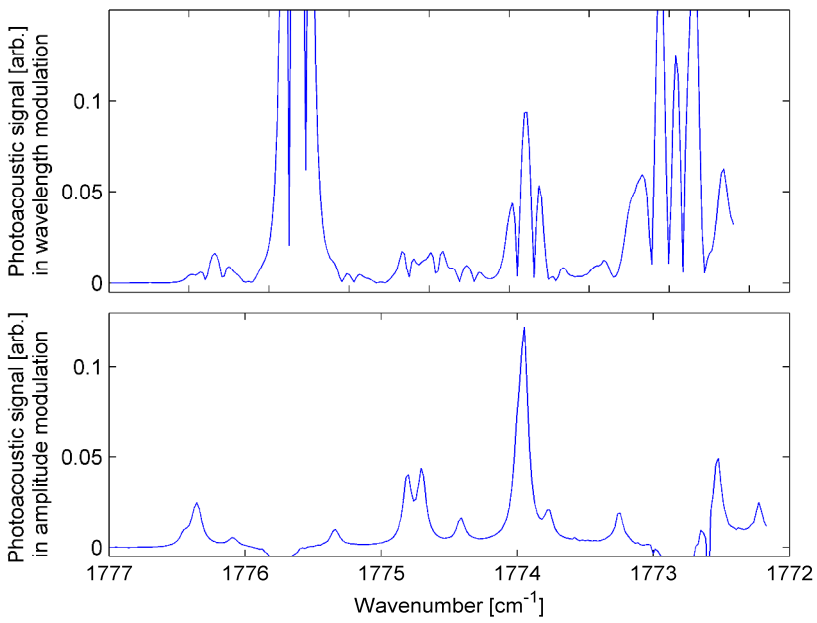

Figure 22. *Upper graph:* Formaldehyde spectrum measured in WM at 2 ppm. *Lower graph:* Formaldehyde spectrum measured in AM at 2 ppm, printed here again to facilitate the comparison with the WM spectrum (reprint from Article III, with the permission from Springer).

The same absorption band was used for the calculation of the figures of merit in WM than for AM. However, no background and no water subtraction were necessary. Due to the absence of the background signal and consequently the absence of background signal instability, the noise *N* in case of WM was taken from the ordinate intercept of the noise regression line in Figure 19. The parameters used for the calculation, the resulting detection limit and the NNEA are shown in Table 9 in the column titled "WM". The achieved detection limit (3σ, 0.951 s) is 1.3 ppb and the NNEA (3σ) reached is 6.04 x 10^{-10} W cm^{-1} $(Hz)^{-1/2}$.

In WM, the achieved detection limit and NNEA are better than in AM by a factor of 1.2. The absence of the background signal in WM reduces the noise *N* compared to AM, which results in better figures of merit. Still, the WM technique can be optimized by adjusting the modulation index. The signal in WM was, indeed, lower than in AM, which comes from the fact that a part of the $2f_{mod}$ signal is redistributed to higher harmonics at a modulation index of 1.5. The maximal signal in the second harmonic for triangular modulation is achieved with a modulation index of 2.8 according to Iguchi [158] and 3.0 to Saarela et al. [159].

6.3.3 Multivariate data analysis

As already introduced in the previous chapters, multivariate data analysis improves the performance of the measurement system if the analyte absorption band extends over more than one data point. By means of the SBC and multivariate data analysis, the detection limit (3σ) for WM is 623 ppt (1773.743–1774.265 cm^{-1}, 30 spectral points each 0.951 s) and for AM 901 ppt (1773.833–1774.085 cm^{-1}, 15 spectral points each 0.951 s). However, for univariate measurement systems such as the QCL-CEPAS, the measurement time increases when multivariate data is acquired. Assuming that the spectral point with the maximal quotient of absorption coefficient and noise was selected for the univariate data analysis, then the multivariate data analysis cannot improve the detection limit scaled on time. By spending the same measurement time at the spectral point with the highest quotient of absorption coefficient and noise, the estimated detection limit for WM is 237 ppt (1773.959 cm^{-1}, 30 readings each 0.951 s) and for AM 413 ppt (1773.959 cm^{-1}, 15 readings each 0.951 s). As a result, multivariate data analysis is only justified if a particular reason calls for it and a common case is the spectral interference in a multi-compound sample.

6.3.4 Future system improvements

Possible improvements of the measurement system are assessed hereafter:

1. The modulation index can be optimized and a different wavelength modulation waveform can be selected. According to Iguchi [158] and Saarela et al. [159] the $2f_{mod}$ signal can be maximized with the quasi-square or shaped waveform. Compared to the triangular waveform used in this work, Saarela et al. reported a 1.40 and 1.27 times higher photoacoustic signal for the quasi-square and the shaped waveform, respectively [159].
2. The microphone raw signal was FFT transformed via power density calculation. A phase sensitive detection can improve the performance by a factor of √2. Reading the signal with a lock-in amplifier instead can improve the performance by another factor of √2. In sum, the improvement can be about as high as a factor of 2.
3. The QCL should be optimized to match the wavelength of the formaldehyde absorption band with the highest absorption coefficient. The highest absorption coefficient between 1620 and 1840 cm^{-1} is at 1769.466 cm^{-1} with a 1.10 times higher absorption coefficient compared to this study. In the case of AM, the Q-branch of the vibrational level sitting at 1745.826 cm^{-1} offers a factor of 1.38 larger absorption coefficient, however with an FWHM of ≈ 0.5 cm^{-1}.
4. In AM, water vapor in concentrations higher than 100 ppb disturbs the formaldehyde detection, because the formaldehyde band sits on the tail of a

water band as shown in Figure 21. The interference needs to be resolved by a second spectral measurement point. Assuming the same integration time for both points, only half of the measurement time can be spent to measure the analyte, which will decrease the performance by a factor of $\sqrt{2}$, but resolves the interference of water.

5. After the laser wavelength of the QCL is adjusted to the maximum absorption coefficient as suggested under point 3, its output power should be increased as well. Nowadays, commercially available CW DFB QCLs offer up to 300 mW of output power. Since the higher power lets the background signal rise, WM will derive a greater benefit from a more powerful light source than AM.

Assuming the case where all discussed improvements are applied, the univariate detection limit (3σ, 0.951 s) in AM can be as good as 0.36 ppb and for WM 0.07 ppb. A further advance in the detection limit can be realized by a longer measurement time.

6.3.5 Summary and outlook

In this chapter, a novel combination of mid-IR QCL and CEPAS was realized and its performance tested in the trace gas measurement of formaldehyde. The achieved univariate detection limit (3σ, 0.951 s) is 1.6 ppb and the NNEA (3σ) 7.32 x 10^{-10} W cm^{-1} $(Hz)^{-1/2}$ in AM and 1.3 ppb and 6.04 x 10^{-10} W cm^{-1} $(Hz)^{-1/2}$ in WM. In Article III, a comparison with previous studies carried out in the field of photoacoustic formaldehyde detection is made. The comparison clearly showed that the QCL-CEPAS system presented here reached at its minimum one magnitude better NNEA, even without resonant operation of the cell. The QCL-CEPAS system presented here fits in a 19” rack, is man-portable, reaches sub-ppb detection limits and can be used in industrial environments. With minor modifications, the system is ready for most of the measurement applications listed in the introduction, i.e., industrial emission and process gas measurement of formaldehyde, environmental and indoor and urban area formaldehyde monitoring, and with a longer integration time, the system can also be applied in diagnostics. With the discussed improvements, the univariate detection limit (3σ, 0.951 s) could be as low as 0.36 ppb in AM and 0.07 ppb in WM.

In the future vision, QCLs will offer higher output power while becoming cheaper, covering additional spectral regions, i.e., will be available for more gases, they may even increase in tunability, and several QCL chips may be arranged in an array. The progress in QCL technology will facilitate future trends of the QCL-CEPAS measurement system. Setups with a combination of QCL and other light sources are currently being tested and might help in multi-compound samples. QCL-CEPAS has the ability to become a standard method for trace gas analysis both in and outside the laboratory.

7. BTX analysis at ppb level using optical parametric oscillator (OPO)

This chapter presents the work published in Article IV.

7.1 Background

The request for better sensitivity was the starting point of the QCL work in the previous chapter. The built QCL-CEPAS measurement system reached superior sensitivity and measured the analyte selective. In general, the selectivity of narrow bandwidth DFB laser-based systems can be quite good and sufficient [17,19,36,160]. However, the tunability of these lasers is limited to a few wavenumbers [21,31,65,77]. In case of spectral interference or when performing multi-compound analysis, a broader spectral coverage is needed [31,35,161]. While offering a broader tunability, the optical power should not suffer, as is the case for FT-IRs. Different tunable mid-IR sources exist, but most of them are subjected to certain technical limitations. Light sources appropriate for industrial and environmental applications should offer the following performance features: wide tunability, robustness, high optical power output, low power consumption, room temperature operation and compactness, and light weight [34,162]. Optical parametric oscillators are such sources that offer a high optical output power, broader tuning range than DFB-QCLs and cover the interesting 3–4 μm region, where QCLs are still rare [21,31,114,162]. Of late, the very first OPO-CEPAS combination was built and detection limits (1σ, 1s) of 190 ppt for HCN and (1σ, 30 s) of 65 ppt for CH_4 were reported by Peltola et al. in [114]. Regardless of the performance, this system is still in a laboratory state and is not capable of operation in environmental and industrial surroundings. The novel and compact OPO from Cobolt fulfills the performance features listed above, and therefore it is a suitable light source for environmental and industrial measurement applications. Until now, it is the first commercially available OPO that comes in a compact package of 125 x 70 x 45 mm (LxWxH) and offers an optical output power of ~100 mW.

In this work, a novel small-sized measurement system based on OPO and CEPAS, suitable for industrial and environmental measurement applications was assembled. Its performance was tested in the measurement of benzene, toluene

and *p*-, *m*- and *o*-xylene (BTX). The analysis of BTX was chosen, since they pose a very demanding measurement application. Benzene, toluene, and the three xylene isomers usually occur in mixtures while having a similar molecular structure, which makes their discrimination difficult and requires multi-compound analysis.

BTX are frequently used chemicals in industry because they are chemical precursors used in many production processes and they are common solvents. Apart from the industry, BTX can also be found indoors. It typically outgases from products, cleaning agents, printings, paints and wood panels, but tobacco smoke also contributes largely to the indoor BTX concentration [14]. Besides industry and indoor air, benzene is also part of natural resources as for example crude oil and natural gas [14]. Since benzene is not completely removed during crude oil processing, the ready-made fuel still contains around 1% benzene [15]. Therefore, traffic is the main source for benzene pollution in the urban atmosphere [52,163]. Once released into the atmosphere, benzene has a long lifetime compared to toluene and xylene, due to its lower reactivity [14,164]. The environmental effects of BTX are related to global warming, ozone depletion and low level ozone formation, as already explained in Chapter 2.3. Human exposure to BTX causes problems with the nervous system as well as irritation of the skin, eyes and respiratory organs [165]. The effects visible only after the long term are damage to heredity, embryo and breeding [165]. Benzene attracts special attention, since it is carcinogenic causing e.g., leukemia [165] and therefore is considered as the most harmful BTX compound to human health. The 8 h workplace exposure to benzene is 0.5 ppm and for toluene and the xylenes 50 ppm [53]. Further, the EU proposed an annual average limit value in urban areas of 5 µg m^{-3} (~1.5 ppb) [52].

These facts and the obligation to determine the emissions give rise to the development of robust, reliable, selective and sensitive BTX measurement methods. Possible BTX measurement applications are environmental monitoring, indoor and urban air quality analysis as well as process and emission measurement in industry.

7.2 Experimental

7.2.1 Measurement setup

The experimental setup used here is almost the same as for the QCL in Chapter 6, only the light source module is replaced by the OPO module and the data acquisition module is modified to serve the OPO. Therefore, the PA detector module is not described here again.

The OPO module (Cobolt OPO™, tunable from 3237–3296 nm) contained the OPO including control unit and the thermoelectric temperature adjustment system equipped with a passive cooler. The most important parameters of the OPO are shown in Table 10. More detailed information, such as the general description, technical specifications and the performance and stability testing are reported in [162]. The collimated coherent idler beam of the OPO was conducted through the photoacoustic cell to the laser power meter (Thorlabs S302C) placed on the

other side of the PA cell. No aperture was used in this setup, because the beam diameter of 1.6 mm was smaller than the cell diameter of 4 mm. The OPO light beam was modulated at 135 Hz by a mechanical tuning fork chopper sitting in between the OPO module and the PA cell.

Table 10. Parameters of the OPO.

	Value
Wavelength [nm]	3237–3296
Optical power output [mW]	88–103, wavelength depending, see Figure 24
Bandwidth [nm]	1.3
Beam diameter [mm]	1.6
Repetition rate [kHz]	10
Pulse width [ns]	4
Pulse energy [µJ]	10

The data management and acquisition module was used to control the OPO by communicating with the OPO controller and reading the microphone signal from the DSP unit. The time domain signal from the microphone, which is proportional to the cantilever movement, was transformed to frequency domain via FFT (power spectrum) and the amplitude of the photoacoustic signal was recorded at the modulation frequency. The photoacoustic spectrum was created by combining the amplitude of the photoacoustic signal with the actual OPO wavelength provided by the OPO controller. Figure 23 shows an illustration of the measurement setup.

7.2.2 Measurement parameters

The OPO was tuned from 3237 to 3296 nm with a spectral interval of 0.1 nm. The measurement time at each spectral point was 0.951 s, resulting in a total measurement time of ~9 min for a full spectral scan. The temperature of the cell and the sample gas was adjusted to 50 °C. In this work the sample gas pressure was chosen to be 950 mbar, because the observed bands of BTX are rather broad (FWHM >50 nm).

Also here, the high resolution FT-IR reference spectra from PNNL [132] are used for modeling purposes. The PNNL spectra measured at 1013 mbar and 50 °C were chosen.

7.2.3 Gas supply

First, methane (AGA, custom blend of 10 ppm methane in nitrogen) and water vapor were measured to test the measurement system. The water vapor test gas

was prepared in a semi-quantitative way by adding ambient air to the synthetic air (AGA, 5.0), which was the dilution gas for all gas mixtures.

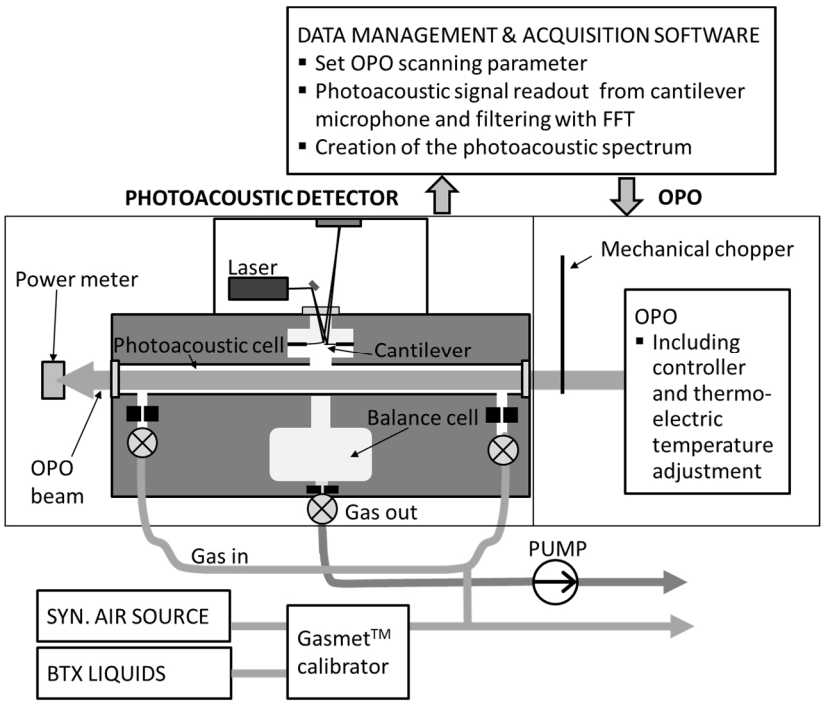

Figure 23. Illustration of the OPO-CEPAS measurement setup (reprint from Article IV, with the permission from Elsevier).

The BTX analyte gas mixtures were prepared by the Gasmet™ calibrator [145]. The calibrator uses a syringe to feed the liquid analyte into an evaporation chamber through which the synthetic air flows with a defined flow rate. The liquid analytes, all procured from Sigma-Aldrich, were benzene (anhydrous, 99.8%), toluene (anhydrous, 99.8%), *m*-xylene (anhydrous, ≥ 99%), *o*-xylene (anhydrous, 97%) and *p*-xylene (anhydrous, ≥ 99%). A design of experiments was established and it included the measurement of each analyte at three different concentrations between 0.20 to 15 ppm. There were plans to measure more diluted concentrations, but due to limitations of the Gasmet™ calibrator that was not possible in practice. The spectra measured at the following concentrations were used for calibration: benzene 10.05 ppm, toluene 9.85 ppm, *p*-xylene 14.5 ppm, *o*-xylene 8.05 ppm and *m*-xylene 9.90 ppm; and for the cross-selectivity number calculation: benzene 5.05 ppm, toluene 9.85 ppm, *p*-xylene 7.20 ppm, *o*-xylene 4.96 ppm and *m*-xylene 9.90 ppm.

7.3 Results and discussion

7.3.1 Verification of the measured data

Before the actual BTX measurement, the setup was tested with methane and water as test gases. Methane and water were chosen because of their rich rotational band spectrum in the region covered by the OPO. Figure 24 shows the measured as well as the PNNL reference spectrum of methane and water. It can be seen that the measured analyte bands occur at the same spectral position as in the reference spectra. The band intensities are a function of the instrument response curve and the OPO excitation bandwidth, and if these two are taken into account, the intensities match. The system response is dominated by the emitted laser power, which increases with longer wavelengths as shown in Figure 24, too. The shape of the measured bands is broader than the bands in the reference spectra. The reason for this is the broad (FWHM = 1.3 nm) OPO excitation bandwidth, which is moreover the limiting factor for the spectral resolution of the measurement system.

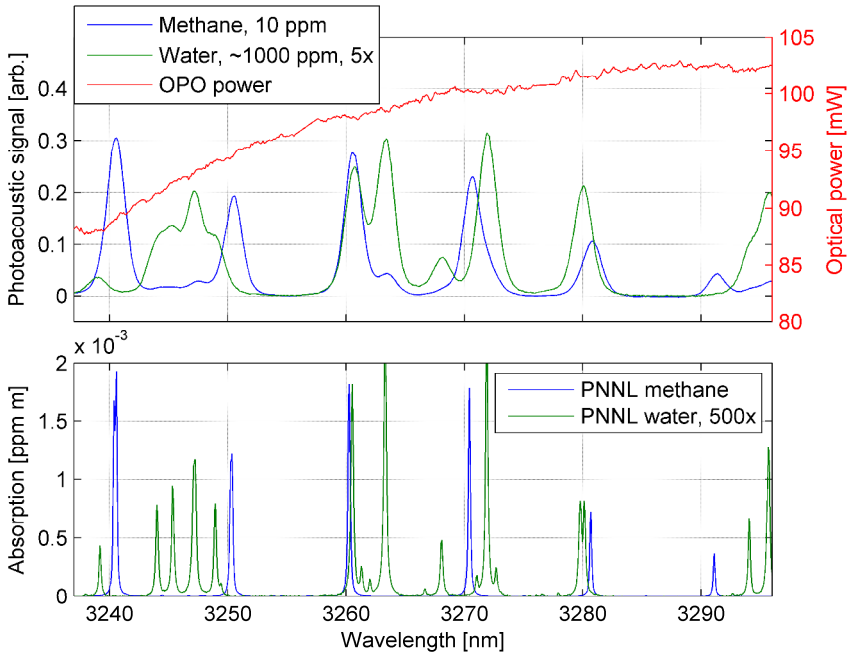

Figure 24. *Upper graph:* Measured methane and water (5x magnified) spectra and the optical power output of the OPO. *Lower graph:* PNNL reference spectra of methane and water (500x magnified) (reprint from Article IV, with the permission from Elsevier).

If the excitation bandwidth is wider than the absorption band, as is the case here, only the photons having the same frequency as the absorption band can be absorbed. As a result, the OPO used here performs best in the measurement of bigger molecules such as benzene, toluene and xylenes that have an absorption band broader than FWHM 1.3.

7.3.2 Noise characterization

The noise measurements were done in the same way as for the QCL setup, with the PA cell filled with synthetic air to 950 mbar and the signal recorded for 2 min with a single measurement time of 0.951 s. The records were done with the OPO turned off and in operation at 10 different wavelengths distributed over the whole spectral range. The PA signal with the OPO off did not increase over the time, but with the OPO on, the signal increased from the start to the end in average by 5.7%. As already discussed in the QCL chapter, the signal increase comes from water molecules desorbing from the cell interior and increasing the PA signal. The water-based signal is not noise and therefore was subtracted in this work with a second-order polynomial. Compared to the QCL work, a second-order polynomial was sufficient because of the ~2 magnitude lower absorption coefficients of water in this region. The residual of the subtraction is the variation in nitrogen signal from which the standard deviation in blocks of 10 successive recording points was calculated. The noise at each wavelength is the average of the 12 standard deviation values. The calculated noise as well as the background signal is shown in Figure 25. The background signal was defined to be the first measurement of each time record.

The noise sources in CEPAS and their suppression were extensively discussed in the noise analysis of the QCL setup, and can therefore be kept sufficiently brief here. As deduced in Chapter 6.3.1, the limiting noise sources in CEPAS are the Brownian noise and the background signal instability [73,74]. The Brownian noise level was evaluated with the OPO switched off and found to be 2.08×10^{-5}. This is in compliance with the QCL work where the Brownian noise was estimated to be 1.99×10^{-5}. With the OPO in operation, the noise varied from the lowest 3.52×10^{-5} to the highest 6.37×10^{-5} with an average of 4.71×10^{-5} over all wavelengths. The noise above the Brownian noise level is due to the background signal instability. In the QCL setup, the background signal instability was 2.85×10^{-5} and the background signal 1.50×10^{-2} at a laser power of 47 mW. As can be seen from Figure 25, the noise correlates well with the background signal height except the values at 3275 nm. The biggest contribution to the higher background signal instability is due to a factor ~2 times higher power being emitted by the OPO, leading to a higher background signal. In addition, the relative intensity noise of the OPO, different beam parameters and a probably slightly differing beam alignment through the PA cell can result in a higher background signal.

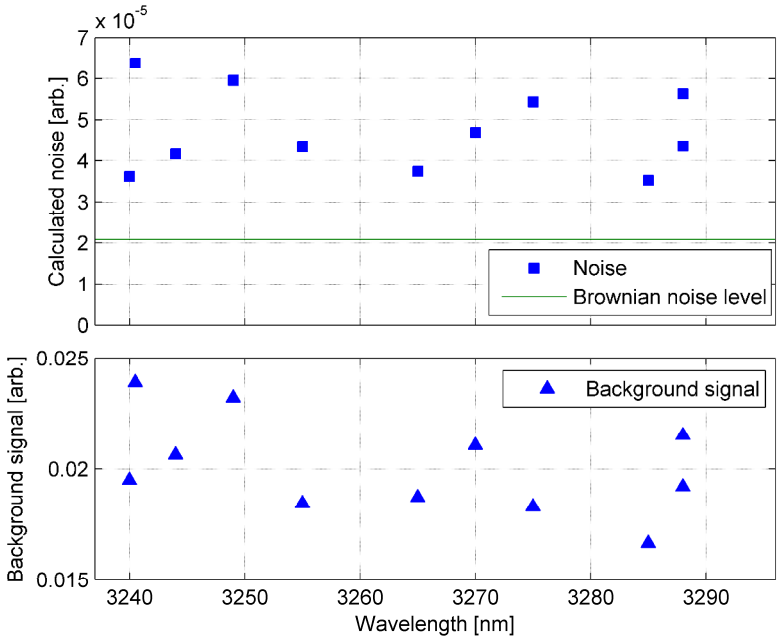

Figure 25. The calculated noise and measured background signal over the wavelength (reprint from Article IV, with the permission from Elsevier).

7.3.3 Data processing

During the experimental work, when the calibrator was supplying the analyte gases, it turned out that for some still unknown reason the calibrator did not keep the analyte concentration stable over time. In other words, the concentration at which the spectra were measured may differ from the set value concentration. To eliminate the uncertainty in concentration, the data is processed as described hereafter. The methane gas used for testing was provided from a gas cylinder and is therefore reliable in concentration and the concentration was stable over time. The signal intensity that the measured spectra should have is called the reference signal intensity and is calculated for each analyte at 3291 nm by dividing the signal intensity of the measured methane by the PNNL methane and multiplying it with the PNNL analyte intensity. Then the signal intensities of the measured BTX spectra were corrected to the reference intensity. This operation assumes an equal PA response for methane and BTX, which is in reality quite similar. The corrections were not blindly adopted; they were rather carefully checked and it turned out that they were in good agreement with the notices during the calibrator operation. The PNNL reference spectra were convoluted to match the spectral bandwidth of the OPO before the above described processing to ensure accurate results that were not falsified by the narrow bandwidths of methane. Also prior to the processing,

the background was subtracted from the measured spectra presuming a linear background over the whole spectral range with the height of 1.80 x 10^{-2}.

The corrected analyte spectra are divided by their concentration to become the response spectra *g* [arb. ppb^{-1}], which will be used later on in the science-based calibration. Due to an internal temperature adjustment, the OPO produced artifact spikes at 3256 and 3275 nm. The spikes were reproducible, both spectral- and time-wise, and thus removed by linear interpolation of the regions 3255.4–3257.7 nm and 3275.8–3277.7 nm. The power emission curve of the OPO shows a small ripple as can be seen in Figure 24, and the ripple occurs in the measured spectra, too. The ripple is not noise as it appears at first glance, since it occurs periodically. The ripples are unflavored in the response spectra for calibration reasons and therefore, the spectra were smoothed using the Savitzky-Golay filter with a span of 25 data points.

Figure 26 shows the resulting and the PNNL reference spectra. As can be seen, the aromatic CH stretch vibrational band of the analytes is so broad that the 59 nm spectral coverage of the OPO can only record a cutout. Compared to the reference spectra, the band positions and the shape are in compliance. The intensities are a function of the system response as discussed for methane and water in Figure 24 and thus are differently pronounced than the response spectra.

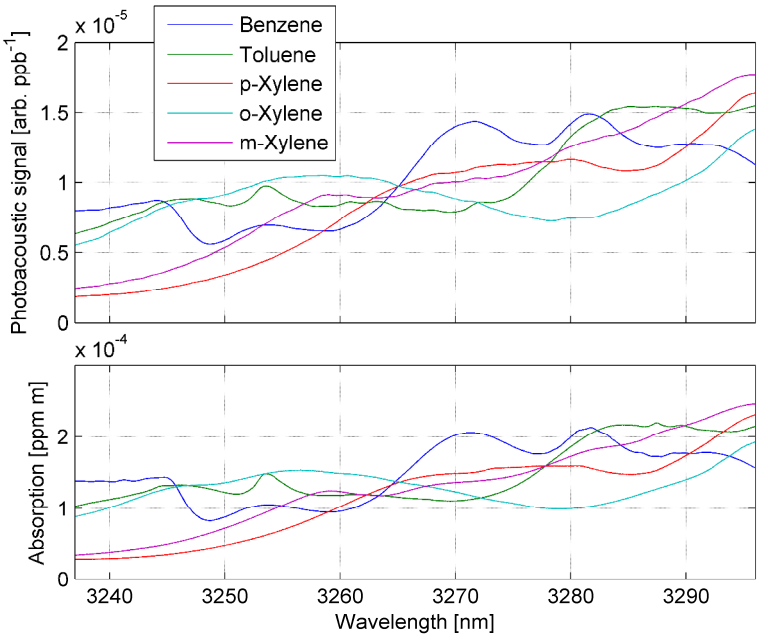

Figure 26. *Upper graph:* The measured response spectra of benzene, toluene and the xylenes. *Lower graph:* PNNL reference spectra of benzene, toluene and the xylenes (reprint from Article IV, with the permission from Elsevier).

7.3.4 Univariate data analysis

Univariate data analysis here can only be used for single-compound analysis, because if more than one analyte is present in the sample, their spectra will interfere. In that case, multivariate data analysis is necessary to resolve the interference, which is shown in the next section. Even if the scope of this work is the multi-compound measurement of BTX, the univariate detection limits are still calculated hereafter for comparison purposes.

The univariate data analysis was done at 3288 nm, because the absorption coefficients of BTX are high and water does not have any major absorption bands. The univariate detection limit for the analytes were calculated by dividing the average of the two noise values at 3288 nm by the signal intensities from the response spectra *g* at 3288 nm. The two noise values at 3288 nm are on average 4.99×10^{-5}, which is a bit higher than the average noise over all wavelengths. Table 11 shows the signal intensities and the univariate detection limits (3σ, 0.951 s), which range from best 9.8 ppb for toluene to worst 16.0 ppb for *o*-xylene, according their absorption coefficients. If the wavelength with the highest absorption coefficient is selected for the individual analyte, then the univariate detection limit can still be improved.

Table 11. Univariate signal intensities and detection limits of the analytes at 3288 nm. The noise was 4.99×10^{-5} (reprint from Article IV, with the permission from Elsevier).

	Signal intensity [arb. ppb^{-1}]	**Detection limit (3σ, 0.951 s) [ppb]**
Benzene	1.25×10^{-5}	12.0
Toluene	1.54×10^{-5}	9.8
p-Xylene	1.14×10^{-5}	13.2
o-Xylene	9.37×10^{-6}	16.0
m-Xylene	1.49×10^{-5}	10.1

The HITRAN and GEISA databases currently do not contain toluene and xylene, and therefore, the absorption coefficients α [cm^{-1}] of the analytes were calculated from the PNNL reference spectra. Using the PNNL spectra creates a slight inaccuracy because these spectra are a function of the FT-IR instrument resolution and are measured at 1013 mbar. The 2012 version of HITRAN features the cross section of benzene, which was used to verify the calculated absorption coefficient of benzene via the PNNL spectra. The difference in the calculated coefficients is <10%, which is sufficient for the purposes here. The minimum detectable absorp-

tion coefficient α_{min} (3σ, 0.951 s) was calculated for each analyte and the average over the five analytes is 4.94 x 10^{-8} cm^{-1}.

If water is present in a concentration higher than ~100 ppm, tiny rotational bands with an absorption coefficient of ~5 x 10^{-7} cm^{-1} (HITRAN, 1 ppm, 10 cm, 323 K, 950 mbar) will start to interfere. To resolve the interference, multivariate data analysis is required.

Besides the spectral scans, the OPO wavelength was fixed to 3288 nm and the PA signal variation over the time recorded at different concentrations. The PA signal of benzene at different concentrations is shown in Figure 27. The signal variation measurements were not processed as the spectra, and therefore the data presented in Figure 27 is the raw data. However, the concentration values shown in Figure 27 were corrected with the response spectra.

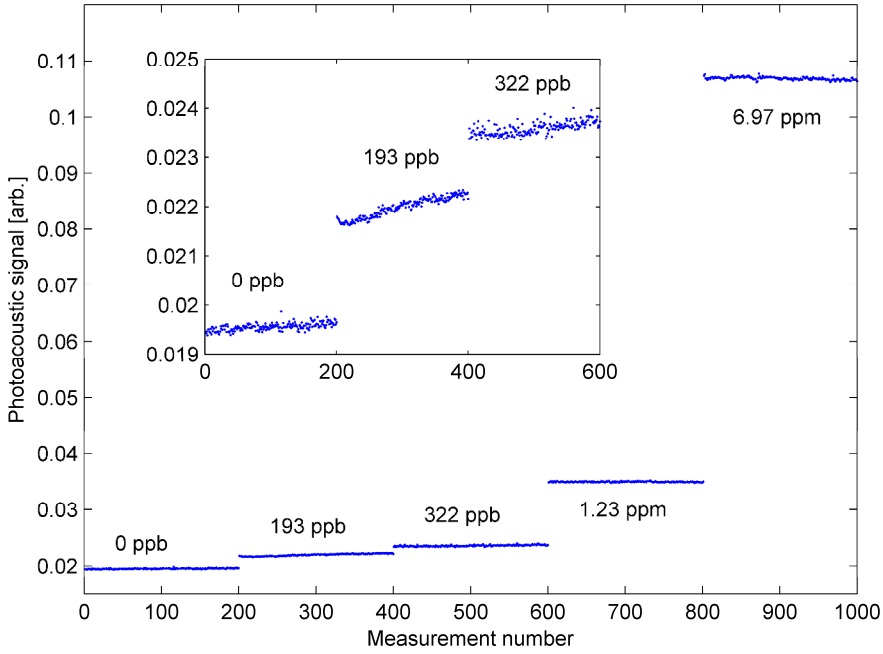

Figure 27. Photoacoustic signal of benzene at 3288 nm and different concentrations. Each measurement number corresponds to 0.951 s measurement time (reprint from Article IV, with the permission from Elsevier).

7.3.5 Multivariate data analysis

The SBC method was used for multivariate data analysis and calibration of the BTX analytes. The response spectra *g* [arb. ppb^{-1}] were used as the analyte signal for the calculation of the regression vector *b* [ppb $arb.^{-1}$]. For each analyte, two individual regression vectors *b* were calculated based on two different analyte

specific noise matrixes Σ [arb.^{2}]. In the multi-compound case, all analytes are present in the sample and each analyte interferes with the determination of all the other analytes. To resolve the interference, the $\Sigma_{\text{multi-compound}}$ contained the instrument noise as well as the interference noise of the other analytes. Resolving the interference consumes more or less signal depending on the extent of the interference, which leads to poorer detection limits. To evaluate how much the detection limits worsens, the $\Sigma_{\text{single-compound}}$ contained only the instrument noise and represents the single-compound case, meaning that only the analyte is present in the sample. The instrument noise was calculated in Chapter 7.3.2. Since the whole spectral range from 3237–3296 nm was calibrated and the noise was only measured at 9 discrete wavelengths, the noise was linearly interpolated and at both ends extrapolated with a linear fit. To make the calibration immune against water vapor, which is often present in samples, water was added to $\Sigma_{\text{multi-compound}}$ as another interferent. The multi-compound calibrations were optimized for selectivity and the influence of the spectral ripples decreased by adding the difference of the measured spectra of each analyte to $\Sigma_{\text{multi-compound}}$.

Figure 28 shows the regression vectors of the analytes and Table 12 the multivariate detection limits in the single- and multi-compound sample. Table 13 shows the cross-selectivity numbers that were calculated with different spectra than those appointed for calibration. Still, the spectra were processed like the calibration spectra as described in Chapter 7.3.3.

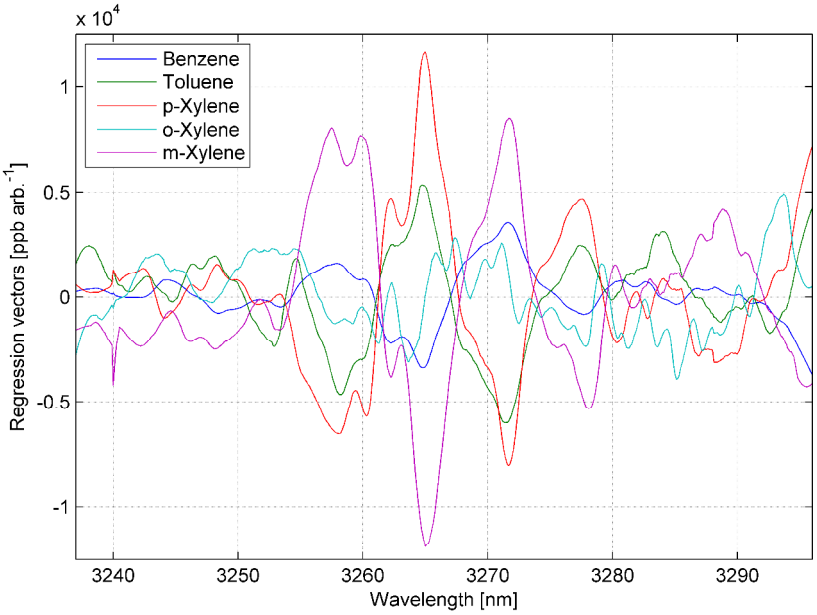

Figure 28. Regression vectors *b* of the analytes benzene, toluene and the three xylenes for the multi-compound calibration (reprint from Article IV, with the permission from Elsevier).

Table 12. Comparison of the multivariate detection limits of the analytes. Single-compound denotes the situation when only the analyte of interest is present in the sample and multi-compound when all other analytes and water interfere (reprint from Article IV, with the permission from Elsevier).

	Detection limit (3σ, 3237–3296 nm, 591 spectral points each 0.951 s) [ppb]	
	Single-compound	Multi-compound
Benzene	0.52	4.3
Toluene	0.51	7.4
p-Xylene	0.59	11.0
o-Xylene	0.61	6.2
m-Xylene	0.52	12.5

The dilemma of univariate measurement in multivariate data analysis was already discussed in Chapter 4 and in the QCL work. For the QCL setup, the detection limit scaled on time could not be improved, and multivariate data analysis was therefore not reasonable. However, in the case of the BTX analysis, multiple univariate measurement points in combination with multivariate data analysis are justified and required to resolve the interference of the analytes. By using all 591 univariate measured spectral points from 3237–3296 nm, the sum of the cross-selectivity numbers per analyte could be kept below 5.00×10^{-2} ppb ppb^{-1}, with an average cross-selectivity number of 3.80×10^{-2} ppb ppb^{-1}. The average of the individual analyte cross-selectivity pairs is 7.60×10^{-3} ppb ppb^{-1}. The cross-selectivity numbers of water are at least one magnitude better, which comes from the fact that the water spectrum is peaky and can more easily be discriminated. The cross-selectivity number of water varied from -2.25×10^{-4} ppb ppb^{-1} for *m*-xylene to -2.84×10^{-5} ppb ppb^{-1} for *o*-xylene, being on average over all analytes 1.22×10^{-4} ppb ppb^{-1}. This number means that the analyte reading will be affected by +1 ppb, if the water concentration varies up to approx. ±5 ppm. This value does not sound too good, but it only expresses the part by which the interferent can vary in concentration. In general, water or any other interferent can be present in a higher concentration if the concentration is stable over time. A stable interferent signal will be included to the operation point spectrum and thus subtracted from the measured spectrum prior to the multiplication, with the regression vector as in Equation (7). The interferent signals that vary over time are of major concern. These need to be considered in the interference assessment and the cross-selectivity numbers needs to be adjusted accordingly. Let us imagine a situation where the sample gas has a humidity of 50% at 20 ºC, which corresponds to a water vapor concentration of ~11.7 kppm. If only ±5 ppm vary over time and the rest of the ~11.7 kppm water vapor are constantly present, then the BTX analyte reading will only be influenced by <1 ppb. In case the humidity changes from 50%

to 40% (~9.3 kppm at 20 °C), for example, then the BTX analyte readings will be biased by ((11.7-9.3) x 10^6 x 1.22 x 10^{-4}) = ~-300 ppb. In this case, the calibration needs to be readjusted, which will result in poorer detection limits of the analytes BTX because a bigger part of the signal is consumed to resolve the water's inference.

Table 13. Cross-selectivities (3237–3296 nm, 591 spectral points, each 0.951 s) in [ppb ppb^{-1}] of the individual analytes, water and in sum. For instance, if toluene's concentration increases by 100 ppb, then it affects the benzene reading by +1.1 ppb (reprint from Article IV, with the permission from Elsevier).

	Interferent →						
Analyte ↓	Benzene	Toluene	*p*-Xylene	*o*-Xylene	*m*-Xylene	Water	Sum
Benzene	0.99	1.09 x 10^{-2}	-8.32 x 10^{-3}	-1.40 x 10^{-2}	-3.72 x 10^{-3}	-5.67 x 10^{-5}	3.70 x 10^{-2}
Toluene	3.83 x 10^{-3}	1.00	1.19 x 10^{-3}	-1.26 x 10^{-2}	1.06 x 10^{-2}	1.34 x 10^{-4}	2.83 x 10^{-2}
p-Xylene	-7.52 x 10^{-3}	-2.39 x 10^{-3}	1.00	9.66 x 10^{-3}	1.11 x 10^{-2}	1.66 x 10^{-4}	3.09 x 10^{-2}
o-Xylene	1.89 x 10^{-2}	-9.67 x 10^{-3}	4.80 x 10^{-3}	0.99	-1.56 x 10^{-2}	-2.84 x 10^{-5}	4.90 x 10^{-2}
m-Xylene	-1.60 x 10^{-3}	1.65 x 10^{-2}	-4.81 x 10^{-4}	2.60 x 10^{-2}	1.00	-2.25 x 10^{-4}	4.47 x 10^{-2}

The resulting multivariate detection limits (3σ, 3237–3296 nm, 591 spectral points each 0.951 s) of the multi-compound sample, where all other analytes and water interfere, ranges from best 4.3 ppb for benzene to worst 12.5 ppb for *m*-xylene. To get a feeling of by how much the detection limit worsens when the interferents are present, the single-compound calibration was conducted. The multivariate single-compound detection limits are better on average by a factor of 15. This rather big loss in signal comes from the fact that the BTX spectra are broad and look quite similar in the measured range, almost like in a near-IR measurement scenario of solids or liquids.

7.3.6 Future system improvements

The measurement system can still be improved and the options are assessed as follows:

1. The application of multivariate data analysis was justified to resolve the interferences, but still the dilemma of the increasing measurement time remains. Therefore, the optimization of the univariate measurement in multivariate data analysis is of major importance. The main variables are the number of spectral points, the wavelengths where the spectral points are measured, and the integration time of each spectral point. Factors that

need to be taken into account are the noise level, absorption coefficients of the analytes and the extent of the interferences, all three wavelength dependent, as well as the measurement system parameters as the system response and the resolution.

In the present work, the resolution of the measurement system was 1.3 nm, but the spectra were measured in steps of 0.1 nm. The measurement time can be reduced to ~4.5 minutes by including only every second measured point in the calibration. As a result, the detection limits will worsen by almost exactly $\sqrt{2}$ to 6.1 ppb for benzene and 18.5 ppb for *m*-xylene, and also the cross-selectivity numbers will worsen on average by a factor of 1.5.

In general, the optimization is always application case specific and will result in a shorter measurement time and a better system performance. Initial work on the development of an optimization tool for an external cavity QCL-CEPAS system was recently reported in [166].

2. The second point is related to improvements of the OPO. To date, the spectral bandwidth of the succeeding OPOs was enhanced to an FWHM of 1.0 nm and electric chopping realized. Electric chopping makes the mechanical tuning fork dispensable, which decreases the system complexity and eliminates the moving parts. Removing the ripple in combination with the improved bandwidth will facilitate better cross-selectivity numbers, possibly to the level of 10^{-4}, maybe even to 10^{-5} ppb ppb^{-1}. Increasing the output power and enabling wavelength modulation of the OPO will finally result in better sensitivity and reduced measurement time. Studies of these subjects are ongoing.
3. The final point here refers to the sampling. Some gases, such as BTX traces, can be adsorbed on the surfaces of the sampling system and the PA cell. Adsorption-desorption processes are not trivial to understand, and in practice they lead to a slow system response and incorrect readings. When designing a measurement system, this should be taken into account and the materials of the sampling system and PA cell should be optimized for the lowest possible adsorption of BTX. For example, the adsorption-desorption processes in a photoacoustic cell for the measurement of ammonia were studied by Schmohl et al. and reported in [167]. The fact that the cell is operated at 50 °C is advantageous, but the gas flow has to be stopped for the measurement, which may support adsorption-desorption processes in the PA cell. Upcoming research will focus on materials with low BTX adsorption as well as on optimizing the sampling parameters.

7.3.7 Summary and outlook

In this work, a state of the art measurement system was built out of CEPAS and OPO. It turned out that the OPO is a superior light source for this application. It

emits light at around 3 µm, where QCLs are rarely available, offers a broader tunability than diode lasers, and supplies more optical power relative to the beam quality. Further, the OPO is small in size and weight, passively cooled, easy to integrate and commercially available, which makes it a suitable light source for measurement setups as presented here.

The assembled measurement system was applied to the analysis of BTX and reached univariate detection limits (3σ, 0.951 s) at 3288 nm of 12.0, 9.8, 13.2, 10.1 and 16.0 ppb for benzene, toluene, *p*-, *m*- and *o*-xylene, respectively. However, univariate data analysis can only be done for single-compound analysis due to the interference. To resolve the spectral interference of the analytes, multivariate data analysis is carried out. The found multivariate detection limits (3σ, 3237–3296 nm, 591 spectral points each 0.951 s) for the multi-compound sample where all other analytes and water interfere were 4.3, 7.4, 11.0, 12.5 and 6.2 ppb for benzene, toluene, *p*-, *m*- and *o*-xylene, respectively. To compare how much signal is consumed to resolve the interferences, a multivariate single-compound calibration was drawn up. It turned out that the single-compound detection limits are better by a factor of ~15, which is due to the fact that the BTX analyte spectra look quite similar in the measured range. The sum of the cross-selectivity numbers could be kept below 5.00×10^{-2} ppb ppb^{-1} with an average cross-selectivity number of 3.80×10^{-2} ppb ppb^{-1}. The cross-selectivity numbers of water were a minimum of one magnitude lower and on average 1.22×10^{-4} ppb ppb^{-1}.

Possible system improvements were assessed and include the optimization of the univariate measurement in multivariate data collection, the OPO, the sampling system materials and the sampling process. These developments can further improve the already high performance of the system, leading to better cross-selectivities, detection limits and faster measurement times.

The performance of the novel measurement system was demonstrated to be suitable for most applications listed in the introduction as industrial and environmental BTX measurement at ppb level. For the urban area monitoring of benzene in cities, a longer measurement time is required, which is in this application not an obstacle. The built system is small-sized, can be arranged in a 19” rack, is passively cooled and requires only a power supply for operation. The whole OPO-CEPAS measurement system including data management and acquisition typically consumes ~60 W and max. 120 W at 230 V. A rugged and portable version is currently being considered and can be built with only minor efforts. In the future, a handheld version may be possible, which requires further progress.

8. General conclusion

Organic molecules with high vapor pressure at room temperature rapidly evaporate into the air and are accordingly classified as volatile organic compounds. The measurement of VOCs is an important need in many applications in industry [17,18], air pollution and atmosphere [19–21], health and well-being [22–26], defense and security [27,28] and many other fields [17,18,21,29,30]. Various analytical techniques have been developed for the measurement of VOCs, including methods based on photoacoustic spectroscopy [32]. Usually, the sensitivity of photoacoustic measurement systems is enhanced by operating the photoacoustic detector at an acoustic resonance frequency [17,34,73,77]. However, this complicates the use of broadly tunable light sources, which are useful in resolving the spectral interference typically occurring in VOC measurement applications. The recently developed optical read-out cantilever microphone enhances the sensitivity without the need for operating the PA cell in resonance [39,73]. This enables setups with broadly tunable light sources without losing sensitivity and thus facilitates the development of CEPAS setups for the measurement of VOCs.

In this thesis, the first industry-ready, robust and portable FT-IR-CEPAS system was presented and its analytical performance tested. The multivariate single-compound detection limits (3σ, 500–4000 cm^{-1}, 25 s) vary from best 2.2 ppm for methane and propene to worst 6.7 ppm for carbon dioxide. In a multi-compound calibration of the analytes methane, carbon dioxide, methanethiol and propene, the detection limits became worse on average only by a factor of 1.4. The average of the sum of the cross-selectivity numbers could be kept at a reasonable level of 9.55 x 10^{-3} ppm ppm^{-1} and the interference of water at 1.81 x 10^{-3} ppm ppm^{-1} on average.

Besides the advantage of the non-resonant operation, the CEPAS detector can also operate at temperatures of up to 180 °C. Some VOC measurement applications, such as the monitoring of industrial emissions, require the measurement of hot sample gas. Therefore, an FT-IR-CEPAS measurement system was built where all parts that are in contact with the gas were heated to 180 °C, including the PA cell and the cantilever. Mid-infrared spectra of 18 VOCs were recorded at 180 °C and the multivariate single-compound detection limits (3σ, 500–4000 cm^{-1}, 8.5 min) ranged from best 0.3 ppm for butyl acetate to worst 2.6 ppm for dichloromethane. For the multi-compound calibration, five VOCs were selected that show

particularly strong spectral overlapping. The sum of the cross-selectivity numbers of tetrachloroethylene, acetone and dimethylformamide were at an acceptable level of 3.10 x 10^{-2} ppm ppm^{-1}, but methyl isobutyl ketone and methanol showed a questionable number of ~0.1 ppm ppm^{-1}. Water interfered with the analyte reading on average by 1.03 x 10^{-3} ppm ppm^{-1}. The multivariate multi-compound detection limits worsen on average by only 1.4 compared to multivariate single-compound detection limits. Water features interfering with the analyte spectra were subtracted from a wide concentration range of 1400 to 100 000 ppm, resulting in an accurate analyte reading. The heated system did not reach the state of the art performance. In a direct comparison of the system working at 50 and 180 °C, the univariate SNR dropped by a factor of 4.6 in the heated state. The reason for that is the non-optimal vibration damping at 180 °C, resulting in a high noise level. An improvement in the vibration isolation is expected to increase the performance to the level similar to the state of the art FT-IR-CEPAS system.

FT-IR-CEPAS is a powerful tool for multi-compound VOC gas measurement applications, where the broad wavelength range helps to resolve the spectral interference between the analytes. Currently the detection limits are at ppm level and with further improvements in the detector and FT-IR, sub-ppm detection limits can be reached within a reasonable measurement time.

For better sensitivity, a novel QCL-CEPAS system was built and its performance tested in the trace gas detection of formaldehyde. The QCL was tunable from 1772 to 1777 cm^{-1} and the formaldehyde band at 1773.959 cm^{-1} was selected for data analysis, where the continuous wave laser emitted 47 mW. The formaldehyde detection limit (3σ, 0.951 s) in wavelength modulation was found to be 1.3 ppb and the NNEA (3σ) 6.04 x 10^{-10} W cm^{-1} $(Hz)^{-1/2}$. Compared to FT-IR-CEPAS, the detection limits improved by a factor of ~1000, but the tunability of narrow bandwidth, mode hop-free QCLs is currently limited to only a few wavenumbers. Thus, interference of several compounds is usually difficult to resolve, even with high spectral resolution of 0.018 cm^{-1} and low gas pressure, as in this case.

To achieve both high sensitivity and multi-compound ability, an OPO-CEPAS setup was built. The OPO offered a higher power of ~100 mW and a broader tunability from 3237 to 3296 nm in steps of 0.1 nm and had a bandwidth of 1.3 nm. Univariate detection limits (3σ, 0.951 s) achieved for benzene, toluene, *p*-, *o*- and *m*-xylene at 3288 nm were 12.0, 9.8, 13.2, 16.0 and 10.1 ppb, respectively. In multivariate detection, where all other analytes and water interfere, the multivariate detection limits (3σ, 3237–3296 nm, 591 spectral points each 0.951 s) varied from 4.3 ppb for benzene to 12.5 ppb for *m*-xylene. The sum of the cross-selectivity numbers per analyte could be kept below 5.00 x 10^{-2} ppb ppb^{-1}, with an average of 3.80 x 10^{-2} ppb ppb^{-1} and an average cross-selectivity number of water of 1.22 x 10^{-4} ppb ppb^{-1}. The OPO used here is compact and commercially available, has a tunable range broader than the QCL, and provides more optical power than the FT-IR, making it a suitable light source for multi-compound VOC analysis.

Ten years have passed since the invention of CEPAS. In recent years, CEPAS has become a mature technique recognized beyond the photoacoustic community.

Nowadays, CEPAS is robust, stable and commercially available for lasers, FT-IRs and broadband light sources. In this work, CEPAS has been successfully applied for the measurement of VOCs. By modifying the CEPAS-based setup, VOC measurement applications with different requirements were served. In addition, this work improved the existing FT-IR-CEPAS technique, developed the heated CEPAS setup, contributed to the development of industrially capable CEPAS measurement systems and laid the foundation for QCL- and OPO-CEPAS gas analyzers, which will become commercially available in the near future.

Bibliography

1. D. R. Crump, "Volatile organic compounds in indoor air," in *Volatile Organic Compounds in the Atmosphere*, R. E. Hester and R. M. Harrison, eds. (The Royal Society of Chemistry, 1995), pp. 109–124.

2. R. G. Derwent, "Sources, distributions, and fates of VOCs in the atmosphere," in *Volatile Organic Compounds in the Atmosphere*, R. E. Hester and R. M. Harrison, eds. (The Royal Society of Chemistry, 1995), pp. 1–15.

3. S. Ojala, S. Pitkäaho, T. Laitinen, N. Niskala Koivikko, R. Brahmi, J. Gaálová, L. Matejova, A. Kucherov, S. Päivärinta, C. Hirschmann, T. Nevanperä, M. Riihimäki, M. Pirilä, and R. L. Keiski, "Catalysis in VOC Abatement," Top. Catal. **54**, 1224–1256 (2011).

4. A. P. Jones, "Indoor air quality and health," Atmos. Environ. **33**, 4535–4564 (1999).

5. United States Environmental Protection Agency, "An Introduction to Indoor Air Quality Volatile Organic Compounds (VOCs)," http://www.epa.gov/iaq/voc.html#Health_Effects.

6. R. Koppmann, "Chemistry of Volatile Organic Compounds in the Atmosphere," in *Handbook of Hydrocarbon and Lipid Microbiology*, K. Timmis, ed. (Springer Berlin Heidelberg, 2010), pp. 267–277.

7. P. J. Crutzen, "The Role of NO and NO2 in the Chemistry of the Troposphere and Stratosphere," Annu. Rev. Earth Planet. Sci. **7**, 443–472 (1979).

8. R. Atkinson, "Gas phase tropospheric chemistry of organic compounds," in *Volatile Organic Compounds in the Atmosphere*, R. E. Hester and R. M. Harrison, eds. (The Royal Society of Chemistry, 1995), pp. 65–90.

9. E. C. Moretti, *Practical Solution for Reducing Volatile Organic Compounds and Hazardous Air Pollutants* (American Institute of Chemical Engineers, 2001).

10. C. Je, R. Stone, and S. G. Oberg, "Development and application of a multi-channel monitoring system for near real-time VOC measurement in a hazardous waste management facility," Sci. Total Environ. **382**, 364–374 (2007).

11. International Agency for Research of Cancer (IARC) of the World Health Organization, "Agents Classified by the IARC Monographs," http://monographs.iarc.fr/ENG/Classification/index.php.

12. R. Friedrich and A. Obermeier, "Chapter 1 - Anthropogenic Emissions of Volatile Organic Compounds," in *Reactive Hydrocarbons in the Atmosphere*, C. N. Hewitt, ed. (Academic Press, 1999), pp. 1–39.

13. "DIRECTIVE 2010/75/EU of 24 November 2010 on industrial emissions (integrated pollution prevention and control)," Off. J. Eur. Union 334, 17–119 (2010).

14. E. Gallego, F. X. Roca, X. Guardino, and M. G. Rosell, "Indoor and outdoor BTX levels in Barcelona City metropolitan area and Catalan rural areas," J. Environ. Sci. **20**, 1063–1069 (2008).

15. F. Palmgren, A. B. Hansen, R. Berkowicz, and H. Skov, "Benzene emission from the actual car fleet in relation to petrol composition in Denmark," Atmos. Environ. **35**, 35–42 (2001).

16. J. Williams and R. Koppmann, "Volatile Organic Compounds in the Atmosphere: An Overview," in *Volatile Organic Compounds in the Atmosphere*, R. Koppmann, ed. (Blackwell Publishing, 2007), pp. 1–32.

17. F. J. M. Harren, G. Cotti, J. Oomens, and S. te L. Hekkert, "Photoacoustic Spectroscopy in Trace Gas Monitoring," in *Encyclopedia of Analytical Chemistry*, R. A. Meyers, ed. (John Wiley & Sons, 2000), pp. 2203–2226.

18. T. Schmid, "Photoacoustic spectroscopy for process analysis," Anal. Bioanal. Chem. **384**, 1071–1086 (2006).

19. M. W. Sigrist, *Air Monitoring by Spectroscopic Techniques* (John Wiley & Sons, 1994).

20. D. E. Heard, *Analytical Techniques for Atmospheric Measurement* (Blackwell Publishing, 2006).

21. F. K. Tittel, D. Richter, and A. Fried, "Mid-Infrared Laser Applications in Spectroscopy," in *Solid-State Mid-Infrared Laser Sources*, I. Sorokina and K. Vodopyanov, eds. (Springer Berlin Heidelberg, 2003), pp. 458–529.

22. B. Buszewski, M. Kesy, T. Ligor, and A. Amann, "Human exhaled air analytics : biomarkers of diseases," Biomed. Chromatogr. **21**, 553–566 (2007).

23. C. Wang and P. Sahay, "Breath Analysis Using Laser Spectroscopic Techniques: Breath Biomarkers, Spectral Fingerprints, and Detection Limits," Sensors (Basel) **9**, 8230–8262 (2009).

24. W. Miekisch, J. K. Schubert, and G. F. E. Noeldge-Schomburg, "Diagnostic potential of breath analysis—focus on volatile organic compounds," Clin. Chim. Acta **347**, 25–39 (2004).

25. M. Phillips, R. N. Cataneo, C. Saunders, P. Hope, P. Schmitt, and J. Wai, "Volatile biomarkers in the breath of women with breast cancer," J. Breath Res. **4**, 1–8 (2010).

26. L. I. B. Silva, A. C. Freitas, T. A. P. Rocha-Santos, M. E. Pereira, and A. C. Duarte, "Breath analysis by optical fiber sensor for the determination of exhaled organic compounds with a view to diagnostics," Talanta **83**, 1586–1594 (2011).

27. C. K. N. Patel, "Laser photoacoustic spectroscopy helps fight terrorism: High sensitivity detection of chemical Warfare Agent and explosives," Eur. Phys. J. Spec. Top. **153**, 1–18 (2008).

28. Y. Sun and K. Y. Ong, *Detection Technologies for Chemical Warfare Agents and Toxic Vapors* (CRC Press, 2004).

29. A. Kosterev, G. Wysocki, Y. Bakhirkin, S. So, R. Lewicki, M. Fraser, F. Tittel, and R. F. Curl, "Application of quantum cascade lasers to trace gas analysis," Appl. Phys. B **90**, 165–176 (2008).

30. C. Haisch, "Photoacoustic spectroscopy for analytical measurements," Meas. Sci. Technol. **23**, 012001 (2012).

31. M. W. Sigrist, R. Bartlome, D. Marinov, J. M. Rey, D. E. Vogler, and H. Wächter, "Trace gas monitoring with infrared laser-based detection schemes," Appl. Phys. B **90**, 289–300 (2008).

32. P. Aragón, J. Atienza, and M. D. Climent, "Analysis of Organic Compounds in Air: A Review," Crit. Rev. Anal. Chem. **30**, 121–151 (2000).

33. R. Muñoz, E. C. Sivret, G. Parcsi, R. Lebrero, X. Wang, I. H. M. Suffet, and R. M. Stuetz, "Monitoring techniques for odour abatement assessment," Water Res. **44**, 5129–5149 (2010).

34. Z. Bozóki, A. Pogány, and G. Szabó, "Photoacoustic Instruments for Practical Applications: Present, Potentials, and Future Challenges," Appl. Spectrosc. Rev. **46**, 1–37 (2011).

35. J. Hodgkinson and R. P. Tatam, "Optical gas sensing: a review," Meas. Sci. Technol. **24**, 012004 (2013).

36. V. Hanyecz, Á. Mohácsi, A. Pogány, A. Varga, Z. Bozóki, I. Kovács, and G. Szabó, "Multi-component photoacoustic gas analyzer for industrial applications," Vib. Spectrosc. **52**, 63–68 (2010).

37. J. Kauppinen, K. Wilcken, I. Kauppinen, and V. Koskinen, "High sensitivity in gas analysis with photoacoustic detection," Microchem. J. 76, 151–159 (2004).

38. K. Wilcken and J. Kauppinen, "Optimization of a microphone for photoacoustic spectroscopy," Appl. Spectrosc. **57**, 1087–1092 (2003).

39. R. E. Lindley, A. M. Parkes, K. A. Keen, E. D. McNaghten, and A. J. Orr-Ewing, "A sensitivity comparison of three photoacoustic cells containing a single microphone, a differential dual microphone or a cantilever pressure sensor," Appl. Phys. B **86**, 707–713 (2007).

40. V. Koskinen, J. Fonsen, J. Kauppinen, and I. Kauppinen, "Extremely sensitive trace gas analysis with modern photoacoustic spectroscopy," Vib. Spectrosc. **42**, 239–242 (2006).

41. M. W. Sigrist, "Trace Gas Monitoring by Laser-Photoacoustic Spectroscopy," Infrared Phys. Technol. **36**, 415–425 (1995).

42. United States Environmental Protection Agency, "Code of Federal Regulations, 40: Chapter 1, Subchapter C, Part 51, Subpart F, 51100," http://cfr.vlex.com/vid/51-100-definitions-19784887.

43. "Council Directive 1999/13/EC of 11 March 1999 on the limitation of emissions of volatile organic compounds due to the use of organic solvents in certain activities and installations," Off. J. Eur. Union **85**, 1–22 (1999).

44. "Directive 2004/42/CE of the European Parliament and of the Council of 21 April 2004 on the limitation of emissions of volatile organic compounds due to the use of organic solvents in certain paints and varnishes and vehicle refinishing products ...," Off. J. Eur. Union **143**, 87–96 (2004).

45. "Directive 2001/81/EC of the European Parliament and of the Council of 23 October 2001 on national emission ceilings for certain atmospheric pollutants," Off. J. Eur. Union **309**, 22–30 (2001).

46. F. I. Khan and A. K. Ghoshal, "Removal of Volatile Organic Compounds from polluted air," J. Loss Prev. Process Ind. **13**, 527–545 (2000).

47. J. Kesselmeier and M. Staudt, "Biogenic Volatile Organic Compounds (VOC): An Overview on Emission, Physiology and Ecology," J. Atmos. Chem. **33**, 23–88 (1999).

48. C. N. Hewitt, X.-L. Cao, C. Boissard, and S. C. Duckham, "Atmospheric VOCs from natural sources," in *Volatile Organic Compounds in the Atmosphere*, R. E. Hester and R. M. Harrison, eds. (The Royal Society of Chemistry, 1995), pp. 17–36.

49. J. Kesselmeier, K. Bode, U. Hofmann, H. Müller, L. Schäfer, A. Wolf, P. Ciccioli, E. Brancaleoni, A. Cecinato, M. Frattoni, P. Foster, C. Ferrari, V. Jacob, J. L. Fugit, L. Dutaur, V. Simon, and L. Torres, "Emission of short chained organic acids, aldehydes and monoterpenes from Quercus ilex L. and Pinus pinea L. in relation to physiological activities, carbon budget and emission algorithms," Atmos. Environ. **31, SI**, 119–133 (1997).

50. J. Mo, Y. Zhang, Q. Xu, J. J. Lamson, and R. Zhao, "Photocatalytic purification of volatile organic compounds in indoor air: A literature review," Atmos. Environ. **43**, 2229–2246 (2009).

51. E. von Schneidemesser, P. S. Monks, and C. Plass-Duelmer, "Global comparison of VOC and CO observations in urban areas," Atmos. Environ. **44**, 5053–5064 (2010).

52. H. Skov, A. Lindskog, F. Palmgren, and C. S. S. Christensen, "An overview of commonly used methods for measuring benzene in ambient air," Atmos. Environ. **35, S1**, S141 – S148 (2001).

53. International Labour Organization, "International Chemical Security Cards," http://www.ilo.org/dyn/icsc/showcard.home.

54. J. Dewulf and H. Van Langenhove, "Anthropogenic volatile organic compounds in ambient air and natural waters: a review on recent developments of analytical methodology, performance and interpretation of field measurements," J. Chromatogr. A **843**, 163–177 (1999).

55. G. Etiope, "Evaluation of a micro gas chromatographic technique for environmental analyses of CO2 and C1–C6 alkanes," J. Chromatogr. A **775**, 243–249 (1997).

56. P. L. Meyer and M. W. Sigrist, "Atmospheric pollution monitoring using CO2-laser photoacoustic spectroscopy and other techniques," Rev. Sci. Instrum. **61**, 1779–1807 (1990).

57. S. Ojala, U. Lassi, and R. L. Keiski, "Testing VOC emission measurement techniques in wood-coating industrial processes and developing a cost-effective measurement methodology," Chemosphere **62**, 113–120 (2006).

58. F. Biasioli, C. Yeretzian, T. D. Märk, J. Dewulf, and H. Van Langenhove, "Direct-injection mass spectrometry adds the time dimension to (B)VOC analysis," TrAC Trends Anal. Chem. **30**, 1003–1017 (2011).

59. J. Frank, H. Fischer, and G. Matz, "P2.9.19 Handheld Sensor Array for Detection of Trace Gases," in *Proceedings of 14th International Meeting on Chemical Sensors* (2012), pp. 1753 – 1756.

60. U. Platt and J. Stutz, "Measurement Techniques for Atmospheric Trace Gas Concentrations and Other Parameters," in *Differential Optical Absorption Spectroscopy*, U. Platt and J. Stutz, eds. (Springer Berlin Heidelberg, 2008), pp. 113–134.

61. P. Griffiths and J. A. De Haseth, *Fourier Transform Infrared Spectrometry*, 2nd ed. (John Wiley & Sons, 2007).

62. U. Platt and J. Stutz, "Differential Absorption Spectroscopy," in *Differential Optical Absorption Spectroscopy*, U. Platt and J. Stutz, eds. (Springer Berlin Heidelberg, 2008), pp. 135–174.

63. K. Schäfer, K. Brockmann, J. Heland, P. Wiesen, C. Jahn, and O. Legras, "Multipass open-path Fourier-transform infrared measurements for nonintrusive monitoring of gas turbine exhaust composition," Appl. Opt. **44**, 2189–2201 (2005).

64. U. Wandinger, "Introduction to Lidar," in *Lidar*, C. Weitkamp, ed. (Springer New York, 2005), pp. 1–18.

65. B. A. Paldus and A. A. Kachanov, "An historical overview of cavity-enhanced methods," Can. J. Phys. **83**, 975–999 (2005).

66. G. Berden and R. Engeln, *Cavity Ring-Down Spectroscopy: Techniques and Applications* (Wiley-Blackwell, 2009).

67. K. H. Michaelian, *Photoacoustic IR Spectroscopy: Instrumentation, Applications and Data Analysis*, 2nd ed. (John Wiley & Sons, 2010).

68. E. L. Holthoff and P. M. Pellegrino, "Sensing Applications Using Photoacoustic Spectroscopy," in *Optical, Acoustic, Magnetic, and Mechanical Sensor Technologies*, K. Iniewski, ed. (CRC Press, 2012), pp. 139–174.

69. A. Elia, P. M. Lugarà, C. Di Franco, and V. Spagnolo, "Photoacoustic techniques for trace gas sensing based on semiconductor laser sources," Sensors (Basel) **9**, 9616–9628 (2009).

70. M. Nägele and M. W. Sigrist, "Mobile laser spectrometer with novel resonant multipass photoacoustic cell for trace-gas sensing," Appl. Phys. B **70**, 895–901 (2000).

71. R. W. Kessler, *Prozessanalytik: Strategien Und Fallbeispiele Aus Der Industriellen Praxis* (Wiley-VCH, 2006).

72. J. Uotila, "Use of the Optical Cantilever Microphone in Photoacoustic Spectroscopy," University of Turku (2009).

73. T. Kuusela and J. Kauppinen, "Photoacoustic Gas Analysis Using Interferometric Cantilever Microphone," Appl. Spectrosc. Rev. **42**, 443–474 (2007).

74. V. Koskinen, J. Fonsen, K. Roth, and J. Kauppinen, "Progress in cantilever enhanced photoacoustic spectroscopy," Vib. Spectrosc. **48**, 16–21 (2008).

75. G. A. West, J. J. Barrett, D. R. Siebert, and K. V. Reddy, "Photoacoustic spectroscopy," Rev. Sci. Instrum. **54**, 797–817 (1983).

76. F. A. McDonald and G. C. J. Wetsel, "Generalized theory of the photoacoustic effect," J. Appl. Phys. **49**, 2313–2322 (1978).

77. A. Miklós, P. Hess, and Z. Bozóki, "Application of acoustic resonators in photoacoustic trace gas analysis and metrology," Rev. Sci. Instrum. **72**, 1937–1955 (2001).

78. A. G. Bell, "On the production and reproduction of sound by light," Am. J. Sci. **S3-20**, 305–324 (1880).

79. A. G. Bell, "LXVIII. Upon the production of sound by radiant energy," Philos. Mag. **11**, 510–528 (1881).

80. W. C. Röntgen, "Über Töne, welche durch intermittierende Bestrahlung eines Gases entstehen," Ann. der Phys. und Chem. **1**, 155–159 (1881).

81. J. Tyndall, "Action of an Intermittent Beam of Radiant Heat upon Gaseous Matter," Proc. R. Soc. **31**, 307–317 (1881).

82. W. H. Preece, "On the Conversion of Radiant Energy into Sonorous Vibrations," Proc. R. Soc. **31**, 506–520 (1881).

83. E. L. Kerr and J. G. Atwood, "The Laser Illuminated Absorptivity Spectrophone: A Method for Measurement of Weak Absorptivity in Gases at Laser Wavelengths," Appl. Opt. **7**, 915–921 (1968).

84. A. C. Bento, D. T. Dias, L. Olenka, A. N. Medina, and M. L. Baesso, "On the application of the photoacoustic methods for the determination of thermo-optical properties of polymers," Brazilian J. Phys. **32**, 483–494 (2002).

85. R. Lewicki, G. Wysocki, A. A. Kosterev, and F. K. Tittel, "Carbon dioxide and ammonia detection using 2 μm diode laser based quartz-enhanced photoacoustic spectroscopy," Appl. Phys. B **87**, 157–162 (2007).

86. A. A. Kosterev, P. R. Buerki, L. Dong, M. Reed, T. Day, and F. K. Tittel, "QEPAS detector for rapid spectral measurements," Appl. Phys. B **100**, 173–180 (2010).

87. I. G. Calasso and M. W. Sigrist, "Selection criteria for microphones used in pulsed nonresonant gas-phase photoacoustics," Rev. Sci. Instrum. **70**, 4569–4578 (1999).

88. B. D. Adamson, J. E. Sader, and E. J. Bieske, "Photoacoustic detection of gases using microcantilevers," J. Appl. Phys. **106**, 114510 (2009).

89. E. D. McNaghten, K. A. Grant, A. M. Parkes, and P. A. Martin, "Simultaneous detection of trace gases using multiplexed tunable diode lasers and a photoacoustic cell containing a cantilever microphone," Appl. Phys. B **107**, 861–871 (2012).

90. A. A. Kosterev, Y. A. Bakhirkin, R. F. Curl, and F. K. Tittel, "Quartz-enhanced photoacoustic spectroscopy," Opt. Lett. **27**, 1902–1904 (2002).

91. A. A. Kosterev, F. K. Tittel, D. V. Serebryakov, A. L. Malinovsky, and I. V. Morozov, "Applications of quartz tuning forks in spectroscopic gas sensing," Rev. Sci. Instrum. **76**, 043105 (2005).

92. V. Spagnolo, P. Patimisco, S. Borri, G. Scamarcio, B. E. Bernacki, and J. Kriesel, "Mid-infrared fiber-coupled QCL-QEPAS sensor," Appl. Phys. B **112**, 25–33 (2013).

93. L. Dong, A. A. Kosterev, D. Thomazy, and F. K. Tittel, "QEPAS spectrophones: design, optimization, and performance," Appl. Phys. B 100, 627–635 (2010).

94. V. Spagnolo, A. A. Kosterev, L. Dong, R. Lewicki, and F. K. Tittel, "NO trace gas sensor based on quartz-enhanced photoacoustic spectroscopy and external cavity quantum cascade laser," Appl. Phys. B 100, 125–130 (2010).

95. N. Petra, J. Zweck, A. A. Kosterev, S. E. Minkoff, and D. Thomazy, "Theoretical analysis of a quartz-enhanced photoacoustic spectroscopy sensor," Appl. Phys. B **94**, 673–680 (2009).

96. V. Spagnolo, P. Patimisco, S. Borri, G. Scamarcio, B. E. Bernacki, and J. Kriesel, "Part-per-trillion level detection of SF6 using a single-mode fiber-coupled quantum cascade laser and a quartz enhanced photoacoustic sensor," Proc. SPIE **8631**, 86310Z (2013).

97. Y. Ma, R. Lewicki, M. Razeghi, and F. K. Tittel, "QEPAS based ppb-level detection of CO and N2O using a high power CW DFB-QCL," Opt. Express **21**, 1008–1019 (2013).

98. M. Horstjann, Y. A. Bakhirkin, A. A. Kosterev, R. F. Curl, F. K. Tittel, C. M. Wong, C. J. Hill, and R. Q. Yang, "Formaldehyde sensor using interband cascade laser based quartz-enhanced photoacoustic spectroscopy," Appl. Phys. B **79**, 799–803 (2004).

99. A. A. Kosterev and F. K. Tittel, "Ammonia detection by use of quartz-enhanced photoacoustic spectroscopy with a near-IR telecommunication diode laser," Appl. Opt. **43**, 6213–6217 (2004).

100. M. Köhring, A. Pohlkötter, U. Willer, M. Angelmahr, and W. Schade, "Tuning fork enhanced interferometric photoacoustic spectroscopy: a new method for trace gas analysis," Appl. Phys. B **102**, 133–139 (2010).

101. A. Manninen, J. Sand, J. Saarela, T. Sorvajärvi, J. Toivonen, and R. Hernberg, "Electromechanical film as a photoacoustic transducer," Opt. Express **17**, 16994–16999 (2009).

102. J. Saarela, J. Sand, T. Sorvajärvi, A. Manninen, and J. Toivonen, "Transversely Excited Multipass Photoacoustic Cell Using Electromechanical Film as Microphone," Sensors (Basel) **10**, 5294–5307 (2010).

103. P. Sievilä, V.-P. Rytkönen, O. Hahtela, N. Chekurov, J. Kauppinen, and I. Tittonen, "Fabrication and characterization of an ultrasensitive acousto-optical cantilever," J. Micromech. Microeng. **17**, 852–859 (2007).

104. P. Sievilä, J. Fonsen, O. Hahtela, N. Chekurov, J. Kauppinen, and I. Tittonen, "Optically Detected, Framed Silicon Cantilever for High Precision Acoustic Sensing," in *Proceedings of TRANSDUCERS 2007 - International Solid-State Sensors, Actuators and Microsystems Conference* (IEEE, 2007), pp. 2605–2608.

105. T. Laurila, H. Cattaneo, V. Koskinen, J. Kauppinen, and R. Hernberg, "Diode laser-based photoacoustic spectroscopy with interferometrically-enhanced cantilever detection," Opt. Express **13**, 2453–2458 (2005).

106. J. Uotila and J. Kauppinen, "Fourier transform infrared measurement of solid-, liquid-, and gas-phase samples with a single photoacoustic cell," Appl. Spectrosc. **62**, 655–660 (2008).

107. J. Kauppinen, V. Koskinen, J. Uotila, and I. Kauppinen, "Extremely sensitive CWA analyzer based on a novel optical pressure sensor in photoacoustic gas analysis," Proc. SPIE **5617**, 115–127 (2004).

108. J. Fonsen, V. Koskinen, K. Roth, and J. Kauppinen, "Dual cantilever enhanced photoacoustic detector with pulsed broadband IR-source," Vib. Spectrosc. **50**, 214–217 (2009).

109. T. Kuusela, J. Peura, B. A. Matveev, M. A. Remennyy, and N. M. Stus', "Photoacoustic gas detection using a cantilever microphone and III–V mid-IR LEDs," Vib. Spectrosc. **51**, 289–293 (2009).

110. A. M. Parkes, K. A. Keen, and E. D. McNaghten, "Trace gas detection using a novel cantilever-based photoacoustic spectrometer with multiplexed optical fiber-coupled diode lasers and fiber-amplification," Proc. SPIE **6770**, 67701C (2007).

111. V. Koskinen, J. Fonsen, K. Roth, and J. Kauppinen, "Cantilever enhanced photoacoustic detection of carbon dioxide using a tunable diode laser source," Appl. Phys. B **86**, 451–454 (2007).

112. T. Laurila, H. Cattaneo, T. Pöyhönen, V. Koskinen, J. Kauppinen, and R. Hernberg, "Cantilever-based photoacoustic detection of carbon dioxide using a fiber-amplified diode laser," Appl. Phys. B **83**, 285–288 (2006).

113. H. Cattaneo, T. Laurila, and R. Hernberg, "Photoacoustic detection of oxygen using cantilever enhanced technique," Appl. Phys. B **85**, 337–341 (2006).

114. J. Peltola, M. Vainio, T. Hieta, J. Uotila, S. Sinisalo, M. Metsälä, M. Siltanen, and L. Halonen, "High sensitivity trace gas detection by cantilever-enhanced photoacoustic spectroscopy using a mid-infrared continuous-wave optical parametric oscillator," Opt. Express **21**, 10240–10250 (2013).

115. J. Uotila, "A new design of the differential photoacoustic gas detector combined with a cantilever microphone," Eur. Phys. J. Spec. Top. **153**, 401–404 (2008).

116. J. Uotila, "Comparison of infrared sources for a differential photoacoustic gas detection system," Infrared Phys. Technol. **51**, 122–130 (2007).

117. J. Uotila, V. Koskinen, and J. Kauppinen, "Selective differential photoacoustic method for trace gas analysis," Vib. Spectrosc. **38**, 3–9 (2005).

118. I. Kauppinen, A. Branders, J. Uotila, S. Sinisalo, J. Kauppinen, and T. Kuusela, "Sensitive and Fast Gas Sensor for Wide Variety of Applications Based on Novel Differential Infrared Photoacoustic Principle," Tech. Mess. **79**, 17–22 (2012).

119. T. Laurila, H. Cattaneo, V. Koskinen, J. Kauppinen, and R. Hernberg, "Diode laser-based photoacoustic spectroscopy with interferometrically-enhanced cantilever detection: erratum," Opt. Express **14**, 4195 (2006).

120. T. Laurila, H. Cattaneo, T. Pöyhönen, V. Koskinen, J. Kauppinen, and R. Hernberg, "Cantilever-based photoacoustic detection of carbon dioxide using a fiber-amplified diode laser: erratum," Appl. Phys. B **83**, 669 (2006).

121. Gasera Ltd., "Gas analyzers," http://www.gasera.fi/products/gas-analyzers/.

122. R. Marbach, "Multivariate Kalibrierung, Selektivität und die SBC-Methode," Chemie Ing. Tech. **82**, 453–466 (2010).

123. R. Marbach, "Multivariate Calibration: A Science-Based Method - Part 1," Pharm. Manuf. **6**, 42–47 (2007).

124. R. Marbach, "Methods to significantly reduce the calibration cost of multichannel measurement instruments," U.S. patent 6,629,041 B1 (2003).

125. United States Food and Drug Administration, "Guidance for Industry: PAT – A Framework for Innovative Pharmaceutical Development, Manufacturing, and Quality Assurance," www.fda.gov/downloads/Drugs/Guidances/ucm070305.pdf.

126. R. Marbach, "A new method for multivariate calibration," J. Near Infrared Spectrosc. **13**, 241–254 (2005).

127. R. Marbach, "Multivariate Calibration: A Science-Based Method - Part 2," Pharm. Manuf. **6**, 44–47 (2007).

128. J. Kuligowski, M. Martínez Galera, M. D. Gil García, M. J. Culzoni, H. C. Goicoechea, S. Garrigues, G. Quintás, and M. de la Guardia, "Science based calibration for the extraction of "analyte-specific" HPLC-DAD chromatograms in environmental analysis," Talanta **83**, 1158–1165 (2011).

129. R. Marbach, "On Wiener filtering and the physics behind statistical modeling," J. Biomed. Opt. **7**, 130–147 (2002).

130. A. D. Mcnaught and A. Wilkinson, *IUPAC. Compendium of Chemical Terminology (the "Gold Book")*, 2nd ed. (Wiley-Blackwell, 1997).

131. G. L. Long and J. D. Winefordner, "Limit of detection: A closer look at the IUPAC definition," Anal. Chem. **55**, 712–724 (1983).

132. S. W. Sharpe, T. J. Johnson, R. L. Sams, P. M. Chu, G. C. Rhoderick, and P. A. Johnson, "Gas-Phase Databases for Quantitative Infrared Spectroscopy," Appl. Spectrosc. **58**, 1452–1461 (2004).

133. M. Ahro and J. Kauppinen, "Nonlinearity of Beer's Law in Gas-Phase FT-IR Spectroscopy," Appl. Spectrosc. **55**, 50–54 (2001).

134. Gasmet Technologies Oy, "FT-IR gas analyzer," www.gasmet.fi/files/26/GASMET_Dx-4000_Technical_Data_(v1.1).pdf.

135. Frost & Sullivan, *European Volatile Organic Compounds Control Equipment Markets* (2000).

136. E. P. C. Lai, S. Y. Su, E. Voigtman, and J. D. Winefordner, "A simple, corrosion-resistant flow cell for laser-induced photoacoustic spectroscopic detection of high-performance liquid chromatography effluents," Chromatographia **15**, 645–649 (1982).

137. E. P. C. Lai, E. Voigtman, and J. D. Winefordner, "Photoacoustic probe for spectroscopic measurements in condensed matter: convenient and corrosion-resistant," Appl. Opt. **21**, 3126–3128 (1982).

138. T. Sorvajärvi, A. Manninen, J. Toivonen, J. Saarela, and R. Hernberg, "Resonant photoacoustic cell for pulsed laser analysis of gases at high temperature," Rev. Sci. Instrum. **80**, 123103 (2009).

139. H. Jalink and D. Bicanic, "Concept, design, and use of the photoacoustic heat pipe cell," Appl. Phys. Lett. **55**, 1507–1509 (1989).

140. D. Bicanic, H. Jalink, and B. van Veldhuizen, "The compact, resonant heat-pipe photoacoustic cell used for high temperature studies and as a gas chromatographic detector," Meas. Sci. Technol. **1**, 247–249 (1990).

141. D. Bicanic, M. Chirtoc, M. Lubbers, and H. Jalink, "A photoacoustic detector of the total carbon content in soil water solutions," Meas. Sci. Technol. **4**, 1016–1020 (1993).

142. H. A. Beck, Z. Bozóki, and R. Niessner, "Screening of Pentachlorophenol-Contaminated Wood by Thermodesorption Sampling and Photoacoustic Detection," Anal. Chem. **72**, 2171–2176 (2000).

143. J. Stenberg, R. Hernberg, and J. Vattulainen, "Analysis of pollutant chemistry in combustion by in situ pulsed photoacoustic laser diagnostics," Appl. Opt. **34**, 8400–8408 (1995).

144. R. Kästle and M. W. Sigrist, "Temperature-dependent photoacoustic spectroscopy with a Helmholtz resonator," Appl. Phys. B **63**, 389–397 (1996).

145. Gasmet Technologies Oy, "Gasmet calibrator," http://www.gasmet.fi/na/products/gas_sampling_units_accessories.

146. M. Fehér, Y. Jiang, J. P. Maier, and A. Miklós, "Optoacoustic trace-gas monitoring with near-infrared diode lasers," Appl. Opt. 33, 1655–1658 (1994).

147. A. Varga, Z. Bozóki, M. Szakáll, and G. Szabó, "Photoacoustic system for on-line process monitoring of hydrogen sulfide (H2S) concentration in natural gas streams," Appl. Phys. B **85**, 315–321 (2006).

148. World Health Organization (WHO), "Formaldehyde: Concise International Chemical Assessment Document 40," http://www.inchem.org/documents/cicads/cicads/cicad40.htm.

149. I. M. Ritchie and R. G. Lehnen, "Formaldehyde-related Health Complaints of Residents Living in Mobile and Conventional Homes," Am. J. Public Health **77**, 323–328 (1987).

150. T. Malaka and A. M. Kodama, "Respiratory Health of Plywood Workers Occupationally Exposed to Formaldehyde," Arch. Environ. Health **45**, 288–294 (1990).

151. T. Salthammer, S. Mentese, and R. Marutzky, "Formaldehyde in the Indoor Environment," Chem. Rev. **110**, 2536–2572 (2010).

152. K. T. Morgan, "A Brief Review of Formaldehyde Carcinogenesis in Relation to Rat Nasal Pathology and Human Health Risk Assessment," Toxicol. Pathol. **24**, 291–307 (1997).

153. Finnish Institute of Occupational Health, "Formaldehyde: Effects to health and exposure," http://www.ttl.fi/fi/kemikaaliturvallisuus/ainekohtaista_kemikaalitietoa/formaldehydi/formaldehydin_terveysahaitat_ja_ltistuminen/sivut/default.aspx.

154. A. Wehinger, A. Schmid, S. Mechtcheriakov, M. Ledochowski, C. Grabmer, G. A. Gastl, and A. Amann, "Lung cancer detection by proton transfer reaction mass-spectrometric analysis of human breath gas," Int. J. Mass Spectrom. **265**, 49–59 (2007).

155. T. Gensty and W. Elsäßer, "Semiclassical model for the relative intensity noise of intersubband quantum cascade lasers," Opt. Commun. **256**, 171–183 (2005).

156. T. Gensty, W. Elsäßer, and C. Mann, "Intensity noise properties of quantum cascade lasers," Opt. Express **13**, 2032–2039 (2005).

157. L. S. Rothman, I. E. Gordon, A. Barbe, D. C. Benner, P. F. Bernath, M. Birk, V. Boudon, L. R. Brown, A. Campargue, J.-P. Champion, K. Chance, L. H. Coudert, V. Dana, V. M. Devi, S. Fally, J.-M. Flaud, R. R. Gamache, A. Goldman, D. Jacquemart, I. Kleiner, N. Lacome, W. J. Lafferty, J.-Y. Mandin, S. T. Massie, S. N. Mikhailenko, C. E. Miller, N. Moazzen-Ahmadi, O. V. Naumenko, A. V. Nikitin, J. Orphal, V. I. Perevalov, A. Perrin, A. Predoi-Cross, C. P. Rinsland, M. Rotger, M. Šimečková, M. A. H. Smith, K. Sung, S. A. Tashkun, J. Tennyson, R. A. Toth, A. C. Vandaele, and J. Vander Auwera, "The HITRAN 2008 molecular spectroscopic database," J. Quant. Spectrosc. Radiat. Transf. **110**, 533–572 (2009).

158. T. Iguchi, "Modulation waveforms for second-harmonic detection with tunable diode lasers," J. Opt. Soc. Am. B Opt. Phys. **3**, 419–423 (1986).

159. J. Saarela, J. Toivonen, A. Manninen, T. Sorvajärvi, and R. Hernberg, "Wavelength modulation waveforms in laser photoacoustic spectroscopy," Appl. Opt. **48**, 743–747 (2009).

160. M. Wolff and H. G. Groninga, "Photoacoustic sensor for VOCs: first step towards a lung cancer breath test," Proc. SPIE **5862**, 58620G (2005).

161. F. G. Bijnen, H. Zuckermann, F. J. Harren, and J. Reuss, "Multicomponent trace-gas analysis by three intracavity photoacoustic cells in a CO laser: observation of anaerobic and postanaerobic emission of acetaldehyde and ethanol in cherry tomatoes," Appl. Opt. **37**, 3345–3353 (1998).

162. J. Hellström, P. Jänes, G. Elgcrona, and H. Karlsson, "Compact and efficient nanosecond pulsed tuneable OPO in the mid-IR spectral range," Proc. SPIE **8733**, 87330A (2013).

163. G. A. Pilidis, S. P. Karakitsios, and P. A. Kassomenos, "BTX measurements in a medium-sized European city," Atmos. Environ. **39**, 6051–6065 (2005).

164. J. G. Calvert, R. Atkinson, K. H. Becker, R. M. Kamens, J. H. Seinfeld, T. J. Wallington, and G. Yarwood, *The Mechanisms of Atmospheric Oxidation of the Aromatic Hydrocarbons* (Oxford University Press, 2002).

165. World Health Organization (WHO), "Benzene: Int. Programme of Chemical Safety, Environmental Health Criteria No. 150," http://www.inchem.org/documents/ehc/ehc/ehc150.htm.

166. A. Ulrici, R. Seeber, M. Calderisi, G. Foca, J. Uotila, M. Carras, and A. M. Fiorello, "A feature selection strategy for the analysis of spectra from a photoacoustic sensing system," Proc. SPIE **8545**, 85450K (2012).

167. A. Schmohl, A. Miklos, and P. Hess, "Effects of adsorption–desorption processes on the response time and accuracy of photoacoustic detection of ammonia," Appl. Opt. **40**, 2571–2578 (2001).

ARTICLE I

Fourier transform infrared photoacoustic multicomponent gas spectroscopy with optical cantilever detection

In: Applied Spectroscopy **64**, pp. 293–297.

Fourier Transform Infrared Photoacoustic Multicomponent Gas Spectroscopy with Optical Cantilever Detection

CHRISTIAN BERND HIRSCHMANN,* JUHO UOTILA, SATU OJALA, JUSSI TENHUNEN, and RIITTA LIISA KEISKI

Mass and Heat Transfer Process Laboratory, Department of Process and Environmental Engineering, FI-90014 University of Oulu, Finland (C.B.H., S.O., R.L.K.); VTT, Photonics and Measurement Solutions, Kaitoväylä 1, FI-90570 Oulu, Finland (C.B.H., S.O., J.T.); and Gasera Ltd., Tykistökatu 4, FI-20520 Turku, Finland (J.U.)

The sensitivity of photoacoustic spectroscopy was improved with the invention of optical cantilever detection (PAS-OCD). However, the ability of present PAS-OCD devices to carry out multicomponent detection is poor. To overcome this, a Fourier transform infrared photoacoustic spectrometer with optical cantilever detection (FT-IR-PAS-OCD) prototype was assembled. In this article, the first evaluation and performance tests of the prototype are described. Selectivity, sensitivity, and the linearity of the signal response are evaluated. The linear response was studied for methane and carbon dioxide and confirmed in the whole analyzed concentration range from 500 to 3500 ppm and from 2500 to 17500 ppm, respectively. The calculated signal-to-noise ratio (SNR) and limit of detection were 2027 and 0.5 ppm for methane and 1362 and 4 ppm for carbon dioxide, with a measurement time of 100 seconds. Selectivity was studied with a multicomponent gas mixture of propene, methane, carbon dioxide, and methylmercaptane. The results indicate that a quantitative analysis of all components in the mixture is possible using the FT-IR-PAS-OCD.

Index Headings: **Photoacoustic spectroscopy; PAS; Fourier transform infrared spectroscopy; FT-IR spectroscopy; Cantilever microphone; Optical cantilever detection; OCD; Multicomponent gas mixture; Linearity.**

INTRODUCTION

Fourier transform infrared (FT-IR) spectrometers, based on the absorption principle, and optical detectors are working very close to their theoretical performance limits.[1,2] The sensitivity of conventional IR absorption techniques can only be enhanced by increasing the optical path length.[1–3] However, increasing the optical path length leads to large, bulky cells that are difficult to construct and to nonlinearities.[4] These nonlinearities become particularly noticeable when wet gases are measured, since both the analyte and the water have a nonlinear response.[4,5] To summarize, it is not possible to significantly improve the sensitivity of the conventional IR absorption technique. To achieve higher sensitivity, new techniques, such as photoacoustic methods, which offer a zero background signal, must be used.[1–5]

The existing and common photoacoustic methods using capacitive microphones for detection of photoacoustic signals are subject to restrictions, such as the nonlinear pressure response. The nonlinearity is caused by the material, which has to stretch out radially under the pressure variation.[1,3,5] The second big drawback is the poor sensitivity, which is due to the "breathing effect" of the microphone. This breathing or "damping" effect is caused by the air flow between the rigid electrode and the flexible membrane.[1,5,6] Further, the response of the membrane also depends on the tension, which is a function of temperature. Since, the membrane response is also dependent on temperature, the thermal stability of the membrane microphone is bad.[7]

To overcome these limitations, Kauppinen, from the University of Turku, Finland, invented the optical readout cantilever microphone in the recent past. This optical microphone is not subject to the physical limitations of the condenser microphone, allowing improvements to the sensitivity and the dynamic range.[1,5–8] Using the optical cantilever detection (OCD) technique, the photoacoustic method can be 100 times more sensitive than with conventional capacitive microphones.[2,9,10]

So far, photoacoustic gas spectroscopy using optical cantilever detection (PAS-OCD) has only been set up with lasers, diode lasers, or blackbody radiators with filters. Consequently, the sensitivity has been enhanced by the optical microphone, but the selectivity of filters and the multicomponent ability of both filters and laser devices is still poor. To improve the multicomponent ability, a new combination of the PAS-OCD system with a highly selective but broadband detecting technique, such as FT-IR with a black body radiator, can be set up. This combination of both the sensitive optical cantilever microphone and the selective FT-IR has been realized by GASERA (Finland) in an FT-IR-PAS-OCD prototype. In this paper the FT-IR-PAS-OCD prototype spectrometer is introduced and the first performance tests are reported.

PROTOTYPE SPECTROMETER FOR FOURIER TRANSFORM INFRARED PHOTOACOUSTIC GAS SPECTROSCOPY USING OPTICAL CANTILEVER DETECTION

Figure 1 shows the schematic design and Table I gives an overview of the specific parameters of the FT-IR-PAS-OCD spectrometer. Light is generated by the broadband IR source, irradiated to the Michelson interferometer, and modulated by the moving mirror, beam splitter, and fixed mirror. The output of the interferometer is modulated light, where each infrared wavelength is modulated at a different frequency. From the interferometer, the modulated light is guided into the photoacoustic sample cell. Acoustical waves, generated by the sample, are detected with the optical cantilever microphone inside the cell. For the displacement measurement of the cantilever, a second interferometer (not shown in Fig. 1) is applied. In this interferometer the cantilever acts as the moving mirror. The spatial change of the interference fringes of the laser light beam are measured by four photodiodes. The phase of this interference signal is proportional to the cantilever

Received 21 August 2009; accepted 10 December 2009.
* Author to whom correspondence should be sent. E-mail: Christian.Hirschmann@vtt.fi.

0003-7028/10/6403-0293$2.00/0

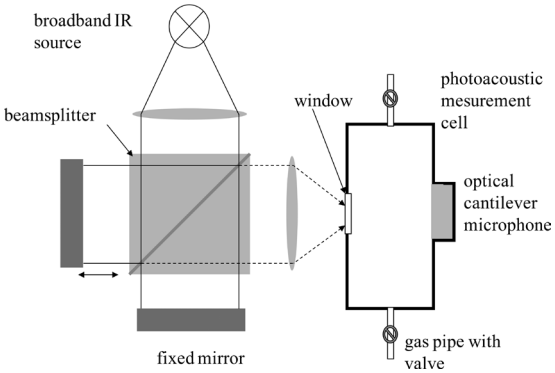

FIG. 1. Schematic design of the FT-IR-PAS using optical cantilever detection.

displacement and the photoacoustic signal. To become a photoacoustic spectrum, the output signal of the optical microphone is Fourier transformed by the software. The function of the optical readout cantilever microphone and the generation and mathematical modeling of the photoacoustic signal are exactly explained in Ref. 5. Additional information about the performance of the same kind of photoacoustic cell and the normalized sensitivity values (NNEA) can be found in Ref. 2. Basically, the flow of sample gas through the photoacoustic cell has to be stopped for the measurement due to the acoustic noise generated by the flow. This limits the system somewhat in terms of continuous measurements. The total time for a measurement is the sum of the used integration time (in this article 100 seconds) plus the time for purging and refilling the cell, which is about 10 seconds.

TABLE I. Specifications of the FT-IR-PAS-OCD system.

	Parameter	Value
FT-IR interferometer	Manufacturer	Bruker Optik GmbH
	Model	Matrix series, IRcube
	Resolution	Variable: min 0.6 cm^{-1}
	Mirror velocity	1.6 and 5 kHz
	Spectral range	200-6000 cm^{-1}
	Beam splitter	KBr–Germanium
	Window material	KBr
	Aperture	Variable: 3, 4 mm
	Focal legth of collimating mirror	69 mm
	Focal legth of focusing mirror	76.2 mm
	Focal spot size	4.4 mm
	Collimated interferometer output beam diameter	25 mm
Sample cell	Material	Aluminium, inside coated with nickel and gold
	Volume	<8 mL
	Length	100 mm
	Optical length	Because of a mirror at the other end: 200 mm
	Radius	4.5 mm
	Internal geometry	Cylindrical
	Window radius	4.5 mm
	Window coating	Gold
	Window material	BaF_2
	Temperature	50 °C, maximum
	Pressure	470 mbar
	Resonance frequency	Above 480 Hz (@ 500 mbar pressure)
	Resonant mode	Nonresonant
Cantilever	Dimensions (length, thickness, width)	6 mm, 10 μm, 1.5 mm
	Gap between the frame	<5 μm

EXPERIMENTAL

Measurement Setup. The experimental setup included the analyte gas and nitrogen for the dilution in separate bottles with pressure reducers, pressure control unit with over pressure valve, and sample reservoir made out of steel. For a precise adjustment of the gas flow, two mass flow controllers were used (Brooks Instrument, model 5878-2 for analyte gas, AALBORG mass flow meter GFM17 for nitrogen). A schematic of the assembly is shown in Fig. 2. After the gas flows were set to the desired rates, two gas pipes were connected together by a T-piece. After blending, the maximal pressure of the blended gas could be set with the pressure control unit (Tekmar-Dohrmann, part no: 14-3938-000). The pressure of the gas conducted into the photoacoustic device was limited to 1.3 atm due to the sensitive cantilever. The pressure control unit was set to this value and the over pressure valve guarantied that no pressure higher than that was applied to the spectrometer. Before the gas pipe was connected to the spectrometer, the last step of the sample preparation was done: The gas flowed into a bottle that acted as a reservoir. In case of a sample change, the pump built in the photoacoustic device vacuumed the sample through the pipe system into the photoacoustic sample cell. If the sampling reservoir were not installed, and the sampling system changed the sample, then the pressure in the system and even the gas flow through the mass controllers would change, caused by the vacuum pump. On that account, the one-liter sample reservoir was installed to buffer the pressure variations.

Gases. The analyte gases used were propene, methylmercaptane, and a blend of methane and carbon dioxide. The methane and carbon dioxide blend was mixed by the supplier Linde Gas/AGA. The gases were diluted with nitrogen, due to the high concentrations of the purchased gases and gas mixtures (propene 5000 ppm, methane 10000 ppm, and carbon dioxide 50000 ppm). Dilution was performed with the self built dilution apparatus. For the selectivity experiment methylmercaptane was utilized as delivered (2000 ppm), propene and

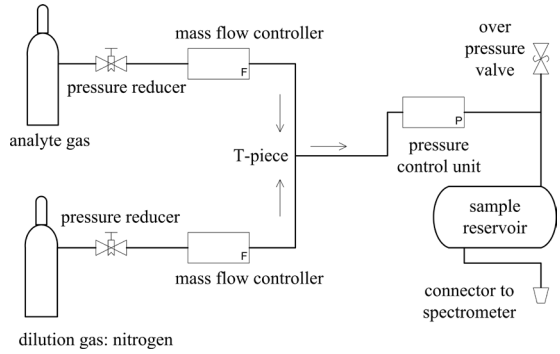

FIG. 2. Schematic drawing of the gas sampling system.

methane were diluted to 1000 ppm, and carbon dioxide was diluted to 5000 ppm. In the sensitivity and the linearity experiment, only methane and carbon dioxide were used. The sensitivity experiment was carried out with 1000 ppm of methane and 5000 ppm of carbon dioxide. For the linearity experiment, the two gases are diluted to several concentrations: for methane, 500, 800, 1000, 1500, 2000, and 3500 ppm; and the corresponding dilutions for carbon dioxide, 2500, 4000, 5000, 7000, 10000, and 17500 ppm. Different concentrations of methane and carbon dioxide in the gas bottle led to the differences in the diluted concentrations.

Measurement Parameters. The measurement parameters for the different experiments are shown in Table II.

RESULTS AND DISCUSSION

Selectivity. A multicomponent gas mixture of several gases with absorption bands in narrow regions would be ideal to describe the selectivity of the spectrometer. Due to the presented gas mixing apparatus, it was not possible to mix more than two gases. For this scope, the spectra of the individual gases were measured consecutively. After that, the spectra were combined in to a "resulting" spectrum. Figure 3 shows the spectra of the single gases and the resulting combined spectrum. The raw spectra were background corrected and the water bands were subtracted with the Photoacoustic FT-IR Analysis software from GASERA.

In some ranges the spectra of the three organic carbon compounds are strongly overlapping, such as in the region of stretch (str) C–H, C–H_2, and C–H_3 vibration occurring from 2900 to 3150 cm^{-1}. However, the region of deformation (def) vibrations still contains areas where the single spectra are not overlapping. It is not a problem to set up a quantitative calibration of the four components by means of multivariate calibration methods, such as partial least square regression (PLS) or science based calibration (SBC). Also, it would still be possible to use the classical "one wavelength calibration method" in areas without spectral overlap, such as for methane at 669 or 1270 cm^{-1}, carbon dioxide at 2355 cm^{-1}, propene at 1665 or 910 cm^{-1}, and methylmercaptane at 1090 cm^{-1}.

Using the weaker pronounced deformation vibrations compared to the strong pronounced stretch vibrations, the signal-to-noise ratio (SNR) will drop, along with the associated sensitivity.

The selectivity can also be described in a graphical way, using the rotational vibrational spectrum of methane. Figure 4 shows the measured rotational vibrational spectrum of methane, which was measured with a resolution of 4 cm^{-1}. The minimal resolution of this device can still be lower, up to 0.6 cm^{-1}. With the used resolution of 4 cm^{-1} it was possible to discriminate between the single rotational levels of the vibrational transition.

TABLE II. Measurement parameters for the gases.

Sample	Methane carbon dioxide blend	Methylmercaptane, propene
Spectral interval [cm^{-1}]	200–6000	200–6000
Resolution [cm^{-1}]	4	4
Aperture [mm]	4	4
Averaged spectra	5	10
Gain	5	10
Mirror velocity [kHz]	1.6	1.6

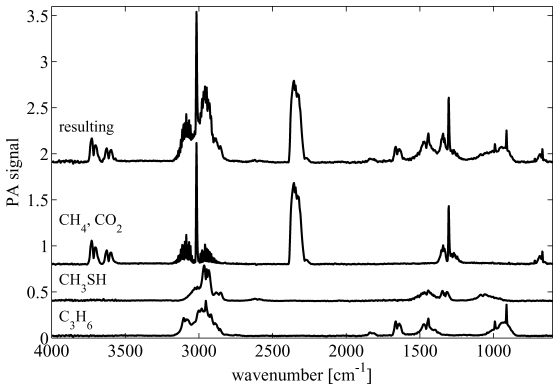

FIG. 3. Single spectra and the resulting combined methane (1000 ppm), carbon dioxide (5000 ppm), propene (1000 ppm), and methylmercaptane (2000 ppm) spectrum.

Sensitivity. The SNR is a meaningful attribute and relates the height of the gained signal to the noise. The signal S was found by searching for the maximum of the absorption band in the raw spectrum. In order to obtain the correct calculation, the offset of the band had to be subtracted from the peak height. To calculate the noise N, a straight line was fitted through the spectrum where no absorption signal occurred. Then the standard deviation of the variation of the measured data points to the fitted line was calculated. One standard deviation was used as the noise. Spectral positions of signals were at 3017 cm^{-1} for the str C–H vibration of methane and 2356 cm^{-1} for the asymmetrical (asym) str C=O vibration of carbon dioxide. For calculation of the noise the spectral area between 3200 and 3250 cm^{-1} was used for both gases. SNR was calculated for the concentration of 1000 ppm methane and 5000 ppm carbon dioxide. The PA signal for methane was 1.30 (arbitrary units) and for carbon dioxide was 0.87, and the noise for both gases was 6.42×10^{-4}. Hence, a SNR for methane of 2027 and for carbon dioxide of 1362 was achieved. To calculate the limit of detection, the concentration was divided by the SNR, as

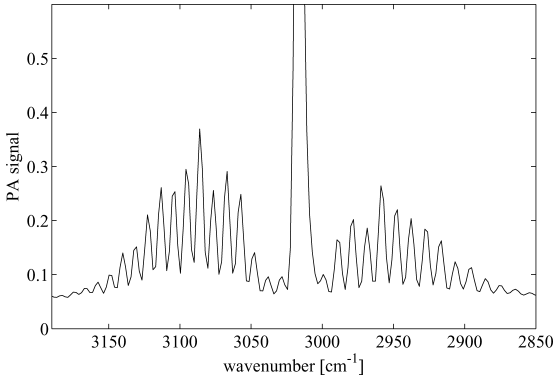

FIG. 4. Rotational vibrational spectrum of methane at the str C–H absorption band.

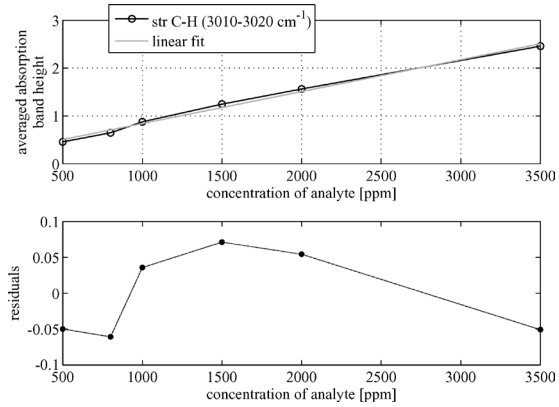

FIG. 5. Linearity analysis of the str C–H band of methane in the blend with carbon dioxide; (**top**) averaged band height on the concentration with the fitted lines; (**bottom**) residuals of the fit.

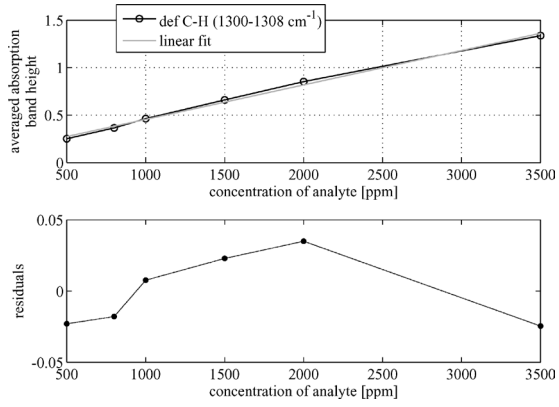

FIG. 6. Linearity analysis of the def C–H band of methane in the blend with carbon dioxide; (**top**) averaged band height on the concentration with the fitted lines; (**bottom**) residuals of the fit.

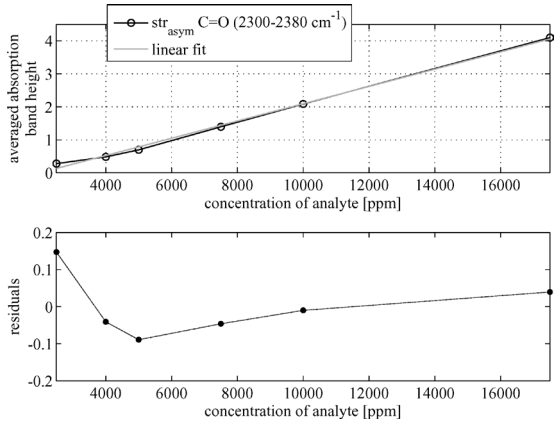

FIG. 7. Linearity analysis of the asym str C=O band of carbon dioxide in the blend with methane; (**top**) averaged band height on the concentration with the fitted lines; (**bottom**) residuals of the fit.

follows: for methane 1000 ppm/2027 = 0.5 ppm and for carbon dioxide 5000 ppm/1362 = 4 ppm.

Previous estimations assumed that the sensitivity of the FT-IR-PAS-OCD would be not as good as PAS-OCD devices using laser or blackbody radiators with filters because the light throughput is limited by the interferometer. Still, the presented data shows that it is possible to detect methane in trace gas concentrations around 1 ppm with a measurement time of 100 seconds. Compared to the existing literature of photoacoustic-OCD measurements, it can not beat the laser- and filter-based methods. Fonsen et al.[6] achieved a detection limit for methane of 0.5 ppm with a measurement time of only 5 seconds, using an electrically modulated broadband infrared source combined with a filter. Kauppinen et al.[1] achieved a detection limit for methane of 0.8 ppb with a measurement time of 100 seconds using a blackbody radiator and an optical filter. Uotila et al.[11] found a detection limit for methane of 13 ppb using the selective differential photoacoustic method. The measurement time was 0.37 seconds and the effective absorption path length was one meter.

The FT-IR-PAS-OCD spectrometer still has the advantage of improved selectivity and multicomponent detection ability; as opposed to filter devices, for which one measurement corresponds to only one measured gas, FT-IR-PAS-OCD can detect several components in one measurement, as demonstrated here with methane and carbon dioxide. To demonstrate the full power of the instrument, a mixture of several gases should be used to compare the devices. Then the measurement time can even be compared to the amount of the number of measured components, which will further highlight the advantages of FT-IR-PAS-OCD. The future application of FT-IR-PAS-OCD will be in the area of multicomponent measurements, in which more than two gases would be measured, or in the measurement of only one gas, mixed with interfering gases. These applications can be found in both the laboratory and in industry.

Linearity. The signal response in PAS is said to be linear.[1,3] In order to test this claim, gas dilutions of higher concentration were prepared, in addition to low concentration gases. Authors of actual PAS-OCD articles have focused quite often on trace gas detection. However, for industrial applications, the high concentration area is also interesting. A linear response of the signal is particularly interesting, because in practice a nonlinear calibration requires many measurements and a complex fitting algorithm.[11] During this testing, the examined methane gas concentration ranged from 500 ppm up to 3500 ppm and for carbon dioxide it ranged from 2500 to 17500 ppm.

For the analysis, the absorption bands were averaged over the whole absorption band in the following ranges: str C–H from 3010 to 3020 cm^{-1}, def C–H from 1300 to 1308 cm^{-1}, and asym str C=O from 2300 to 2380 cm^{-1}. This procedure was done for each gas concentration. Figures 5, 6, and 7 show the averaged absorption band height versus the corresponding concentration for the three bands: str C–H, def C–H, and asym str C=O.

According to the graphics, the measured data for methane as well as for carbon dioxide follows a linear absorption function. The measured data points show an averaged deviation to the

linear fit for str C–H of 5.38×10^{-2}, def C–H of 2.18×10^{-2}, and asym str C=O of 6.22×10^{-2}. These deviations could be explained by the self-assembled gas dilution setup. For more precise issues, like a calibration, it would be better to order test gases with certified concentrations to avoid errors caused by self-mixing the gases, or the concentration of the self-mixed gases should be verified with certainty by another method.

Apart from the deviation, which can be explained by the self-made apparatus, the linearity of the PAS signal is given in the examined concentration area. This is a huge gain for industrial applications. Only one gas concentration is needed to set up a quantitative calibration. Even re-calibration, after instrument servicing or a light source change, is simple. The quantitative water subtraction should also be easy, which will be studied in further investigations.

CONCLUSION

The newly invented FT-IR-PAS-OCD prototype has been set up and the first performance tests are reported here. Compared to PAS-OCD devices based on filters and lasers, the selectivity and the multicomponent detection ability is enormously increased. Sensitivities of filter- and laser-based devices could not be reached with the existing prototype. In the future, the sensitivity can be increased by enlarging the light source and the aperture without the need to tightly focus the small detector. This can be done, because the linear signal response enables the effective least squares fit, even if different components show high cross interference. In the high concentration range the response of the gained signal is still linear. In any field of gas measurements a linear response is a very interesting feature for industrial applications. Linearity allows low-cost calibration and simple adaption to different problems.

ACKNOWLEDGMENTS

The authors wish to thank GASERA Ltd., Finland, for the excellent technical support and the permission to publish an article about the device. Further, the authors acknowledge the financial support of the Baden-Württemberg scholarship from the Federal State of Baden-Württemberg, Germany.

1. J. Kauppinen, K. Wilcken, I. Kauppinen, and V. Koskinen, Micromech. J. **76,** 151 (2004).
2. V. Koskinen, J. Fonsen, K. Roth, and J. Kauppinen, J. Appl. Phys. B **86,** 451 (2007).
3. V. Koskinen, J. Fonsen, J. Kauppinen, and I. Kauppinen, Vib. Spectrosc. **42,** 239 (2006).
4. V. Koskinen, J. Fonsen, K. Roth, and J. Kauppinen, Vib. Spectrosc. **48,** 16 (2008).
5. T. Kuusela and J. Kauppinen, Appl. Spectrosc. Rev. **42,** 443 (2007).
6. J. Fonsen, V. Koskinen, K. Roth, and J. Kauppinen, Vib. Spectrosc. **50,** 214 (2009).
7. P. Sievila, V. P. Rytkönen, O. Hahtela, N. Chekurov, J. Kauppinen, and I. Tittonen, J. Micromech. Microeng. **17,** 852 (2007).
8. P. Sievila, J. Fonsen, O. Hahtela, N. Chekurov, J. Kauppinen, and I. Tittonen, "Optically detected, framed silicon cantilever for high precision acoustic sensing", Solid-State Sensors, Actuators and Microsystems Conference (Lyon, France, 2007), p. 2605.
9. R. E. Lindley, A. M. Parkes, K. A. Keen, E. D. McNaghten, and A. J. Orr-Ewing, J. Appl. Phys. B **86,** 707 (2007).
10. A. Olafsson, G. I. Hansen, A. S. Loftsdottir, and S. Jakobsson, "FT-IR photoacoustic trace gas detection", in *Photoacoustic and Photothermal Phenomena: 10th Interntional Conference*, F. Scudieri and M. Bertolotti, Eds. (1999), p. 208.
11. J. Uotila, V. Koskinen, and J. Kauppinen, Vib. Spectrosc. **38,** 3 (2005).

ARTICLE II

FT-IR-cPAS – New photoacoustic measurement technique for analysis of hot gases: A case study on VOCs

In: Sensors (Basel) **11**, pp. 5270–5289.

Sensors **2011**, *11*, 5270-5289; doi:10.3390/s110505270

OPEN ACCESS

sensors

ISSN 1424-8220

www.mdpi.com/journal/sensors

Article

FT-IR-cPAS—New Photoacoustic Measurement Technique for Analysis of Hot Gases: A Case Study on VOCs

Christian Bernd Hirschmann [1,2,*], Niina Susanna Koivikko [2], Jussi Raittila [3], Jussi Tenhunen [1], Satu Ojala [1,2], Katariina Rahkamaa-Tolonen [1], Ralf Marbach [1], Sarah Hirschmann [2] and Riitta Liisa Keiski [2]

[1] Photonic Devices and Measurement Solutions, VTT Technical Research Centre of Finland, Kaitoväylä 1, FI-90570 Oulu, Finland; E-Mails: jussi.tenhunen@vtt.fi (J.T.); satu.ojala@oulu.fi (S.O.); katariina.rahkamaa-tolonen@vtt.fi (K.R.-T.); ralf.marbach@vtt.fi (R.M.)

[2] Mass and Heat Transfer Process Laboratory, Department of Process and Environmental Engineering, University of Oulu, FI-90014 Oulu, Finland; E-Mails: niina.koivikko@oulu.fi (N.S.K.); sarah.hirschmann@oulu.fi (S.H.); riitta.keiski@oulu.fi (R.L.K.)

[3] Gasera Ltd., Tykistökatu 4, FI-20520 Turku, Finland; E-Mail: jussi.raittila@gasera.fi (J.R.)

* Author to whom correspondence should be addressed; E-Mail: christian.hirschmann@vtt.fi; Tel.: +358-40-187-7447; Fax: +358-20-722-2320.

Received: 7 April 2011; in revised form: 4 May 2011 / Accepted: 12 May 2011 / Published: 16 May 2011

Abstract: This article describes a new photoacoustic FT-IR system capable of operating at elevated temperatures. The key hardware component is an optical-readout cantilever microphone that can work up to 200 °C. All parts in contact with the sample gas were put into a heated oven, incl. the photoacoustic cell. The sensitivity of the built photoacoustic system was tested by measuring 18 different VOCs. At 100 ppm gas concentration, the univariate signal to noise ratios (1σ, measurement time 25.5 min, at highest peak, optical resolution 8 cm^{-1}) of the spectra varied from minimally 19 for o-xylene up to 329 for butyl acetate. The sensitivity can be improved by multivariate analyses over broad wavelength ranges, which effectively co-adds the univariate sensitivities achievable at individual wavelengths. The multivariate limit of detection (3σ, 8.5 min, full useful wavelength range), *i.e.*, the best possible inverse analytical sensitivity achievable at optimum calibration, was calculated using the SBC method and varied from 2.60 ppm for dichloromethane to 0.33 ppm for butyl acetate. Depending on the shape of the spectra,

which often only contain a few sharp peaks, the multivariate analysis improved the analytical sensitivity by 2.2 to 9.2 times compared to the univariate case. Selectivity and multi component ability were tested by a SBC calibration including 5 VOCs and water. The average cross selectivities turned out to be less than 2% and the resulting inverse analytical sensitivities of the 5 interfering VOCs was increased by maximum factor of 2.2 compared to the single component sensitivities. Water subtraction using SBC gave the true analyte concentration with a variation coefficient of 3%, although the sample spectra (methyl ethyl ketone, 200 ppm) contained water from 1,400 to 100k ppm and for subtraction only one water spectra (10k ppm) was used. The developed device shows significant improvement to the current state-of-the-art measurement methods used in industrial VOC measurements.

Keywords: volatile organic compound (VOC); photoacoustic spectroscopy (PAS); science based calibration (SBC); elevated temperature measurement

1. Introduction

In environmental pollutant and exhaust gas analyses, the emitted gas concentrations can be very low, and thus difficult to qualify and even more challenging to quantify. In spite of the technical progress of recent years, one of the most demanding and still unresolved needs is the reliable measurement of volatile organic compounds (VOC) [1,2]. VOC emissions cause atmospheric pollution and damage the stratospheric ozone layer. By reacting with nitrogen oxides, they create smog in the lower atmosphere which reduces the quality of air and finally harms human health [3-5]. Some VOCs can even be carcinogenic and genotoxic for humans. Besides humans, VOCs have a harmful effect on the whole environment including flora and fauna [6-8]. It is not surprising that the demand for measuring and monitoring of environmental pollutants has increased in recent years [9]. In industry, VOCs are released primarily from organic solvents, which are frequently used in a wide range of different industrial sectors, like chemical and pharmaceutical plants, painting facilities, *etc.* [10]. Abatement technologies for VOC emissions exist and are sometimes applied. However, the abatement cannot be completely validated, because the crucial point is the lack of accurate, continuous and reliable VOC measurement and monitoring technology. The success of the installed abatement unit is difficult to prove, if the outlet gas of the abatement system cannot be analyzed reliably.

Measuring VOC emissions is challenging. The problem in measuring them is that VOCs can occur in small concentrations (for example in measurements of odorous), but also in very high concentrations. In addition, they show a wide variety in their chemical composition [11-14]. In practice, emission streams are almost always mixtures of several compounds (including moisture and carbon dioxide) whose concentration values are not constant. These facts make the analysis of VOC emissions demanding. Requirements for the measurement system are sensitivity, selectivity and multi component ability. Sometimes the emissions contain corrosive compounds, which make the requirements for the measurement system even tougher. For industrial applications, the system has to be robust and contamination resistant. The presence of water vapor should not influence the

measurement, since water is frequently present in industrial measurements. In addition, if the system is used for continuous monitoring or in the scope of process analysis to process control purposes, the system needs to have on-line measurement capability. Until today, there has only been the FT-IR transmission spectroscopy using whitecells, which satisfies most of the requirements mentioned. The transmission technique, however, suffers from certain disadvantages, like the poor stability in a rough and corrosive industrial environment, the non-linear signal response and the high calibration effort. It also suffers from the interference of moisture. In return, photoacoustic spectroscopy has the ability to overcome the limitations mentioned.

By selecting a cantilever enhanced microphone as photoacoustic detector that has been developed in the past few recent years [15-21] photoacoustic spectroscopy, especially the cantilever enhanced one, has several advantages compared to state-of-the-art transmission spectroscopy. One valuable advantage, which can be very useful in industrial emission measurements, is the linearity in signal response. Short optical path lengths of only a few centimeters enable the linear response and opens the door for easy water subtraction, because not only the analyte but also the water absorption behaves linearly [9,18,19,21,22]. The improved photoacoustic detection also provides a linear dynamic range of at least four magnitudes with one point calibration. Together with Science Based Calibration (SBC) [23-25], cantilever enhanced photoacoustic spectroscopy allows low cost calibration and adaptation to different measurement tasks and chemical species. The water subtraction allows accurate process measurements even when water vapor is present, because the water can easily be subtracted and bands, which are overlapping or even lying under the water band can be analyzed [22]. However, the combination of FT-IR and cPAS (cantilever enhanced photoacoustic spectroscopy) was previously realized only for ambient temperatures and up to 50 °C. In some gas measurement applications, especially in industrial emission measurements, the gases to be measured are hot and need to be kept hot in order to avoid condensation. Therefore, the whole measurement system has to be heated. The target of the present approach was to build an FT-IR-cPAS measurement system working at an elevated temperature up to 180 °C and test the sensitivity performance of the system by measuring several different VOCs.

2. Experimental Section

2.1. FT-IR-cPAS Prototype

The FT-IR-cPAS measurement system consist of three parts, an FT-IR to provide and modulate the light, a photoacoustic cell with an optical cantilever readout (cPAS) to detect the photoacoustic signal and a gas exchange unit to circulate the sample through the measurement system. Bio-Rad's research grade FTS 6000 was used as FT-IR in the experiments. Since the photoacoustic effect is slow, low frequency modulation, *i.e.*, slow mirror drive, of the IR light is essential in photoacoustic FT-IR spectroscopy. Bio-Rad's FTS 6000 slowest scanning speed is 2.5 kHz relating to the modulation frequency of the HeNe laser (wavelength of HeNe laser is 632.8 nm, 15,802.8 cm^{-1}). To maximize the signal to noise ratio (SNR), the frequency band for the measurement has to be below the resonance frequency of the cantilever. The resonance of the cantilever in the cell is around 4,800 cm^{-1} (~750 Hz) with a scanning speed of 2.5 kHz. All considerable parameters of the FT-IR are listed in Table 1.

Table 1. Instrument parameters of FT-IR and cPAS cell.

Parameter	Value	Parameter	Value
FT-IR interferometer			
Manufacturer	Bio-Rad	model	FTS 6000
Resolution	8 cm^{-1}	mirror velocity	2.5 kHz
Spectral Range	400–8,000 cm^{-1}	beam splitter	KBr
Aperture	11.94 mm	focal spot size	11.94 mm
Co-Added Scans	300		
Photoacoustic Sample Gas Cell			
Manufacturer	Gasera	model	PA101h
Material	stainless steel, inside gold	gas volume	about 8 mL
Diameter	4.0 mm	length	100 mm
Internal Geometry	cylindrical	optical path length	200 mm
Window Diameter	13 mm	temperature range	15–200 °C
Window Material	BaF_2	sample pressure	0–2 bar
Resonant Mode	non-resonant		
Cantilever			
Material	silicon, gold coated	thickness	10 μm
Length	5 mm	resonance frequency	750 Hz
Width	1.2 mm	gap between frame and cantilever	<5 μm

The cantilever enhanced photoacoustic cell (cPA cell) manufactured by Gasera, Finland, was optimized for elevated temperatures. The cell was then integrated into the measurement setup described here. Compared to common photoacoustic detectors, the readout mechanism of the photoacoustic signal is different. Pressure waves, generated in the cell, create a force on the silicon cantilever, the displacement of which is observed optically with an interferometric setup. The position of the cantilever is presented as an analog signal via digital to analog converter and routed to the FT-IR as analog detector interferogram signal. More information about the improved photoacoustic cell, including the detailed principle of operation, quantitative modeling as well as details of the interferometric readout can be found in the following references [15,17-21,26-28]. Table 1 shows the important cell parameters.

The PA cell is optically connected to the FT-IR by an ellipsoidal mirror, which images the focus of the sample compartment to the input aperture of the PAS cell. The light beam leaving the FT-IR has a diameter of 11.94 mm in the focus. The ellipsoidal mirror decreases the beam diameter by 3:1 to 3.98 mm, which is ideal for the PA cell with a diameter of 4 mm. The gas exchange system used was designed, built and tested by VTT. The main effort in designing and building was to find components, which can withstand rather high temperatures (up to 180 °C) and corrosive environment. The corrosion resistance is also important later on in industry, when unknown gases enter the measurement system. In addition, the system should be transportable to be able to carry it to industrial sites. An oven design was chosen to solve the heating problem. All components that needed to be heated were put into the self-built oven. The materials for the parts in contact with the sample gas were chosen to be PTFE or stainless steel grade SS316, sometimes coated with a Silcosteel coating. However, some parts could not be procured in high resistance quality. The function of the gas exchange system is to clean the sample cell by purging it with fresh sample gas, adjusting the pressure of the fresh sample gas inside the cell and after the measurement, purging the cell again with fresh

sample gas. For that purpose, the gas exchange unit contains the following parts: 0.5 µm particle filter at the inlet, membrane pump to forward the gas through the system, valves to seal the sample in the photoacoustic cell, a pressure sensor to monitor the sample pressure inside the cell and a control system to monitor the interaction of all components and the temperature inside the oven.

2.2. Chemicals—Model VOCs

The need of industry to measure certain VOCs directed the gas selection in this study. The selected model gases and their boiling points are shown in Table 2. All VOCs were measured at the concentrations of 100 ppm and 200 ppm (all the ppm values in this article are given as mol-ppm) diluted in nitrogen. The boiling point is an important value for the measurements because the VOCs are typically liquids in normal conditions and need to be vaporized for the measurement. For the same reason, the compounds can condense easily inside the measurement apparatus if the temperature inside the measurement set-up decreases to a certain level.

Table 2. Model VOCs used in the experiments.

VOC	Boiling point	VOC	Boiling point
acetone	56	methoxypropanol acetate	146
n-butanol	117	methyl acetate	60
butyl acetate	126	methyl ethyl ketone	80
dichloromethane	40	methyl isobutyl ketone	118
dimethylformamide	153	perchloroethylene	121
ethanol	78	toluene	111
isobutanol	108	*o*-xylene	144
isopropanol	83	*m*-xylene	139
methanol	65	*p*-xylene	138

2.3. Experiments

The VOC vapor generator consists of a mass flow controller for adjusting the carrier gas flow, a syringe pump for feeding the organic liquid and a vaporizer to vaporize the liquid. The feed rate of the syringe pump is calculated and adjusted for each VOC and each concentration. The evaporation temperature was chosen to always be 5 °C above the boiling point of the organic liquid. To avoid condensation and to ensure the vaporization, the connection line to the gas exchange system was heated up to 180 °C. For bypassing the sample gas and avoiding overpressures in the system, a T-connection conducted excess gas into exhaust. A scheme of the VOC vapor generator is shown in Figure 1. The sample gas pressure inside the photoacoustic cell was set always set at 1.3 bar.

Figure 1. Schematic set up of the VOC vapor generator.

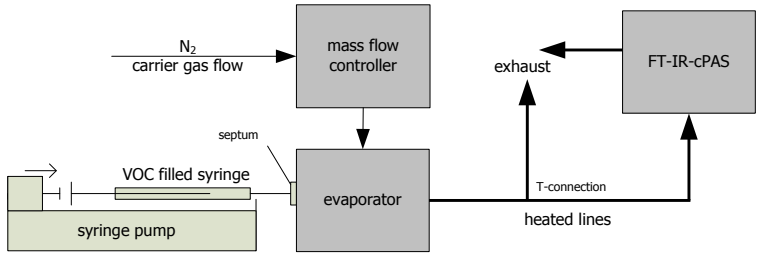

3. Results and Discussion

The first section of this chapter will go into details of the data pre-treatment with the background subtraction as its main issue. It will explain why the background subtraction is important here and how the problem was solved. After that, the second section will expand on the sensitivity of the newly built photoacoustic system. Sensitivity will be analyzed based on the univariate signal to noise ratio (SNR) and the multivariate limit of detection (LoD). The third section will analyze the selectivity and multi component ability by an SBC calibration with five interfering VOCs. In the fourth section, the ability of water subtraction will be tested. Finally, an overall evaluation section will discuss the most important findings. The amplitude of the PA single beam signal is measured in arbitrary units hereafter called PA signal intensity or 'PAI' for short.

3.1. Data Pre-Treatment

The output of a Fourier Transformation is a complex vector or in other words a complex spectrum consisting of a real and imaginary part. Calculating the magnitude spectrum via the phase correction [29] is the default setting of the majority of FT-IR software. Three main facts enable the phase correction in conventional transmission spectroscopy: the signal is at a high level at almost all wavelengths, the phase is a 'slow' function of the wavenumber and the absorption phenomena taking place in the sample does not affect the signal phase. Else in photoacoustic spectroscopy, the signal is practically zero at wide spectral regions, since only the narrow bands of the sample form the signal. Further, the delay in time between the absorption of the light and the proceeding of the photoacoustic effect, which results in the generation of the pressure wave, creates sample dependent phase changes. For these reasons, the magnitude PA spectrum is typically calculated directly as magnitude value from the real and imaginary parts. Looking from the chemical aspect, the measured PA signal consists of two parts; the signal from the analyte in gas phase and the signal from the cell (background). Since these two phenomena have different time delays or phases, the straightforward subtraction of the magnitude spectrum of the cell lead to incorrect results, especially if the measured photoacoustic signal of the analyte is small. Instead, a complex correction can be used as explained in Figure 2.

Figure 2. Complex background subtraction strategy at one, arbitrary wavenumber illustrated with vectors in the complex plain. The measured signal with analyte in the cell (grey) contains the signal from both analyte and cell. The measured signal from dry N_2 (red) only contains the signal from the cell. The desired pure analyte signal (blue) results from the complex background subtraction of the measured cell signal from the measured sample signal.

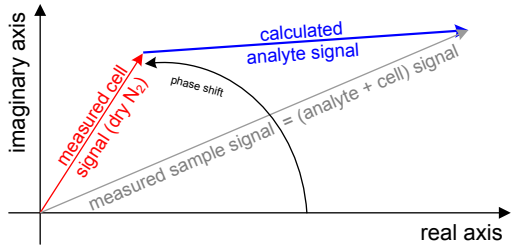

The measured interferograms (I) gained from the photoacoustic detector were treated by a complex Fast Fourier Transformation (FFT), giving out the complex signal (S) as real ($_r$) and imaginary ($_i$) part. To make things easier here, S is the signal at one wavenumber:

$$I \xrightarrow{FFT} S_{r,i} \tag{1}$$

The background signal of the cell, measured with pure, dry nitrogen ($Sb_{r,i}$) (red arrow in Figure 2), is removed by subtracting its real and imaginary parts from the measured sample signal ($Ss_{r,i}$) (grey arrow) resulting in the complex calculated analyte signal $Sa_{r,i}$ (blue arrow):

$$Sa_{r,i} = Ss_{r,i} - Sb_{r,i} \tag{2}$$

Finally, the magnitude analyte spectrum (Sa_m) is calculated as power spectrum:

$$Sa_m = \sqrt{Sa_r^{\,2} + Sa_i^{\,2}} \tag{3}$$

Toluene's spectrum at 100 ppm was selected to show the differences between the two background subtraction methods. On the one hand, the background was calculated in the complex plain and after that the power spectrum, which will hereafter be called 'complex subtraction'. On the other hand, the magnitude of the toluene and background spectra were calculated and after that subtracted hereafter called 'magnitude subtraction'. The visual result of the subtraction is shown in Figure 3.

Figure 3. Comparison of the background subtraction performed as complex and magnitude as an example of toluene at 100 ppm. To make this figure well arranged, the result spectrum of the complex subtraction is plotted with an offset of +0.005 PAI and the result spectrum for the magnitude subtraction with +0.05 PAI.

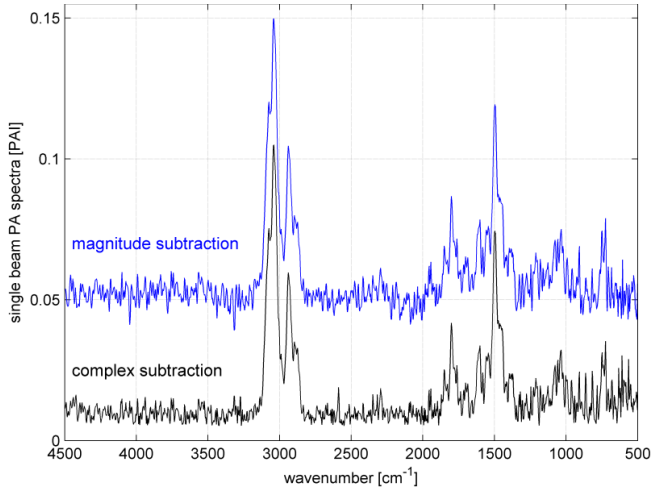

It can be seen in the figure that the peak heights of the absorption band at 1,500 and 3,000 cm^{-1} are identical independent of the subtraction method used. However, the baseline of the spectrum resulting from the complex subtraction is smoother and the amplitude of the noise seems to be smaller. This visual observation can be proven by calculating the coefficient of variation (CV) of the spectral regions where no absorption occurs. It turns out that the CV is smaller by a factor of 3.5 for the complex

subtraction than for the magnitude in the spectral range between 2,200 and 2,800 cm^{-1}. Still, for both subtraction methods the background in the region from 500 to 1,400 cm^{-1} looks somehow higher than the background in the region between 2,200 and 2,800 cm^{-1}. This is due to two weak pronounced toluene absorption bands, the C-H in plane bending (1,000 to 1,100 cm^{-1}) and the C-H out of plane bending (720 to 820 cm^{-1}). Those two absorption bands are slightly higher than the surrounding noise and hence impute a higher noise level.

In photoacoustic spectroscopy, when no phase correction can be performed, the background should be subtracted in the complex plain. In this way, higher precision is achieved resulting in smaller noise residuals in the spectrum and a higher signal to noise ratio, compared to the magnitude background correction. Still, since the power spectrum is used at the final stage, the method suffers from the fact that the noise in absolute values cannot become negative numbers, which shifts the spectrum to slightly higher values on the ordinate. The slight offset shift can be corrected with an offset correction.

3.2. Single Component Analysis

The signal to noise ratio (SNR) is calculated by dividing the univariate signal S by the noise N. The standard deviation of each VOC spectrum was calculated in the region from 2,400 to 2,800 cm^{-1}. Because the amount of data points was too small to make a precise noise estimation (51 optical resolved points), all the calculated standard deviation values were averaged. The signal and the noise are given in Table 3. N is the RMS noise with the magnitude of one standard deviation (1σ). The equivalent measurement time for each VOC of 900 averaged scans was 25.5 min at a resolution of 8 cm^{-1}.

Table 3. Signal to noise ratio (SNR) and its calculation parameters for each VOC: wavelength where the signal was taken and corresponding signal height. N is the RMS noise of the region 2,400–2,800 cm^{-1} with the magnitude of one standard deviation (1σ). N is for all VOCs 3.53e−3, since the standard deviation was averaged over all VOCs. The concentration of each VOC was 100 ppm.

VOC	Signal at wave-number [cm^{-1}]	Signal [PAI]	SNR
acetone	1,744	4.02e−01	114
ethanol	1,053	1.08e−01	31
isobutanol	1,042	2.21e−01	63
isopropanol	2,978	1.73e−01	49
methanol	1,057	1.59e−01	45
n-butanol	2,943	2.07e−01	59
perchloroethylene	910	5.61e−01	159
methoxypropanol acetate	1,242	1.12e+00	316
methyl acetate	1,246	8.18e−01	232
methyl ethyl ketone	1,744	2.16e−01	61
methyl isobutyl ketone	1,724	2.68e−01	76
o-xylene	2,940	6.71e−02	19
m-xylene	2,940	6.71e−02	19
p-xylene	1,508	7.33e−02	21
dimethylformamide	1,724	7.27e−01	206
dichloromethane	1,277	1.21e−01	34
butyl acetate	1,234	1.16e+00	329
toluene	3,040	1.00e−01	28

The calculated SNR values for the 18 VOCs varies a lot, from 19 (the lowest) for o-xylene to 329 (the highest) for butyl acetate. SNR is a meaningful parameter to describe the relation of the signal to the noise. What does for o-xylene mean: The univariate signal of 100 ppm o-xylene at 2,940 cm^{-1} is 19 times larger than the estimated noise between 2,400 and 2,800 cm^{-1}.

Calculating univariate characterization parameters such as the SNR presented here downgrades the performance of the FT-IR-cPAS. This is due to FT-IR-cPAS being a multivariate measurement instrument which measures the photoacoustic signal at several and not just at a single wavenumber. An analyte band spreading over several wavenumbers, is underestimated in the univariate (SNR) case, because the gained information about the photoacoustic signal at all the other wavenumbers (the rest of the photoacoustic spectrum) is neglected. The multivariate limit of sensitivity should be used to calculate the limit of detection (LoD) in spectroscopy. Equation (4) is a part of the recently presented science based method or science based calibration (SBC). More information about the SBC and its mathematical derivation can be found in [23-25]:

$$\mathrm{BEC} = \sqrt{\frac{1}{g^T \cdot \Sigma^- \cdot g}} \tag{4}$$

where BEC is the background noise equivalent concentration [ppm], $\sum^-$ the covariance matrix of the noise [PAI^2], g the response spectrum of the analyte as column vector [$PAI \cdot ppm^{-1}$] and g^T the response spectrum of the analyte as row vector [$PAI \cdot ppm^{-1}$]. The International Union for Pure and Applied Chemistry (IUPAC) defined the LoD as follows: "The limit of detection is derived from the smallest measure that can be detected with reasonable certainty for a given analytical procedure" [30]. Whereby, 3 standard deviations (3σ) are recommended for calculating the LoD [31]. The case when the measured signal has the same magnitude as the noise (1σ) is called background noise equivalent concentration (BEC).

The diagonal of the ∑ matrix was filled with the smoothed standard deviation of 3 measured dry nitrogen spectra. ∑ was computed from the instrument noise; no other interference or noise source than the sampling noise was taken into account. Hence, the LoD values presented here will be discussed as best possible ones for the FT-IR-cPAS. The noise was determined with 300 scans which corresponds to a measurement time of 8.5 min at a resolution of 8 cm^{-1}. For both the noise and the analyte signal, the full spectral area from 500 to 4,500 cm^{-1} was used. Table 4 shows the LoD (3σ) for each VOC. One more interesting parameter is the comparison between uni- and multivariate LoD, or in other words how much the multivariate LoD performs better. First, the univariate LoD is calculated as:

$$\text{univariate LoD} = \frac{\text{gas concentration}}{\text{SNR}} = \frac{100\ \text{ppm}}{\text{SNR}\ [\,]} \tag{5}$$

The LoD ratio, which can be found in Table 4, relates the univariate LoD with the multivariate BEC (each 1σ) as:

$$\mathrm{LoD}_{\mathrm{ratio}} = \frac{\mathrm{LoD}_{\mathrm{univariate}}\,[\mathrm{ppm}]}{\mathrm{BEC}_{\mathrm{multivariate}}\,[\mathrm{ppm}]}. \tag{6}$$

Table 4. LoD for each measured VOC as 3σ. For both the noise and the analyte signal, the full spectral area from 500 to 4,500 cm^{-1} was used. The concentration of each VOC was 100 ppm. The LoD ratio relates the uni- with the multivariate LoD and is an indicator of how much better the multivariate LoD performs.

VOC	LoD (3σ) [ppm]	LoD ratio: (uni/multi)variate [ ]
acetone	0.55	4.9
ethanol	1.70	5.9
isobutanol	0.83	5.7
isopropanol	1.00	6.2
methanol	1.50	4.4
n-butanol	0.81	6.3
perchloroethylene	0.85	2.2
methoxypropanol acetate	0.33	2.9
methyl acetate	0.36	3.6
methyl ethyl ketone	1.10	4.3
methyl isobutyl ketone	0.83	4.7
o-xylene	1.70	9.2
m-xylene	1.80	8.8
p-xylene	1.90	7.8
dimethylformamide	0.56	2.9
dichloromethane	2.60	3.4
butyl acetate	0.33	3.0
toluene	1.70	6.1

The LoD data in Table 4 is pessimistic because of a numerical particularity of FT-instruments. Before FT transformation, the interferogram is usually appended with zeros to the largest power-of-2 number (…512, 1,024, 2,048…). This enables efficient computation using the Fast Fourier Transformation (FFT) algorithm but also interpolates the resulting spectral data points. In other words, neighboring spectral points are not independent from each other, since even the high frequency electronic noise (affecting the interferogram) has been interpolated in the spectra. This could be described by putting non-zero elements on the side diagonals in the noise matrix ∑. To avoid this time-consuming step, the LoD is calculated with empty side diagonals (as explained above). Then, the correction factor f in Equation (7) has to be taken into account to become accurate again:

$$\text{factor f} = \sqrt{\frac{\text{numerical FFT points}}{\text{optical resolved points}}} = \sqrt{\frac{2048}{987}} = \sqrt{2.07} \tag{7}$$

Hence, the expected LoD values are better by factor $\approx\sqrt{2}$ than the ones stated here. Multivariate analysis improves the sensitivity relative to univariate analysis because, graphically speaking, the sensitivity of many wavelengths is "added up". The best possible sensitivity for a certain wavenumber range is given by Equation 4 and in practice achieved by so-called "matched filter" calibration [23-25]. Table 4 shows the improvements, which are between 2.2 for perchloroethylene and 9.2 for *o*-xylene. The multivariate method gains from more and broader signal bands. Figure 4 shows the spectra of perchloroethylene and *p*-xylene. Perchloroethylene's spectrum shows only one fine absorption band, which is covered by 16 data points. Making a generalization, the fine band almost represents the univariate case itself. The factor of improvement is low. An opposite extreme is *p*-xylene, where the

spectral features are relatively broad but tiny and slightly larger than the noise level. This case gains from the relative broad band around 3,000 cm^{-1} covered by 69 data points.

Figure 4. Two extreme cases for multivariate data analysis: spectra of perchloroethylene (PCE) and *p*-xylene. Perchloroethylene shows one fine absorption band, which does not gain that much from multivariate data analysis. *Vice versa*, *p*-xylene gains from multivariate analysis, because its spectrum has tiny but several absorption bands, from which one is relatively broad.

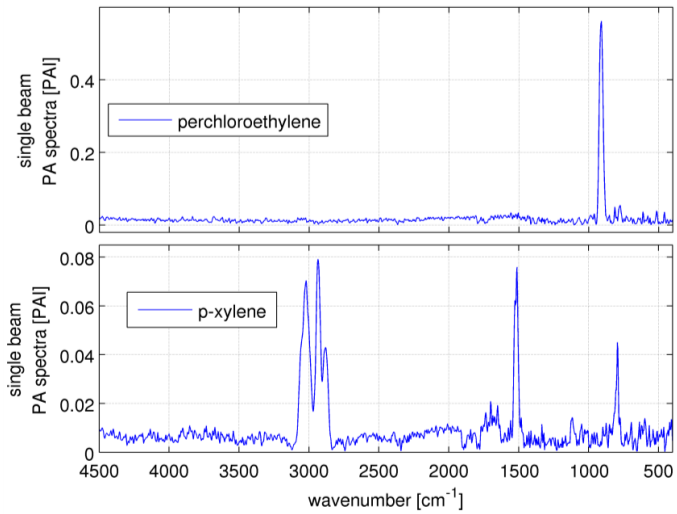

The LoD numbers are adequate according to the emission limits stated by Directive 2010/75/EU. Directive 2010/75/EU appoints the emission limit of 20 $mg \cdot Nm^{-3}$ for VOCs with the hazard statement H341 or H351 (earlier R-label R40 and R68) and 2 $mg \cdot Nm^{-3}$ stated with H340, H350, H350i, H360D or H360F (earlier R45, R46, R49, R60 and R61) (Nm^3 stands for norm cubic meter and refers to a temperature of 273.15 K and a pressure of 101.3 kPa) [32]. Three of the model VOCs fall under the regulation of Directive 2010/75/EU. Table 5 shows the VOCs, their H-statement, emission limit and experimentally gained LoD.

Table 5. Emission limits according Directive 2010/75/EU and the experimentally achieved LoD with a measurement time of 8.5 min.

VOC	H-statement	Emission limit concentration [$mg \cdot Nm^{-3}$]	Emission limit [ppm]	LoD (3σ) [ppm]
dichloromethane	H351	20	5.5	2.60
dimethylformamide	H360D	2.0	0.6	0.56
perchloroethylene	H351	20	2.8	0.85

The presented detection limits are only true if no other spectral interference or noise component is present. If other components such as other VOCs are present and interfering (overlapping the spectra) the detection limit will increase. The next section will evaluate the interferences of analytes in a multi component mixture.

3.3. Multi Component Analysis

Multi component ability and selectivity (*i.e.*, the interferences between the analytes) will be shown with an SBC calibration. Five VOCs were selected to set up a quantitative multi component calibration. The VOCs were acetone, perchloroethylene, methyl isobutyl ketone, dimethylformamide and methanol. In addition, water was added as an interferent, since it is frequently present in industrial measurements. Figure 5 shows the spectra of the five selected VOCs and water. The calibration was set up with VOC spectra of 200 ppm and water of 5,000 ppm. For each VOC, one SBC calibration was set up including the interference noise of the four other VOCs and water. The standard deviation of the interfering VOCs (how much the concentration of the interferent can change in the subsequent measurements) was set to 500 ppm and water 1,000 ppm. Further, the noise matrix contained the hardware noise floor and offset noise. The calculated b-vectors alias regression vectors are shown in Figure 6.

Figure 5. Selectivity experiment: Spectra of the five VOCs and water.

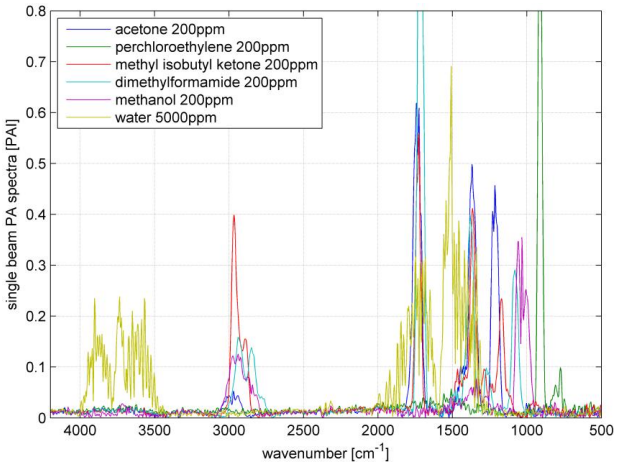

Figure 6. Selectivity experiment: b-vectors of the five calibrations.

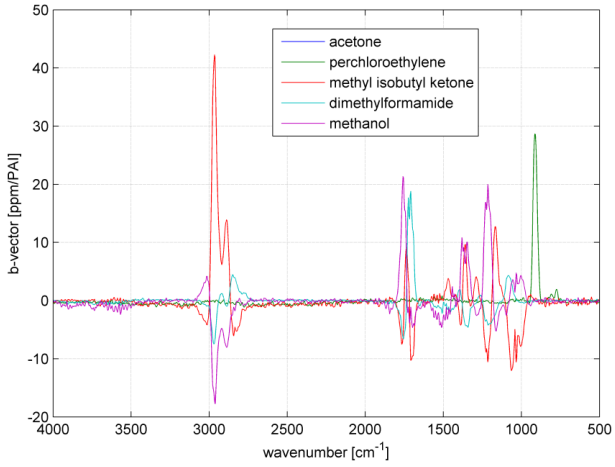

As it can be seen in Figure 5, the spectra overlap heavily. However, the b-vectors contain negative elements, which will cancel out the interferences. Figure 7 shows an example how a b-vector and its multiplication 'work'. In this example the concentration of the analyte acetone will be calculated using the b-vector of acetone that includes the interferent information of all four interfering VOCs. To keep the overview and not make this example to complicated only methanol was chosen as interferent. The sample gas contains 100 ppm of acetone and 100 ppm of methanol (spectra in upper graph in Figure 7). The measured sample gas spectrum will be multiplied with acetone's b-vector to achieve the sample's acetone concentration. Dependent on the shape and the amplitude of the b-vector and the spectrum, the concentration accumulates at each wavenumber. The lower graph in Figure 7 shows the accumulated multiplication curve starting from 500 cm^{-1} and ending at 3,500 cm^{-1}. The concentration increases with the analyte bands at 1,200, 1,350 and 1,750 cm^{-1}. However, the methanol band at 1,050 cm^{-1} lifted the concentration too high, which is compensated by the negative b-vector elements at 2,900 cm^{-1} resulting in an acetone concentration of 102 ppm.

Figure 7. Sample spectrum, b-vector and result calculation: A schematic demonstration. The upper graph shows the sample spectrum (analyte and interferent spectra plotted separate), in the middle the b-vector for the analyte acetone and the lower graph the resulting cumulative sum of the vector multiplication of b-vector and sample spectrum (accumulation starts from 500 cm^{-1}).

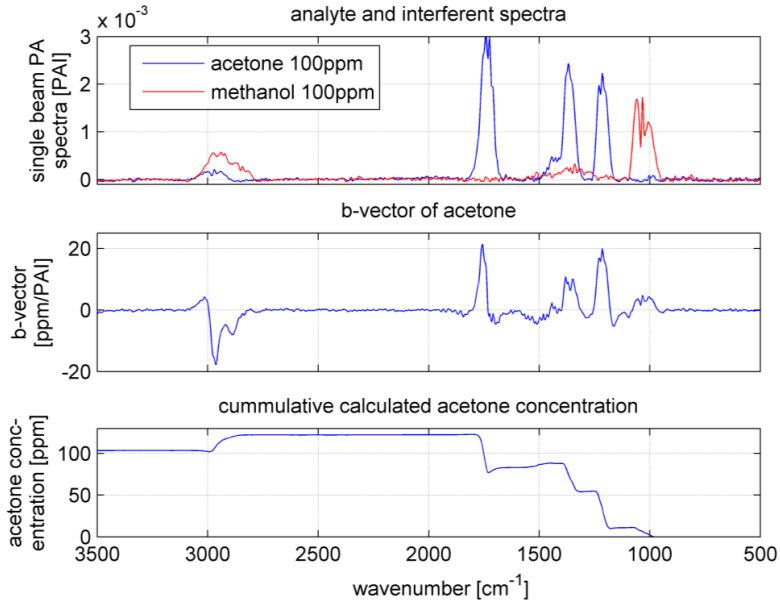

A numerical expression of the selectivity is the cross selectivity, which is calculated between the five VOCs. The 100 ppm spectra of the VOCs are divided by 100 and multiplied by the b-vector of each VOC. Table 6 shows the calculated cross selectivities. A cross selectivity of 0.10 (10%) means, if the interferent changes e.g., by 100 ppm, the analyte concentration will change by 10 ppm.

Table 6. Cross selectivity's of the five VOCs and water in [ppm·ppm^{-1}]. For example, when measuring acetone and perchloroethylene's concentration increases by 100 ppm, the measured acetone value will decrease by 1 ppm.

	Interferent						
analyte ↓	**acetone**	**perchloro -ethylene**	**methyl isobutyl ketone**	**dimethyl-formamide**	**methanol**	**water**	**sum**
acetone	1.00	−0.010	0.008	0.002	0.020	<0.001	0.037
perchloroethylene	−0.012	1.00	−0.007	<0.001	0.008	<0.001	0.029
methyl isobutyl ketone	−0.004	−0.020	1.00	−0.067	−0.011	0.002	0.098
dimethylformamide	0.005	<0.001	−0.004	1.00	−0.020	−0.002	0.036
methanol	−0.013	0.002	−0.034	−0.086	1.00	0.004	0.130

Most of the pairs show cross selectivities below 0.01 (1%). Four pairs have 2% and three exceptions which are >2%. The average cross selectivity is <2%. The calibration is pretty immune against water, since the water cross selectivities are below 0.2%. Due to the additional interference noise, the detection limits have changed. Table 7 shows the detection limits for the multi component analysis and compare it with the single component measurements. The detection limits went up for all VOCs due to the overlapping of the spectra. Acetone shows the highest increase of factor, 2.2. The detection limit of the four other VOCs have not increased by more than a factor of 2.

Table 7. Comparison of the detection limits: single *versus* and multi component. The single component detection limits (Table 4) were calculated without interference noise. The multi component detection limits including the interference of 4 other VOCs and water.

VOC	**LoD (3σ) [ppm]**	
	Single	**Multi**
acetone	0.55	1.20
methanol	1.50	1.85
perchloroethylene	0.85	1.00
methyl isobutyl ketone	0.83	1.41
dimethylformamide	0.50	0.71

3.4. Water Subtraction

Humid samples are a major challenge in the analysis of IR spectra, when the spectrum of water overlaps the spectrum of the analyte as seen in Figure 8. Still, to be able to use the overlapping region for data analysis, in particular quantitative data analysis, the water has to be subtracted. In this experiment, the concentration of methyl ethyl ketone (MEK) was always 200 ppm, while water was added to the samples in concentrations spreading from 1,400 ppm to 100k ppm. The measured spectra are shown in Figure 9. The subtraction of water was done with a SBC calibration, where MEK was the analyte of interest. One water spectra (10k ppm) was added as an interferent in the calibration, so that the b-vector will cancel out the water features and predict the true MEK concentration. A second calibration was set up without adding water as an interferent. Both b-vectors are shown in Figure 10.

Figure 8. Demonstration of water overlapping with the analyte: If the pure MEK sample (blue) contains water (green), the measured spectra will be the sum of both (red).

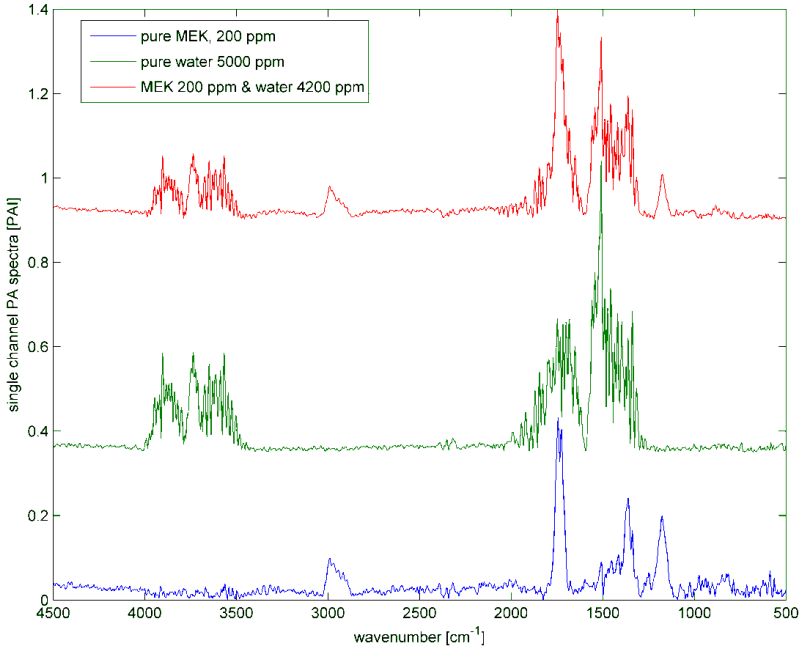

Figure 9. Water subtraction experiment: MEK concentration was always 200 ppm while the water concentration were 1,400, 4,200, 12k, 35k and 100k ppm.

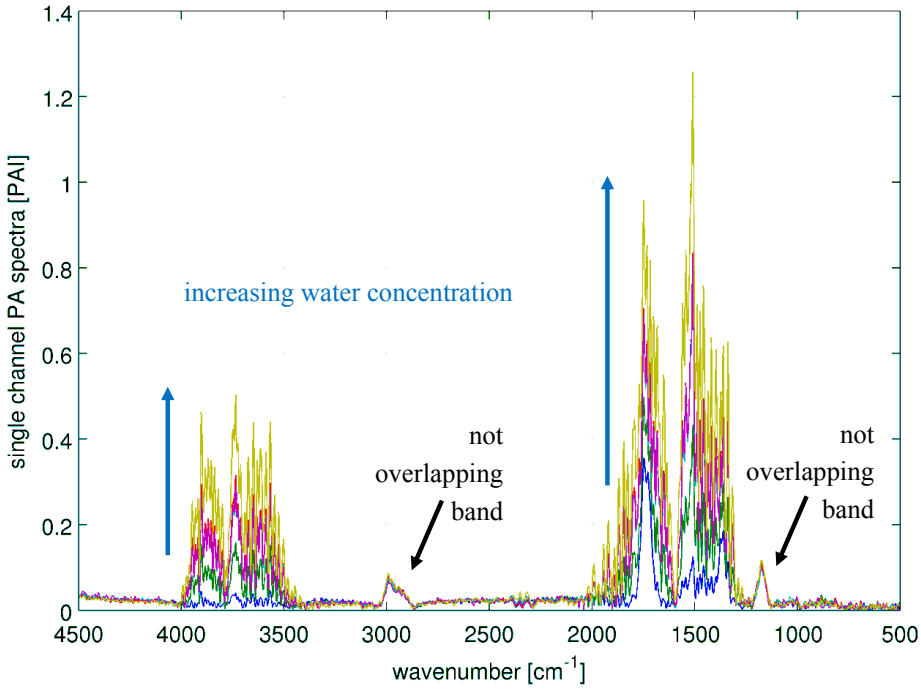

Figure 10. Water subtraction experiment: b-vectors. The blue b-vector was calculated with water as an interferent. It shows negative elements, which will cancel out the interference of water. The red b-vector, without the information of water interference, does not show negative elements.

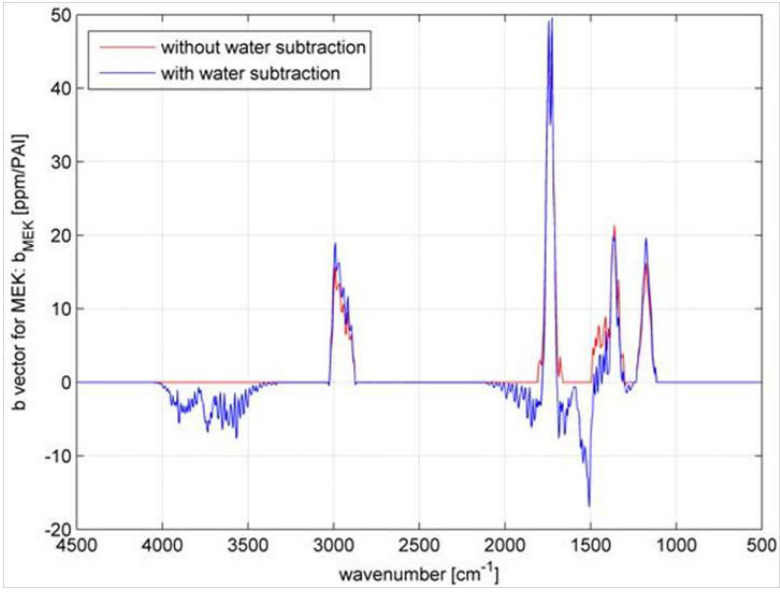

The results of the water subtraction experiment are shown in Table 8. If the interference of water is not cancelled out by the calibration, the calculated MEK concentrations increase with increasing water concentrations. If the information of the water interference is added to the calibration, it will calculate the true MEK concentration with a coefficient of variation (CV) of 3%.

Table 8. Water subtraction experiment: results of the analysis using the water subtracted and not water subtracted calibration.

MEK concentration [ppm]	Water concentration [ppm]	Calculated MEK concentration [ppm]	
		without subtraction	with subtraction
200	1,400	238	202
200	4,200	336	196
200	12k	481	198
200	35k	453	187
200	100k	650	200

The variation of the calculated MEK concentration is not induced by the calibration method. The variation seen here can be explained by the experimental deviation of the true MEK concentration, since the CV of the area of the non-overlapping band (2,850–3,050 cm^{-1}) is 4.5%. The variation in the MEK concentration can be explained by the gas feeding system, which may have several points of uncertainty. One possibility can be the time instability of the syringe feed, which would cause direct changes in the true analyte concentration.

3.5. Overall Evaluation

Reflecting back to the introduction, the listed needs for an industrial emission measurement system are: selectivity, sensitivity, multi component ability, corrosion resistance, high measurement temperature, low influence of water vapor, online capability and robustness. The temperature was successfully increased to 180 °C, which is high enough for emission measurements. Corrosion resistance was realized on a basic level, since all components were SS316. Better corrosion resistance (PTFE, Silcosteel coating) was achieved for some parts, but a few (e.g., the valves) were SS316.

For single component measurements, the detection limits were in compliance with the statutory emission limits. For the five component mixture with water, the detection limits only increased by a maximum factor of 2.2. Still, the gained sensitivity couldn't reach the state of the art (too long measurement time), which is due to the non optimal alignment and coupling of the cell to the FT-IR. In these experiments, a high resolution FT-IR was used. By having a high resolution spectrometer, the aperture is limited to a certain size, which is, on the other hand, the bottleneck for sensitivity. Bio-Rad's FT-IR has a maximal aperture size for 4 cm^{-1} of resolution (11.94 mm), although the spectra were measured with 8 cm^{-1} resolution, where light power was lost. In future, the sensitivity can be increased by selecting a low resolution FT-IR with a much higher light throughput.

The low cross selectivities of the five component calibration and the successful water subtraction showed that the resolution of 8 cm^{-1} is still good enough to offer selectivity. By increasing the resolution (e.g., to 4 cm^{-1} or even better), the cross selectivities might improve, but the SNR will drop down for the same measurement time. An application specific tradeoff between selectivity and sensitivity has to be found. For the case presented here, the resolution better than 8 cm^{-1} was not needed.

The presence of water influenced the calibration less than 0.2%. The water subtraction was studied in more detail and the subtraction turned out to be accurate (within a CV of 3%) with only one water 'library' spectrum. This is a big benefit for measurement applications where water is present, since no complex water libraries are needed and the subtraction itself is easier due to the linear behavior (scaling of the 10k ppm subtraction spectrum fit the 1,400 ppm as well as the 100k ppm).

In principle, the device is ready for process analysis, although the measurement time needs to be decreased in the upcoming investigations (optimization of the FT-IR coupling). One drawback is the restriction of the non continuous flow, *i.e.*, the gas flow needs to be stopped and the valves closed for measurement. This is a disadvantage for continues monitoring and for certain gases due to possibly occurring adsorption phenomena especially when the cell is not heated. The last point is the robustness for industrial use. Since this is difficult to evaluate in a laboratory, further studies are planned to test the system under real industrial conditions.

4. Conclusions

Photoacoustic FT-IR spectroscopy was successfully brought to high temperatures up to 180 °C. The performance of the novel heated FT-IR-cPAS system was studied by laboratory VOC measurements. It turned out that a complex background correction has to be performed to correct the phase shift of the photoacoustic signal after the FFT. Sensitivity was explored as univariate SNR (1σ) and multivariate LoD (3σ). The multivariate analysis using SBC was up to 9.2 times better compared to the univariate

analysis (both 1σ). SNR (1σ) numbers for the 18 measured VOCs were varying between 19 (the lowest) for *o*-xylene and 329 (the highest) for butyl acetate at a measurement time of 25.5 min. In the same way, the multivariate LoD (3σ) varied between 2.60 ppm (worst) for dichloromethane to 0.33 ppm (best) for butyl acetate within 8.5 min. The LoDs of the VOC were in compliance with the statutory emission limits stated by Directive 2010/75/EU for single compound measurement. Selectivity and multi component ability were shown by an SBC calibration with 5 VOCs and water. On visual inspection, the six spectra overlapped heavily. Still, the cross selectivity (the numerical expression of the selectivity) could be kept below 2% for most of the interference pairs. The resulting detection limits increased by a maximum factor of 2.2. The successful subtraction of water could be shown by another SBC calibration which calculated the true analyte concentration with a variation coefficient of 3%, although the variation in the water concentration covered almost three magnitudes (1,400 to 100k ppm) and the used subtraction water spectrum had the concentration of 10k ppm. Even though the FT-IR-cPAS technology shows some weaknesses (e.g., the sample gas stream needs to be stopped for the measurement) it provides features which are superior compared to transmission spectroscopy as the water subtraction ability or the easiness of calibration. Therefore it is worth, developing it further to reach an industrial ready technology.

Acknowledgements

The work presented here was done within the EU-FP7-SME-Project 'ZERO-VOC'. The authors acknowledge the funding of the European Union. Further, the authors want to express their gratitude to the whole ZERO-VOC consortium for the support and the excellent collaboration. The consortium is: Innovació i Recerca Industrial i Sostenible SL (project coordinator, RTD Spain), Centro de Producción de Pinturas SL (Spain), Relox Technik GmbH (Germany), Ehovoc Oy (Finland), Gasera Ldt. (Finland), LNL Elektrik Elektronik Bilisim ve Danismanlik Ltd. Sti. (Turkey), Fermion Oy (Finland), Sensotran SL (Spain), University of Oulu (RTD, Finland) and VTT Technical Research Centre of Finland (RTD, Finland). More information about the ZERO-VOC project can be accessed under: www.zero-voc.eu.

References

1. Ojala, S.; Lassi, U.; Keiski, R.L. Testing VOC Emission Measurement Techniques in Wood-Coating Industrial Processes and Developing a Cost-Effective Measurement Methodology. *Chemosphere* **2006**, *62*, 113-120.
2. Ojala, S.; Pitkäaho, S.; Laitinen, T.; Niskala, N.; Brahmi, R.; Gaálová, J.; Matejova, L.; Kucherov, A.; Päivärinta, S.; Hirschmann, C.; *et al.* Catalysis in VOC Abatement. *Catal. Today* **2010**, in press.
3. Crutzen, P.J. The Role of NO and NO_2 in the Chemistry of the Troposphere and Stratosphere. *Annu. Rev. Earth Planet. Sci.* **1979**, *7*, 443-472.
4. Moretti, E.C.; Mukhopadhyay, N. VOC Control: Current Practices and Future Trends. *Chem. Eng. Progr.* **1993**, *89*, 20-26.
5. Khan, F.I.; Kr Ghoshal, A. Removal of Volatile Organic Compounds from Polluted Air. *J. Loss Prev. Process Indust.* **2000**, *13*, 527-545.

6. Hester, R.E. Volatile Organic Compounds in the Atmosphere. In *Issues in Environmental Science and Technology*, 4th ed.; Ronald, E., Harrison, R.M., Eds.; American Chemical Society: Washington, DC, USA, 1996; pp. 1-149.
7. Von Schneidemesser, E.; Monks, P.S.; Plass-Duelmer, C. Global Comparison of VOC and CO Observations in Urban Areas. *Atmos. Environ.* **2010**, *44*, 5053-5064.
8. Gibson, N.B.; Costigan, G.T.; Swannell, R.P.J.; Woodfield, M.J. Volatile Organic Compound (VOC) Emissions during Malting and Beer Manufacture. *Atmos. Environ.* **1995**, *29*, 2661-2672.
9. Lindley, R.E.; Parkes, A.M.; Keen, K.A.; McNaghten, E.D.; Orr-Ewing, A.J. A Sensitivity Comparison of Three Photoacoustic Cells Containing a Single Microphone, a Differential Dual Microphone or a Cantilever Pressure Sensor. *Appl. Phy. B* **2007**, *86*, 707-713.
10. Moretti, E.C. *Practical Solution for Reducing Volatile Organic Compounds and Hazardous Air Pollutants*; American Institute of Chemical Engineers: New York, NY, USA, 2001; p. 150.
11. Muñoz, R.; Sivret, E.C.; Parcsi, G.; Lebrero, R.; Wang, X.; Suffet, I.H.; Stuetz, R.M. Monitoring Techniques for Odour Abatement Assessment. *Water Res.* **2010**, *44*, 5129-5149.
12. Sun, R.; Zobel, N.; Neubauer, Y.; Cardenas Chavez, C.; Behrendt, F. Analysis of Gas-Phase Polycyclic Aromatic Hydrocarbon Mixtures by Laser-Induced Fluorescence. *Opt. Laser Eng.* **2010**, *48*, 1231-1237.
13. Van Geem, K.M.; Pyl, S.P.; Reyniers, M.; Vercammen, J.; Beens, J.; Marin, G.B. On-Line Analysis of Complex Hydrocarbon Mixtures Using Comprehensive Two-Dimensional Gas Chromatography. *J. Chromatogr. A* **2010**, *1217*, 6623-6633.
14. Passant, N.R.; Richardson, S.J.; Swannell, R.P.J.; Gibson, N.; Woodfield, M.J.; van der Lugt, J.P.; Wolsink, J.H.; Hesselink, P.G.M. Emissions of Volatile Organic Compounds (VOCs) from the Food and Drink Industries of the European Community. *Atmos. Environ. Gen. Top.* **1993**, *27*, 2555-2566.
15. Uotila, J.; Koskinen, V.; Kauppinen, J. Selective Differential Photoacoustic Method for Trace Gas Analysis. *Vib. Spectrosc.* **2005**, *38*, 3-9.
16. Uotila, J. Comparison of Infrared Sources for a Differential Photoacoustic Gas Detection System. *Infrared Phys. Technol.* **2007**, *51*, 122-130.
17. Laurila, T.; Cattaneo, H.; Koskinen, V.; Kauppinen, J.; Hernberg, R. Diode Laser-Based Photoacoustic Spectroscopy with Interferometrically-Enhanced Cantilever Detection. *Opt. Express* **2005**, *13*, 2453-2458.
18. Kauppinen, J.; Wilcken, K.; Kauppinen, I.; Koskinen, V. High Sensitivity in Gas Analysis with Photoacoustic Detection. *Microchem. J.* **2004**, *76*, 151-159.
19. Koskinen, V.; Fonsen, J.; Kauppinen, J.; Kauppinen, I. Extremely Sensitive Trace Gas Analysis with Modern Photoacoustic Spectroscopy. *Vib. Spectrosc.* **2006**, *42*, 239-242.
20. Koskinen, V.; Fonsen, J.; Roth, K.; Kauppinen, J. Progress in Cantilever Enhanced Photoacoustic Spectroscopy. *Vib. Spectrosc.* **2008**, *48*, 16-21.
21. Kuusela, T.; Kauppinen, J. Photoacoustic Gas Analysis Using Interferometric Cantilever Microphone. *Appl. Spectrosc. Rev.* **2007**, *42*, 443-474.
22. Hirschmann, C.B.; Uotila, J.; Ojala, S.; Tenhunen, J.; Keiski, R.L. Fourier Transform Infrared Photoacoustic Multicomponent Gas Spectroscopy with Optical Cantilever Detection. *Appl. Spectrosc.* **2010**, *64*, 293-297.

23. Marbach, R. On Wiener Filtering and the Physics Behind Statistical Modeling. *J. Biomed. Opt.* **2002**, *7*, 130-147.
24. Marbach, R. A New Method for Multivariate Calibration. *J. Near Infrared Spectrosc.* **2005**, *13*, 241-254.
25. Marbach, R. Multivariate Kalibrierung, Selektivität Und Die SBC-Methode. *Chem. Ing. Tech.* **2010**, *82*, 453-466.
26. Fonsen, J.; Koskinen, V.; Roth, K.; Kauppinen, J. Dual Cantilever Enhanced Photoacoustic Detector with Pulsed Broadband IR-Source. *Vib. Spectrosc.* **2009**, *50*, 214-217.
27. Koskinen, V.; Fonsen, J.; Roth, K.; Kauppinen, J. Cantilever Enhanced Photoacoustic Detection of Carbon Dioxide Using a Tunable Diode Laser Source. *Appl. Phy. B* **2007**, *86*, 451-454.
28. Wilcken, K.; Kauppinen, J. Optimization of a Microphone for Photoacoustic Spectroscopy. *Appl. Spectrosc.* **2003**, *57*, 1087-1092.
29. Griffiths, P.; De Haseth, J.A. *Fourier Transform Infrared Spectrometry*, 2nd ed.; Wiley: Hoboken, NJ, USA, 2007.
30. IUPAC. *Compendium of Chemical Terminology*, 2nd ed.; International Union of Pure and Applied Chemistry (IUPAC): Research Triangle Park, NC, USA, 1997.
31. Long, G.L.; Winefordner, J.D. Limit of Detection: A Closer Look at the IUPAC Definition. *Anal. Chem.* **1983**, *55*, 712-724.
32. Directive 2010/75/EU of the European Parliament and of the Council of 24 November 2010 on industrial emissions (integrated pollution prevention and control). *OJEU* **2010**, *L 334/17*, 1-103.

ARTICLE III

Not available in the electronic version

ARTICLE IV

Trace gas detection of benzene, toluene, *p*-, *m*- and *o*-xylene with a compact measurement system using cantilever enhanced photoacoustic spectroscopy and optical parametric oscillator

In: Vibrational Spectroscopy **68**, pp. 170–176.

Vibrational Spectroscopy 68 (2013) 170–176

Contents lists available at ScienceDirect

Vibrational Spectroscopy

journal homepage: www.elsevier.com/locate/vibspec

Trace gas detection of benzene, toluene, *p*-, *m*- and *o*-xylene with a compact measurement system using cantilever enhanced photoacoustic spectroscopy and optical parametric oscillator

C.B. Hirschmann[a,b,*], S. Sinisalo[c], J. Uotila[c], S. Ojala[a,b], R.L. Keiski[a]

[a] Mass and Heat Transfer Process Laboratory, Department of Process and Environmental Engineering, University of Oulu, 90014 Oulu, Finland
[b] Photonics and Measurement Solutions, VTT Technical Research Centre of Finland, Kaitoväylä 1, 90571 Oulu, Finland
[c] Gasera Ltd., Tykistökatu 4, 20520 Turku, Finland

ARTICLE INFO

Article history:
Received 16 May 2013
Received in revised form 8 July 2013
Accepted 15 July 2013
Available online 24 July 2013

Keywords:
Photoacoustic spectroscopy
Cantilever microphone
Optical parametric oscillator
Benzene
Toluene
Xylenes

ABSTRACT

A compact measurement system based on a novel combination of cantilever enhanced photoacoustic spectroscopy (CEPAS) and optical parametric oscillator (OPO) was applied to the gas phase measurement of benzene, toluene, and *o*-, *m*- and *p*-xylene (BTX) traces. The OPO had a band width (FWHM) of 1.3 nm, was tuned from 3237 to 3296 nm in steps of 0.1 nm and so spectra of BTX at different concentrations were recorded. The power emitted by the OPO increased from 88 mW at 3237 nm to 103 mW at 3296 nm. The univariate detection limits (3σ, 0.951 s) for benzene, toluene, *p*-, *m*- and *o*-xylene at 3288 nm were 12.0, 9.8, 13.2, 10.1 and 16.0 ppb, respectively. Multivariate data analysis using science-based calibration was used to resolve the interference of the analytes. The multivariate detection limits (3σ, 3237–3296 nm, 591 spectral points each 0.951 s) for benzene, toluene, *p*-, *m*- and *o*-xylene in the multi-compound sample, where all other analytes and water interfere were 4.3, 7.4, 11.0, 12.5 and 6.2 ppb, respectively. Without interferents, the multivariate detection limits varied between 0.5 and 0.6 ppb. The sum of the cross-selectivities (3237–3296 nm, 591 spectral points, each 0.951 s) per analyte were below 0.05 ppb/ppb, with an average of 0.038 ppb/ppb. The cross-selectivity of water to the analytes was on average 1.22×10^{-4} ppb/ppb. The OPO is small in size ($L \times W \times H$ 125 × 70 × 45 mm), commercially available, and easy to operate and integrate to setups. The combination with sensitive CEPAS enables compact measurement systems for industrial as well as environmental trace gas monitoring.

1. Introduction

BTX is a common acronym in petrochemical industry that stands for benzene, toluene and the three xylene isomers. The demand of BTX in industry is high, since they are very common starting chemicals used in production processes and they are also frequently used as solvents. Benzene occurs in natural resources as crude oil and natural gas [1], and processed fuels still contains around 1% of benzene [2]. Thus, urban atmospheric benzene originates mainly from traffic [3,4]. Benzene is stable in the atmosphere and has low reactivity compared to toluene and xylene, that enables benzene a long atmospheric lifetime [1,5]. The typical environmental effects are related to global warming, ozone depletion and low level ozone formation, to mention only a few [6]. Besides urban air, BTX occurs in indoor air, too. It can outgas from commodities, cleaning agents, printings, paints and wood panels, but also tobacco smoke contributes largely to the indoor BTX concentration [1]. Humans may be exposed to the BTX *via* skin, by swallowing or, most commonly, *via* breathing. BTX exposure causes skin and eye irritation problems, the irritation of respiratory organs and problems with nervous system [7]. In addition, they are dangerous to heredity, embryo and breeding [7]. Among BTX, benzene is the most harmful compound to human health, since it is proven to be carcinogenic causing for example leukemia [7], and therefore, the European Union proposed a limit value of 5 $\mu g\,m^{-3}$ (~1.5 ppb) for benzene as an annual average for urban areas [3]. The workplace exposure during 8 h for benzene is 0.5 ppm and for toluene and the xylenes 50 ppm [8]. Despite recent reductions in emissions and due to the obligations to follow up the emissions, the development of robust, reliable, selective and sensitive measurement methods is needed. Potential BTX measurement applications are versatile and include environmental, urban, indoor, as well as industrial gas monitoring.

Photoacoustic spectroscopy (PAS) has certain advantages over the conventional transmission spectroscopy as PAS is a zero-background method, it provides a wide dynamic range and the

* Corresponding author at: Mass and Heat Transfer Process Laboratory, Department of Process and Environmental Engineering, University of Oulu, 90014 Oulu, Finland. Tel.: +358 401 877447; fax: +358 294 482304.
E-mail addresses: christian.hirschmann@oulu.fi, christian.hirschmann@vtt.fi (C.B. Hirschmann).

0924-2031/$ – see front matter © 2013 Elsevier B.V. All rights reserved.
http://dx.doi.org/10.1016/j.vibspec.2013.07.004

Table 1
The OPO parameters.

Parameter	Value
Wavelength	3237–3296 nm
Bandwidth	1.3 nm
Beam diameter	1.6 mm
Power	88–103 mW, wavelength depending
Repetition rate	10 kHz
Pulse width	4 ns
Pulse energy	10 μJ

photoacoustic signal usually responds linear to the analyte [9–12]. The sensitivity is commonly improved by operating the photoacoustic detectors in a resonant mode [9–13]. However, using resonant mode requires exact adjustment and perpetuation of the resonance frequency. This complicates setups with broadly tunable light sources. The optical read-out cantilever microphone offers improved sensitivity without the need for resonance enhancement [14–21]. Combinations with FT-IRs [22–24] and broad band light sources [17,19,25] have been demonstrated and are nowadays commercially available [26,27].

In multi-compound samples, as in the BTX case, tunable light sources can be used to resolve the spectral interference between the analytes. Several types of tunable mid-IR sources exist; however most are not fulfilling all of the following performance features required for environmental and industrial applications such as wide tunability, robustness, high optical power, low power consumption, and compactness and light weight [28]. The recently developed optical parametric oscillator (OPO) from Cobolt meets all the mentioned features making it a suitable light source for environmental and industrial measurements. To the authors' knowledge, this OPO is the first commercially available OPO capable of delivering ~100 mW in a compact package of 125 × 70 × 45 mm ($L \times W \times H$). The very first combination of an OPO and CEPAS was recently reported in [29] and ppt detection limits were reached within a few seconds of measurement time. However, that OPO is larger than the OPO used here and is still in a laboratory state. The objective of this work is to build a novel small-sized measurement system for industrial and environmental measurement applications based on a compact OPO and CEPAS, and demonstrate its performance in the BTX measurement.

2. Experimental

2.1. Measurement setup and parameters

The built measurement setup combines a photoacoustic detector with optical cantilever microphone (Gasera PA201) and a compact OPO (Cobolt OPO™, tunable from 3237 to 3296 nm). Table 1 shows the parameters of the OPO; more information about the OPO as the general description, technical details as well as the performance and stability testing is reported in [28]. The coherent idler beam of the OPO was guided through the photoacoustic cell to the laser power meter (Thorlabs S302C). The photoacoustic cell was made out of aluminum, with a cylindrical shape of 95 mm in length and 4 mm in diameter and the silicon cantilever had the dimensions of 5 × 1.2 × 0.01 mm ($L \times W \times H$). Both, the cell and the cantilever were coated with gold. The BaF_2 windows were not at Brewster angle because the cell was intentionally designed to be used for wavelength modulation. A mechanical tuning fork chopper that was placed between the OPO and the cell modulated the light at 135 Hz. The sample gas was exchanged by the built in gas handling system of the photoacoustic detector. The data management and acquisition software done with LabVIEW was used to control the OPO and to collect and process the digital signal, proportional to cantilever microphone movement. The time domain microphone readout signal was transformed to frequency domain using FFT (power spectrum) and the photoacoustic signal amplitude was recorded at the modulation frequency. The amplitude of the photoacoustic signal *versus* OPO wavelength was combined to form the photoacoustic spectrum. Fig. 1 shows a schematic drawing of the measurement setup.

The spectra were measured from 3237 to 3296 nm in steps of 0.1 nm and an integration time of 0.951 s per spectral point. The total measurement time for one scan was ~9 min. The gas flow through the photoacoustic cell needs to be stopped for the measurement. In the sealed photoacoustic cell, the sample gas pressure was adjusted to 950 mbar and the temperature to 50 °C. Reference spectra from the Pacific Northwest National Laboratory (PNNL) [30] measured at 50 °C and 1013 mbar were used for modeling and comparison purposes in this work.

2.2. Gas supply

The setup was tested first by measuring methane (AGA, custom blend of 10 ppm methane in nitrogen) and water vapor by adding some ambient air to the synthetic air (AGA, 5.0) that was used as buffer gas for all gas mixtures. The BTX analyte gas streams were produced by evaporating benzene (anhydrous, 99.8%), toluene (anhydrous, 99.8%), *m*-xylene (anhydrous, ≥99%), *o*-xylene (anhydrous, 97%) and *p*-xylene (anhydrous, ≥99%), all procured from Sigma–Aldrich, using the Gasmet™ calibrator [31]. The design of experiments included at least 3 different concentrations for each analyte in the range from 0.20 to 15 ppm. More diluted concentrations were not possible due to limitations of the Gasmet™ calibrator. For calibration, the spectra of the following concentrations were used: benzene 10.05 ppm, toluene 9.85 ppm, *p*-xylene 14.5 ppm, *o*-xylene 8.05 ppm and *m*-xylene 9.90 ppm; and for the calculation of the cross-selectivity: benzene 5.05 ppm, toluene 9.85 ppm, *p*-xylene 7.20 ppm, *o*-xylene 4.96 ppm and *m*-xylene 9.90 ppm. All ratios (ppm and ppb) stated in this work refer to volume ratio.

3. Results and discussion

3.1. Testing of the setup and verification of the results

Prior to the BTX analysis, the setup was tested and the measured data verified. Methane and water were the test gases, because both have several narrow rotational bands within the spectral region covered by the OPO. Both the measured and the reference methane and water vapor spectra taken from PNNL are shown in Fig. 2. The spectral band positions of the measured spectra are in compliance with the PNNL spectra. The band intensities are as well in compliance, if the system response and the OPO excitation band width are taken into account. The system response is mainly influenced by the emitted power of the OPO that is rising with longer wavelength as also shown in Fig. 2. Band shape wise, the measured spectra are broader than the PNNL spectra, which comes from the broad (FWHM = 1.3 nm) excitation band width of the OPO that limits the spectral resolution of the measurement system. As the excitation band width is wider than the rotational bands, only a part of the emitted photons are available to become absorbed. Thus, this OPO is better used for the measurement of heavier molecules as benzene, toluene and xylenes, where the analyte band width is far broader than FWHM 1.3 nm and all photons have the chance to become absorbed.

3.2. Noise characterization

To get a clear picture on all possible noise sources, the noise measurements were done in both cases, the OPO in operation and

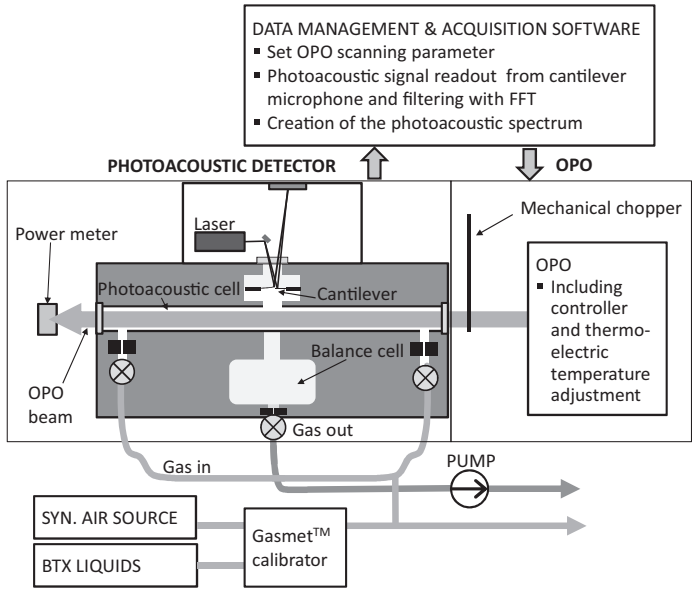

Fig. 1. Schematic drawing of the measurement setup.

as switched off. For the noise characterization measurements, the photoacoustic cell was filled with synthetic air to 950 mbar and the photoacoustic signal was recorded for 2 min with a single measurement time of 0.951 s. The noise measurements with the OPO in operation were done at 10 different wavelengths, spread over the spectral range of the OPO, as shown in Fig. 3. The records with the OPO off showed a stable signal varying around the mean value. With the OPO in operation, the measured signal increased with the record time, from start to end in average by 5.7%. The increase in the signal is due to desorption of water molecules from the cell interior into the gas phase and thus increasing the photoacoustic signal. The signal increase due to water vapor is actually not noise and for an accurate noise characterization of the system, the water increased signal was subtracted. A second-order polynomial fit subtracted the water signal leaving the variation in nitrogen signal as residual. The standard deviation was calculated from the nitrogen signal in blocks of 10 successive recording points, to reduce water signal residuals biasing the standard deviation. The noise, for each of the records, is an average from the 12 independent standard deviation values. Fig. 3 shows the calculated noise as well as the background signal *versus* the wavelength. Due to the increase in the background signal over time, the first measurement of each time record was defined as the background signal.

The sources of the noise in cantilever photoacoustic spectroscopy are discussed in [16,18,32] and case specific in the work [33] where the same setup was used with a quantum cascade laser (QCL) instead of the OPO. In practice, the limiting noise sources for the cantilever photoacoustic detection are Brownian noise and background signal instability [16,18], that is sometimes referred

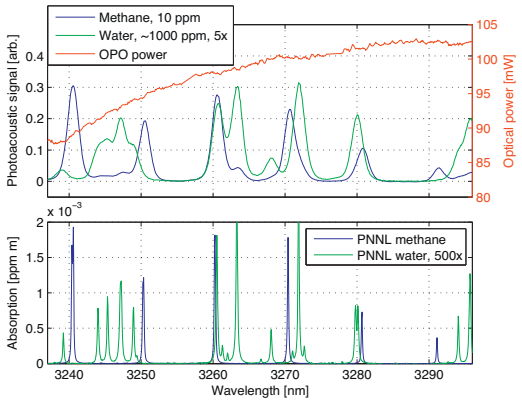

Fig. 2. Upper graph: Measured spectra of methane and water (5× magnified) and the OPO power emission. Lower graph: Reference spectra of methane and water (500× magnified) taken from PNNL.

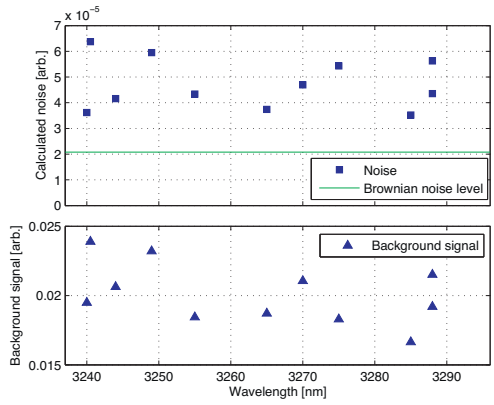

Fig. 3. Noise and background signal *versus* wavelength.

as background noise [10]. Background signal is the photoacoustic signal generated by the walls, windows, as well as dust particles inside the cell. Background signal instability means the variation in the background signal that originates from intensity fluctuation in the radiation source and the precision of the cantilever read-out. These variations create noise even if the background signal can be subtracted [32]. The Brownian noise level, evaluated with the OPO off, was 2.08×10^{-5} (photoacoustic signal is in arbitrary units). The noise with the OPO in operation ranges from the lowest value of 3.52×10^{-5} to the highest value of 6.37×10^{-5} with an average of 4.71×10^{-5} over all wavelengths. The noise on top of the Brownian noise level arises from the background signal instability. In the previous work with an identical setup and mid-infrared QCL [33], the Brownian noise was analyzed to be the same as here. However, the background signal instability was 2.85×10^{-5} at a laser power of 47 mW and with a smaller background signal of 1.50×10^{-2}. The major part of the higher background instability in the OPO setup can be explained by the factor ~2 times higher power emitted by the OPO leading to a bigger background signal. Further points can be the probably somewhat different beam diameter and alignment of the source beams toward the cell, resulting in a different background signal and the relative intensity noise of the OPO.

3.3. Spectral data processing

The BTX analyte gases were prepared using the Gasmet™ calibrator as described in Section 2.2. While operating the calibrator, the authors realized that the concentration supplied by the calibrator was not stable over time. This means, that the true concentration in the cell and the set concentration may differ from each other. To eliminate the uncertainty in concentration, the intensity of the measured spectra was corrected as follows: methane supplied from the gas cylinder is reliable in concentration and the concentration was stable over time. The reference signal intensity for each analyte at 3291 nm was calculated by dividing the intensity at 3291 nm of the measured methane by the PNNL methane and multiplying it with the PNNL analyte intensity. Finally, the intensity of the measured spectra was corrected to the reference intensity. This assumes that the PA cell response is equal to methane and BTX, which is quite true. The correction factors were carefully reviewed and were in agreement with the observations during the operation of the calibrator. Prior to the calculation of the reference signal intensity, the PNNL reference spectra were convoluted to the same spectral bandwidth as the OPO, because of the narrow bands of methane. In addition, the measured spectra were background corrected assuming a linear background over the whole spectral range with the height of 1.80×10^{-2}. For the science-based calibration, the spectral response (arb./ppb) of the analytes is needed and, therefore, the analyte spectra were divided by the concentration. At each 3256 and 3275 nm, the OPO produced an artifact spike in the spectrum due to internal temperature adjustment. The spikes were reproducible and the regions between 3255.4–3257.7 nm and 3275.8–3277.7 nm were linear interpolated. As it can be seen from Fig. 2, the power emission curve of the OPO shows some tiny ripples. To avoid the ripples in the final response spectra, the spectra were smoothed using the Savitzky–Golay filter with a span of 25 data points. The resulting response as well as the PNNL reference spectra are shown in Fig. 4. The band positions and the shape of the measured BTX spectra are in compliance with the PNNL reference spectra. As already mentioned for Fig. 2, the intensities are a function of the measurement system response and therefore, deviate somewhat from the reference spectra. The recorded bands arise from aromatic CH stretching vibrations and as shown in Fig. 4 they are rather broad, which supports the broad excitation band width of the OPO.

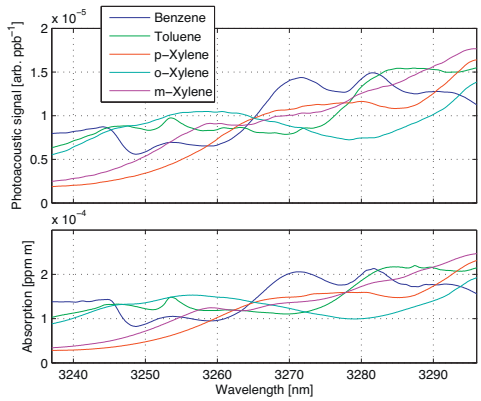

Fig. 4. Upper graph: Measured response spectra of benzene, toluene and the xylenes. Lower graph: PNNL reference spectra of benzene, toluene and the xylenes.

3.4. Univariate data analysis

The criteria for the wavelength selection in the univariate data analysis were high absorption coefficients of the analytes and the absence of water at that wavelength. The wavelength 3288 nm was selected and the signal intensities from the above calculated response spectra at 3288 nm are used for the detection limit calculation. The noise for the univariate analysis is the average of the two noise values at 3288 nm and its value of 4.99×10^{-5} is a bit higher than the average noise. The signal intensities as well as the calculated univariate detection limit are shown in Table 2. The detection limit (3σ, 0.951 s) varies between 9.8 ppb for toluene and 16.0 ppb for *o*-xylene. The difference in the detection limit comes from the different absorption coefficient of the analytes at 3288 nm. The average of the calculated minimum detectable absorption coefficients α_{min} (3σ, 0.951 s) of the five analytes is 4.94×10^{-8} cm^{-1}. The absorption coefficients were calculated from the PNNL spectra, which introduce a slight inaccuracy because the PNNL spectra are a function of the FT-IR instrument resolution and are measured at 1013 mbar compared to the measurements here done at 950 mbar.

The univariate detection limit can still be improved by selecting the wavelength with the highest absorption coefficient for each individual analyte. If more than one analyte is present, multivariate data analysis is crucial to resolve the spectral interference. The univariate detection in the 3288 nm region is immune to water up to a water concentration of 100 ppm. Above that, tiny water bands with a absorption coefficient of approx. 5×10^{-7} cm^{-1} (HITRAN [34], 1 ppm, 10 cm, 323 K, 950 mbar) are rising in the 3288 nm region. If water is present in higher concentrations, the interference needs to be resolved by multivariate data analysis as well.

In addition to the spectra, the OPO was adjusted to 3288 nm and the photoacoustic signal of the analytes was recorded to observe the signal variation over time. Fig. 5 shows the photoacoustic signal of

Table 2
Univariate detection limits of the analytes at 3288 nm.

	Signal intensity [arb./ppb]	Detection limit (3σ, 0.951 s) [ppb]
Benzene	1.25×10^{-5}	12.0
Toluene	1.54×10^{-5}	9.8
p-Xylene	1.14×10^{-5}	13.2
o-Xylene	9.37×10^{-6}	16.0
m-Xylene	1.49×10^{-5}	10.1

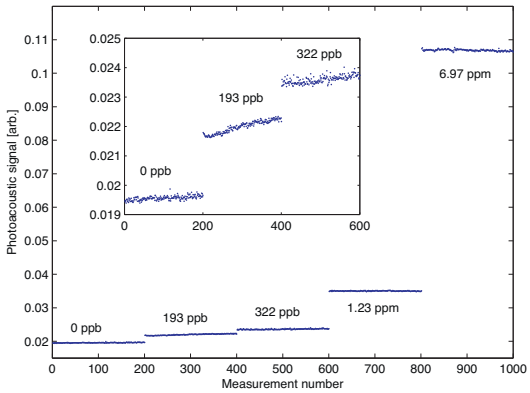

Fig. 5. Photoacoustic signal of benzene over time at 3288 nm and the corresponding concentrations. One measurement corresponds to 0.951 s.

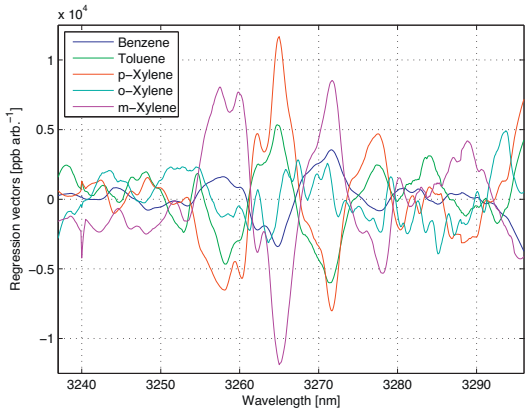

Fig. 6. Calculated regression vectors of benzene, toluene and the xylenes for the multi-compound sample.

benzene at different concentrations. For the sake of visibility and to save space, only the plot for benzene is shown here. The time recordings were not processed as the spectra. The data shown in Fig. 5 is raw data, however the displayed concentration values were corrected with the use of the response spectra.

3.5. Multivariate data analysis

Science-based calibration (SBC) was used for multivariate data analysis. From mathematical view, the SBC-method is a Wiener filter and it combines the earlier separate existing statistical *e.g.* PLS, PCR and physical *e.g.* classical calibration approaches. In case of the SBC-method, compared to the earlier approaches, both estimates of the signal and the noise are explicit *i.e.* controllable by the user. Therefore, the SBC-method offers the advantages of both approaches, the prediction accuracy of the statistical calibration and the simplicity of the classical calibration [37]. More information about the SBC as derivation, formulas, application examples and comparison to other calibration methods is published in [35–38]. The SBC equations used in this work will briefly be stated here for better understanding of the results. The regression vector b is calculated as

$$b = \frac{\sum^{-} g}{g^T \sum^{-} g}, \tag{1}$$

the detection limit DL as

$$DL = 3\sqrt{\frac{1}{g^T \sum^{-} g}}, \tag{2}$$

the cross-selectivity CS as

$$CS_{A/I} = b_A^T g_I, \tag{3}$$

where g is the response spectrum [arb./ppb] written as column vector and g^T as row vector, b is the regression vector [ppb/arb.], $\sum$ is the noise matrix, $\sum^{-}$ is the inverted noise matrix and $CS_{A/I}$ is the cross-selectivity of the interferent I to analyte A [ppb/ppb]. Finally, the concentration of the analyte c_A is calculated as

$$C_A = c_{OP} + b_A^T(S_m - S_{OP}), \tag{4}$$

where c_A is the concentration of the analyte [ppb] of the measured spectrum S_m [arb.], S_{OP} [arb.] the spectrum at the operation point and c_{OP} the concentration [ppb] at the operation point.

The response spectra g, prepared as in Section 3.3 explained are used for the calculation of the regression vectors b. The sigma matrixes are analyte specific and contain the instrument noise and the interference of the other analytes. This sigma matrix represents the 'real case situation', or in other words the multi-compound sample, assuming all analytes to be present in the sample. When all analytes are present, each analyte will interfere the determination of all the other analytes. For comparison, how much the detection limit will be worse when the interference is resolved, a second calibration is set up for each analyte without interfering analytes, assuming only the analyte of interest to be present. This situation is referred to single-compound sample and the sigma matrix contains only the instrument noise. The instrument noise is the noise calculated in Section 3.2. To cover the whole spectral range, the noise was linear interpolated. Outside the measured points, the noise was extrapolated by a linear fit. The multi-compound calibrations were optimized for selectivity and, in addition, water was added as another interferent to make the calibration immune toward water vapor that may be present in the sample. To decrease the influence of the ripples in the spectra, the differences of the measured spectra of each analyte are added to the noise matrix. The calculated regression vectors are shown in Fig. 6 and detection limits of the analytes as single- and multi-compound sample in Table 3. For the calculation of the cross-selectivities (CS) different spectra were used as response spectra than for the calibration. However, the spectra were treated in the same way as the calibration spectra, like described in Section 3.3. The calculated cross-selectivities are shown in Table 4.

With multivariate data analysis, the detection limit can be enhanced compared to univariate. Particular advantage of multivariate data analysis have systems that measure multivariate *i.e.* without increasing the measurement time as for example

Table 3
Multivariate detection limits of the analytes using the full spectral range from 3237 to 3296 nm. Single-compound means the measurement of only the analyte of interest and multi-compound the measurement of the analyte while all other analytes and water interfere.

	Detection limit (3σ, 591 spectral points each 0.951 s) [ppb]	
	Single-compound	Multi-compound
Benzene	0.52	4.3
Toluene	0.51	7.4
p-Xylene	0.59	11.0
o-Xylene	0.61	6.2
m-Xylene	0.52	12.5

Table 4
Cross-selectivities of the analytes and water (3237–3296 nm, 591 spectral points, each 0.951 s) in ppb/ppb. For example, when measuring benzene and toluene's concentration increases by 100 ppb, the measured benzene value will increase by 1.1 ppb.

Analyte	Interferent						
	Benzene	Toluene	*p*-Xylene	*o*-Xylene	*m*-Xylene	Water	Sum
Benzene	0.99	0.011	−0.008	−0.014	−0.004	-5.67×10^{-5}	0.037
Toluene	0.004	1.00	0.001	−0.013	0.011	1.34×10^{-4}	0.028
p-Xylene	−0.008	−0.002	1.00	0.010	0.011	1.66×10^{-4}	0.031
o-Xylene	0.019	−0.010	0.005	0.99	−0.016	-2.84×10^{-5}	0.049
m-Xylene	−0.002	0.017	<−0.001	0.026	1.00	-2.25×10^{-4}	0.045

grating instruments with line or array detector and FT-IRs. However, for measurement systems that are of univariate nature as the system here, additional spectral data points increase the measurement time. If the spectral point with the highest quotient of absorption coefficient and noise was chosen for univariate data analysis, then the detection limit scaled on the measurement time cannot be improved with multivariate data analysis. However, if interferents are present, as in the case here, then multiple univariate measurement points in combination with multivariate data analysis can be used to resolve the interference as shown in the present work where the sum of the cross-selectivities per analyte were below 0.05 ppb/ppb, with an average of 0.038 ppb/ppb. However, resolving the interference consumes signal and the resulting detection limit suffers from that. In this work the multivariate detection limits (3σ, 3237–3296 nm, 591 spectral points each 0.951 s) of the multi-compound sample, where all other analytes and water interfere vary from 4.3 ppb for benzene to 12.5 ppb for *m*-xylene. Without the interference, in the multivariate single-compounds case, the detection limits are better by an average factor of 15. The cross-selectivity of water varied from -2.25×10^{-4} ppb/ppb for *m*-xylene to -2.84×10^{-5} ppb/ppb for *o*-xylene, with an average of 1.22×10^{-4} ppb/ppb. This means that the water concentration can vary by approx. ±5 ppm and only affect the analyte reading by 1 ppb. However, water or any other interferent can be present in higher concentrations if the concentration does not change over time. Only the varying part of the interferent signal needs to be considered in the interference assessment. A non-varying interferent signal will be included in the operation point spectrum and thus be subtracted from the measured spectrum before its multiplication with the *b*-vector as in Eq. (4).

3.6. Outlook and system improvements

For this work an OPO was selected as light source because it has several advantages over other light sources as *e.g.* QCLs. The OPO offers a broader tunability as diode lasers and can supply more optical power relative to the beam quality. Further, QCLs emitting in the 3–4 μm region are sparely commercially available yet. The OPO used here is commercially available, small-sized and easy to integrate to setups. That makes it a suitable light source for industrial and environmental trace gas monitoring.

The built measurement system is ready for most applications stated in Section 1 as process or environmental BTX measurements on ppb level and workplace security control. If the interferences are low, then the system reaches the detection limits for urban area monitoring of benzene in cities. Otherwise, a longer integration time or improvements mentioned following will help to reach the detection limit. The system is small, fits in a 19 in. rack and needs only a power supply for operation. The OPO is passively cooled and the whole OPO-CEPAS system including data management and acquisition consumes typically ~60 W and max. 120 W at 230 V. A portable version of the system could be built without great effort and with more development work maybe a handheld version.

Suggestions for further improvements of the system are:

1. A strategy to optimize the univariate measurement needs to be developed. In this work, the OPO was tuned in steps of 0.1 nm, all spectral points were included to the calibration and the integration time was the same for all points. Since, the spectral resolution of the measurement system is limited to 1.3 nm, the step interval can be chosen wider without losing resolution but saving measurement time. Further, the noise is not evenly distributed over the spectral range, the absorption coefficients of the analytes are wavelength dependent and the interferences as well. Therefore, the univariate measurement can be improved by optimizing the amount of spectral points, the wavelengths where the spectral points are measured at and the integration time at each spectral point. This optimization is always application specific and will result in better system performance and a shorter measurement time. First investigations about the optimization strategy of an external cavity QCL-CEPAS system are recently reported in [39].
2. The cross-selectivities are already on a good level, but they can still be improved by reducing the ripples in the spectra that originates from the OPO. Without the ripples, the CS could possibly be enhanced to the level of 10^{-4}, maybe even to 10^{-5} ppb/ppb. Already during this work the spectral band width of the next assembled OPOs was improved to a FWHM of 1.0 nm. This will facilitate as well for the cross-selectivities, particular for water. Increasing the output power of the OPO will reduce the measurement time or increase the sensitivity.
3. BTX vapor in trace concentrations is adsorbing on the interior of sampling systems and the photoacoustic cells. This can lead to slow response time of the system as well as incorrect readings. Therefore, the sampling system and cell materials need to be optimized for the lowest possible adsorption of BTX as reported for example for ammonia in [40]. Because the gas flow through the cell needs to be stopped for the measurement, the adsorption phenomena happening need to be analyzed and optimized by *e.g.* shortening the measurement time, longer purging time between consecutive measurements, evacuating the cell with lower pressure for longer time and using optimized materials for low adsorption.

4. Conclusions

A compact measurement system based on a novel combination of CEPAS and OPO was set up and its performance demonstrated. The OPO had a FWHM bandwidth of 1.3 nm, was tunable from 3237 to 3296 nm in steps of 0.1 nm and within that range the emitted power increased from 88 to 103 mW. The univariate detection limit (3σ, 0.951 s) for benzene, toluene, *p*-, *m*- and *o*-xylene at 3288 nm was 12.0, 9.8, 13.2, 10.1 and 16.0 ppb, respectively. A multi-compound sample requires multivariate data analysis to resolve the spectral interferences of the analytes. The multivariate detection limit (3σ, 3237–3296 nm, 591 spectral points each 0.951 s) of the multi-compound sample where all other analytes

and water interfere was 4.3, 7.4, 11.0, 12.5 and 6.2 ppb for benzene, toluene, *p*-, *m*- and *o*-xylene, respectively. Without interference, multivariate detection (3σ, 3237–3296 nm, 591 spectral points each 0.951 s) of the analytes varied between 0.5 and 0.6 ppb. The cross-selectivities per analyte were below 0.05 ppb/ppb, with an average of 0.038 ppb/ppb. The cross-selectivity of water was on average 1.22×10^{-4} ppb/ppb.

Possible improvements of the system include (1) optimization strategy for the univariate measurement, (2) reducing the ripples, decreasing the bandwidth and increasing the optical output of the OPO and (3) optimization of the sampling system for lowest possible BTX adsorption. These will improve the performance of the measurement system like the CS that could possibly be enhanced to the level of 10^{-4}, maybe even to 10^{-5} ppb/ppb and the already high sensitivity further increased, leading to better detection limits or faster measurement times.

The system is ready for accurate and routine measurement of BTX in industrial processes, in urban and indoor air as well as for environmental monitoring. The system reaches ppb detection limits in multi-compound analysis of BTX, fits in a 19 in. rack and needs only a power supply. With future improvements a portable and even a handheld system is imaginable.

Acknowledgements

The authors would like to thank Cobolt AB, Sweden (www.cobolt.se) for cooperation and providing the OPO. C.B. Hirschmann acknowledges the financial support of the Graduate School in Chemical Engineering, Finland.

References

[1] E. Gallego, F.X. Roca, X. Guardino, M.G. Rosell, Journal of Environmental Science 20 (2008) 1063.
[2] F. Palmgren, A.B. Hansen, R. Berkowicz, H. Skov, Atmospheric Environment 35 (2001) 35.
[3] H. Skov, A. Lindskog, F. Palmgren, C.S.S. Christensen, Atmospheric Environment 35 (2001) S141.
[4] G.A. Pilidis, S.P. Karakitsios, P.A. Kassomenos, Atmospheric Environment 39 (2005) 6051.
[5] J.G. Calvert, R. Atkinson, K.H. Becker, R.M. Kamens, J.H. Seinfeld, T.J. Wallington, G. Yarwood, Mechanisms of Atmospheric Oxidation of Aromatic Hydrocarbons, Oxford University Press, New York, 2000.
[6] S. Ojala, S. Pitkäaho, T. Laitinen, N. Niskala Koivikko, R. Brahmi, J. Gaálová, L. Matejova, A. Kucherov, S. Päivärinta, C. Hirschmann, T. Nevanperä, M. Riihimäki, M. Pirilä, R.L. Keiski, Topics in Catalysis 54 (2011) 1224.
[7] World Health Organization, Benzene, Int Programme of Chemical Safety, Environmental Health Criteria No. 150, Geneva, Switzerland, 1993.
[8] International Labour Organization, International Chemical Security Cards of Benzene, Toluene and Xylenes, http://www.ilo.org/dyn/icsc/showcard.home (accessed 29.04.2013).
[9] J. Hodgkinson, R.P. Tatam, Measurement Science and Technology 24 (2013) 012004.
[10] Z. Bozóki, A. Pogány, G. Szabó, Applied Spectroscopy Reviews 46 (2011) 1.
[11] A. Elia, P.M. Lugarà, C. Di Franco, V. Spagnolo, Sensors-Basel 9 (2009) 9616.
[12] T. Schmid, Analytical and Bioanalytical Chemistry 384 (2006) 1071.
[13] F.J.M. Harren, G. Cotti, J. Oomens, S. teL. Hekkert, in: R.A. Meyers (Ed.), Encyclopedia of Analytical Chemistry, John Wiley & Sons, Chichester, 2000, pp. 2203–2226.
[14] K. Wilcken, J. Kauppinen, Applied Spectroscopy 57 (2003) 1087.
[15] J. Kauppinen, K. Wilcken, I. Kauppinen, V. Koskinen, Microchemical Journal 76 (2004) 151.
[16] T. Kuusela, J. Kauppinen, Applied Spectroscopy Reviews 42 (2007) 443.
[17] V. Koskinen, J. Fonsen, J. Kauppinen, I. Kauppinen, Vibrational Spectroscopy 42 (2006) 239.
[18] V. Koskinen, J. Fonsen, K. Roth, J. Kauppinen, Vibrational Spectroscopy 48 (2008) 16.
[19] J. Kauppinen, V. Koskinen, J. Uotila, I. Kauppinen, Proceedings of SPIE 5617 (2004) 115.
[20] R.E. Lindley, A.M. Parkes, K.A. Keen, E.D. McNaghten, A.J. Orr-Ewing, Applied Physics B 86 (2007) 707.
[21] I. Kauppinen, A. Branders, J. Uotila, S. Sinisalo, J. Kauppinen, T. Kuusela, Technisches Messen 79 (2012) 17.
[22] C.B. Hirschmann, J. Uotila, S. Ojala, J. Tenhunen, R.L. Keiski, Applied Spectroscopy 64 (2010) 293.
[23] C.B. Hirschmann, N.S. Koivikko, J. Raittila, J. Tenhunen, S. Ojala, K. Rahkamaa-Tolonen, R. Marbach, S. Hirschmann, R.L. Keiski, Sensors-Basel 11 (2011) 5270.
[24] J. Uotila, J. Kauppinen, Applied Spectroscopy 62 (2008) 655.
[25] J. Fonsen, V. Koskinen, K. Roth, J. Kauppinen, Vibrational Spectroscopy 50 (2009) 214.
[26] Gasera Ltd., PA101 – Photoacoustic Low Volume Gas Analysis Module, http://www.gasera.fi/products/ftir-accessories/pa101/ (accessed 29.04.2013).
[27] Gasera Ltd., F10 – Photoacoustic Multi-gas Analyzer, http://www.gasera.fi/products/gas-analyzers/f10/ (accessed 29.04.2013).
[28] J. Hellström, P. Jänes, G. Elgcrona, H. Karlsson, Proceedings of SPIE 8733 (2013) 87330A.
[29] J. Peltola, M. Vainio, T. Hieta, J. Uotila, S. Sinisalo, M. Metsälä, M. Siltanen, L. Halonen, Optics Express 21 (2013) 10240.
[30] S.W. Sharpe, T.J. Johnson, R.L. Sams, P.M. Chu, G.C. Rhoderick, P.A. Johnson, Applied Spectroscopy 58 (2004) 1452.
[31] Gasmet Technologies Oy, Gasmet Calibrator, http://www.gasmet.fi/na/products/gas_sampling_units_accessories (accessed 29.04.2013).
[32] J. Uotila, Use of the Optical Cantilever Microphone in Photoacoustic Spectroscopy, University of Turku, 2009.
[33] C.B. Hirschmann, J. Lehtinen, J. Uotila, S. Ojala, R.L. Keiski, Sub-ppb detection of formaldehyde with cantilever enhanced photoacoustic spectroscopy using quantum cascade laser source, Applied Physics B 111 (2013) 603–610.
[34] L.S. Rothman, I.E. Gordon, A. Barbe, D.C. Benner, P.F. Bernath, M. Birk, V. Boudon, L.R. Brown, A. Campargue, J.-P. Champion, K. Chance, L.H. Coudert, V. Dana, V.M. Devi, S. Fally, J.-M. Flaud, R.R. Gamache, A. Goldman, D. Jacquemart, I. Kleiner, N. Lacome, W.J. Lafferty, J.-Y. Mandin, S.T. Massie, S.N. Mikhailenko, C.E. Miller, N. Moazzen-Ahmadi, O.V. Naumenko, A.V. Nikitin, J. Orphal, V.I. Perevalov, A. Perrin, A. Predoi-Cross, C.P. Rinsland, M. Rotger, M. Šimečková, M.A.H. Smith, K. Sung, S.A. Tashkun, J. Tennyson, R.A. Toth, A.C. Vandaele, J. Vander Auwera, Journal of Quantitative Spectroscopy and Radiative Transfer 110 (2009) 533.
[35] R. Marbach, Journal of Biomedical Optics 7 (2002) 130.
[36] R. Marbach, Journal of Near Infrared Spectroscopy 13 (2005) 241.
[37] R. Marbach, Pharmaceutical Manufacturing 6 (2007) 42.
[38] R. Marbach, Pharmaceutical Manufacturing 6 (2007) 44.
[39] A. Ulrici, R. Seeber, M. Calderisi, G. Foca, J. Uotila, M. Carras, A.M. Fiorello, Proceedings of SPIE 8545 (2012) 85450K.
[40] A. Schmohl, A. Miklos, P. Hess, Applied Optics 40 (2001) 2571.

Series title and number
VTT Science 46

Title	**Cantilever-enhanced photoacoustic spectroscopy in the analysis of volatile organic compounds**
Author(s)	Christian Bernd Hirschmann
Abstract	Accurate and reliable measurement of volatile organic compounds (VOCs) is an important need in many application areas in industry, air pollution and atmosphere, health and well-being, defense and security as well as in many other fields. In this thesis, cantilever-enhanced photoacoustic spectroscopy (CEPAS) has been applied for the measurement of VOCs. A key feature in CEPAS is the non-resonant operational mode of the detector, which enables the broadly tunable wavelength ranges needed to resolve the spectral interferences that are typical in VOC measurement applications. Due to the large variation in VOC applications, the objective of this work was to build several, differently optimized CEPAS measurement systems and characterize their performance in certain applications. The Fourier transform infrared (FT-IR) technique was applied for multi-compound VOC mixtures because of its capability to resolve spectral interference between the compounds. A compact, industry-ready FT-IR-CEPAS system was tested and reached multivariate detection limits (3σ, 25 s) at the single ppm level with the average sum of the cross-selectivity numbers in a four compound mixture being <0.01 ppm ppm^{-1}. To achieve better analytical sensitivity, the CEPAS detector was set up with a quantum cascade laser (QCL). The QCL-CEPAS system provides a univariate detection limit (3σ, 0.951 s) of 1.3 ppb for formaldehyde, which is ~1000 times better than the FT-IR-CEPAS system. However, in case of several compounds, spectral interferences are usually difficult to resolve because the mode hop-free tuning range of QCLs is limited to a few wavenumbers. For sensitive and selective trace gas detection, a compact optical parametric oscillator (OPO) was combined with CEPAS and applied to the multi-compound measurement of benzene, toluene, *p*-, *m*- and *o*-xylene (BTX). The achieved multivariate detection limits (3σ, 3237–3296 nm, 591 spectral points each 0.951 s) were around 10 ppb and the average sum of the cross-selectivity numbers <0.04 ppb ppb^{-1}. Another achievement was the construction of a CEPAS measurement system capable of measuring at gas temperatures up to 180 °C. This enables applications where gases can only be measured in the hot state, e.g. the monitoring of many industrial emissions. Since the cantilever pressure transducer can withstand 180 °C, it was in direct contact with the hot sample gas and the need for cooling the gas or for using a signal tube was eliminated. In summary, this thesis shows that modern CEPAS is a suitable technique for measuring VOCs. CEPAS is now robust and reliable enough for industrial and other applications outside the laboratory. Several measurement systems based on CEPAS and relevant for VOC applications have been demonstrated in this thesis.
ISBN, ISSN	ISBN 978-951-38-8105-4 (Soft back ed.) ISBN 978-951-38-8106-1 (URL: http://www.vtt.fi/publications/index.jsp) ISSN-L 2242-119X ISSN 2242-119X (Print) ISSN 2242-1203 (Online)
Date	December 2013
Language	English
Pages	109 p. + app. 49 p.
Keywords	Cantilever-enhanced photoacoustic spectroscopy, volatile organic compounds, FT-IR, quantum cascade laser, optical parametric oscillator, multi-compound analysis, science-based calibration
Publisher	VTT Technical Research Centre of Finland P.O. Box 1000, FI-02044 VTT, Finland, Tel. +358 20 722 111

Cantilever-enhanced photoacoustic spectroscopy in the analysis of volatile organic compounds

Accurate and reliable measurement of volatile organic compounds (VOCs) is an important need in many application areas in industry, air pollution and atmosphere, health and well-being, defense and security as well as in many other fields. In this thesis, cantilever-enhanced photoacoustic spectroscopy (CEPAS) has been applied for the measurement of VOCs. A key feature in CEPAS is the non-resonant operational mode of the detector, which enables the broadly tunable wavelength ranges needed to resolve the spectral interferences that are typical in VOC measurement applications. Due to the large variation in VOC applications, the objective of this work was to build several, differently optimized CEPAS measurement systems and characterize their performance in certain applications.

In summary, this thesis shows that modern CEPAS is a suitable technique for measuring VOCs. CEPAS is now robust and reliable enough for industrial and other applications outside the laboratory. Several measurement systems based on CEPAS and relevant for VOC applications have been demonstrated in this thesis.

ISBN 978-951-38-8105-4 (Soft back ed.)
ISBN 978-951-38-8106-1 (URL: http://www.vtt.fi/publications/index.jsp)
ISSN-L 2242-119X
ISSN 2242-119X (Print)
ISSN 2242-1203 (Online)